UNIVERSIDADE ESTADUAL PAULISTA - UNESP

CÂMPUS DE JABOTICABAL

DYNAMICS AND CONTROL OF CO_2 EMISSION CYCLES IN HEAT WAVES IN NORTHERN EUROPE AND IN THE DIFFERENT BIOMES OF BRAZIL: CLIMATE RESILIENCE AND MITIGATION MECHANISMS

Marcelo Odorizzi de Campos

Agronomic Engineer

2025

UNIVERSIDADE ESTADUAL PAULISTA - UNESP
CÂMPUS DE JABOTICABAL

DYNAMICS AND CONTROL OF CO_2 EMISSION CYCLES IN HEAT WAVES IN NORTHERN EUROPE AND IN THE DIFFERENT BIOMES OF BRAZIL: CLIMATE RESILIENCE AND MITIGATION MECHANISMS

Marcelo Odorizzi de Campos
Advisor: Prof. Dr. Rouverson Pereira da Silva

Dissertation presented to the Faculty of Agricultural and Veterinary Sciences – Unesp, Jaboticabal Campus, as part of the requirements for obtaining the title of Doctor in Agronomy (plant production).

2025

CATALOGRAPHIC SHEET

C198d

Campos, Marcelo Odorizzi de

Dynamics and control of CO_2 emission cycles in heat waves in northern Europe and in the different biomes of Brazil: climate resilience and mitigation mechanisms / Marcelo Odorizzi de Campos. -- Jaboticabal, 2025

92 p.

Tese (doutorado) - Universidade Estadual Paulista (UNESP), Faculdade de Ciências Agrárias e Veterinárias, Jaboticabal

Orientador: Rouverson Pereira da Silva

1. Climate change. 2. Dioxido de carbono atmosferico. 3. Teor de carbono no solo. 4. Ondas de calor. 5. Zonas climáticas. I. Título.

Sistema de geração automática de fichas catalográficas da Unesp. Dados fornecidos pelo autor(a).

POTENTIAL IMPACT OF THIS RESEARCH

This work aims to support Brazil's challenging mission to meet the goals set in its Nationally Determined Contribution (NDC) and at the 27th United Nations Climate Change Conference (COP27), including: reducing greenhouse gas (GHG) emissions by 37% by 2025 and 43% by 2030 (compared to 2005 levels); restoring at least 12 million hectares of degraded land by 2030; and achieving carbon neutrality by 2050. These targets align directly with the United Nations Sustainable Development Goal (SDG) 13 – Climate Action.

The study emphasizes the integration of social, environmental, and economic dimensions of research in accordance with the SDGs, highlighting how technologies focused on climate resilience and mitigation can positively impact the plant–soil–atmosphere carbon cycle in Brazilian biomes. Environmentally, the work is especially aligned with SDG 12 (Responsible Consumption and Production) and SDG 13 (Climate Action); socially, with SDG 2 (Zero Hunger and Sustainable Agriculture); and economically, with SDG 8 (Decent Work and Economic Growth).

By advancing understanding of how public policies influence the adoption of sustainable land-use practices, this work contributes to strengthening responsible and productive systems. These efforts not only enhance climate resilience and reduce GHG emissions but also improve the profitability and scalability of agroecosystems.

UNIVERSIDADE ESTADUAL PAULISTA

Câmpus de Jaboticabal

CERTIFICADO DE APROVAÇÃO

TÍTULO DA TESE: DYNAMICS AND CONTROL OF CO2 EMISSION CYCLES IN HEAT WAVES IN NORTHERN EUROPE AND IN THE DIFFERENT BIOMES OF BRAZIL: CLIMATE RESILIENCE AND MITIGATION MECHANISMS

AUTOR: MARCELO ODORIZZI DE CAMPOS
ORIENTADOR: ROUVERSON PEREIRA DA SILVA

Aprovado como parte das exigências para obtenção do Título de Doutor em Agronomia (Produção Vegetal), pela Comissão Examinadora:

gov.br Documento assinado digitalmente
ROUVERSON PEREIRA DA SILVA
Data: 11/07/2025 16:17:13-0300
Verifique em https://validar.iti.gov.br

Prof. Dr. ROUVERSON PEREIRA DA SILVA (Participaçao Virtual)
Departamento de Engenharia / FCAV UNESP Jaboticabal

gov.br Documento assinado digitalmente
GUSTAVO ANDRE DE ARAUJO SANTOS
Data: 14/07/2025 14:47:50-0300
Verifique em https://validar.iti.gov.br

Prof. Dr. GUSTAVO ANDRÉ DE ARAÚJO SANTOS (Participaçao Virtual)
Departamento de Engenharia Agricola / Universidade Federal do Maranhão (UFMA) - São Luis/MA

Prof. Dr. NEWTON LA SCALA JUNIOR (Participaçao Virtual)
Departamento de Ciencias Exatas / FCAV UNESP Jaboticabal

gov.br Documento assinado digitalmente
NEWTON LA SCALA JUNIOR
Data: 11/07/2025 17:09:41-0300
Verifique em https://validar.iti.gov.br

gov.br Documento assinado digitalmente
LUCIANO DE SOUZA MARIA
Data: 12/07/2025 06:14:58-0300
Verifique em https://validar.iti.gov.br

Prof. Dr. LUCIANO DE SOUZA MARIA (Participaçao Virtual)
Departament de Ciências do Solo / Universidade do Estado de Mato Grosso (UNEMAT) - Alta Floresta/MT

Faculdade de Ciências Agrárias e Veterinárias - Câmpus de Jaboticabal -
Via de Acesso Professor Paulo Donato Castellane, s/n, 14884900
https://www.fcav.unesp.br/#!/pos-graduacao/programas-pg/agronomia-producao-vegetal/CNPJ: 48.031.918/0012-87.

UNIVERSIDADE ESTADUAL PAULISTA

Câmpus de Jaboticabal

Prof. Dr. ALAN RODRIGO PANOSSO (Participaçao Virtual)
Departamento de Ciencias Exatas / FCAV UNESP Jaboticabal

Documento assinado digitalmente
ALAN RODRIGO PANOSSO
Data: 16/07/2025 09:48:58-0300
Verifique em https://validar.iti.gov.br

Jaboticabal, 06 de junho de 2025

AUTHOR'S RESUME

Marcelo Odorizzi de Campos

Born in Cândido Mota, in the countryside of São Paulo State, on May 22, 1995, son of José Valentim de Campos and Alba Tereza Odorizzi, who worked professionally as a locksmith and a cleaner, respectively. He is currently working in carbon credit origination at Itaú Unibanco S.A., focusing on environmental assets related to Nature-Based Solutions and Technology-Based Solutions. He previously worked as an Agronomist and Carbon Specialist on the carbon credit origination team at MyCarbon (Minerva Foods).

He is currently pursuing a Ph.D. in Agronomy (Plant Production) at São Paulo State University "Júlio de Mesquita Filho" (UNESP), Faculty of Agricultural and Veterinary Sciences (FCAV), Jaboticabal campus – a program rated CAPES 6. At this same institution, he earned his Master's degree in Agronomy (Plant Production) and completed his undergraduate studies in Agronomic Engineering. Additionally, he obtained a second Master's degree in Planning and Analysis of Public Policies from UNESP, Faculty of Human and Social Sciences (FCHS), Franca campus.

He has collaborated in teaching and extension activities with the Centro de Educación y Tecnología (CET) in Bio-Bio, Chile. Furthermore, he carried out part of his Ph.D. research at the University of Trento, Italy.

He has experience in the carbon market, VERRA certification standards, and carbon credit origination, especially for agricultural products and solutions. He is also experienced in modeling the carbon Plant–Soil–Atmosphere continuum in agriculture, particularly in soil carbon stocks and atmospheric CO_2, and is knowledgeable about Brazilian public financing policies for sustainable land-use transitions, such as the ABC Program – Low-Carbon Agriculture.

DEDICATION

I dedicate this work to my father, José Valentim de Campos, my mother, Alba Tereza Odorizzi, and my brothers, Matheus Odorizzi de Campos and Luan Alberto Odorizzi dos Santos.

A special acknowledgment goes to Prof. Luan Odorizzi, the first in our family to earn a bachelor's, master's, and doctoral degree, whose achievements in science paved the way for my own professional development.

With deep affection, I also dedicate this work to my future wife, Dr. Andreísa Flores Braga, whose unwavering support was essential throughout my entire doctoral journey.

ACKNOWLEDGMENTS

I would like to express my deep gratitude to my parents for their unwavering support and encouragement throughout my life. Their dedication and effort have been fundamental in shaping the person I have become. I also wish to express my sincere appreciation to my siblings: to Matheus Odorizzi de Campos, whose simplicity and charisma have always enriched my life, and to Prof. Dr. Luan Alberto Odorizzi dos Santos, whose influence has been essential to both my professional and personal development. Furthermore, a special thanks to Dr. Andreísa Flores Braga, who on September 21, 2024 officially became part of my family, as my wife.

I especially and sincerely thank my advisor, Prof. Dr. Rouverson Pereira da Silva, as well as Prof. Dr. Regina Aparecida Leite de Camargo, Prof. Dr. Newton La Scala Jr., and Prof. Dr. José Marques Júnior, for all the scientific, professional, and personal knowledge they have shared with me throughout my journey. It has been truly rewarding to work with such brilliant scientists - people who are not only highly competent in their fields, but also deeply human.

I also thank the Faculty of Agricultural and Veterinary Sciences – UNESP, Jaboticabal Campus, and the Graduate Program in Agronomy (Plant Production), for the opportunity and support provided for my academic development. This study was financed in part by the Coordenação de Aperfeiçoamento de Pessoal de Nível Superior - Brasil (CAPES) - Finance Code 001

SUMMARY

LIST OF TABLES

DYNAMICS AND CONTROL OF CO_2 EMISSION CYCLES IN HEAT WAVES IN NORTHERN EUROPE AND IN THE DIFFERENT BIOMES OF BRAZIL: CLIMATE RESILIENCE AND MITIGATION MECHANISMS

ABSTRACT: Climate change has been intensifying extreme events, such as heatwaves, which directly impact carbon cycles and ecosystem stability. At the same time, there is growing concern about the rise in global temperatures and its effects on soil carbon stocks, especially in tropical and subtropical regions. In this context, this thesis aimed to assess the effects of heatwaves on carbon dioxide emissions in temperate forests in Europe and to investigate the factors that control soil carbon stocks and atmospheric carbon dioxide concentrations in the main Brazilian biomes. The first study was conducted in northern Europe, where data on atmospheric carbon dioxide concentration, carbon fluxes between the ecosystem and the atmosphere, vegetation growth variables, soil moisture and temperature, as well as climate parameters such as air temperature, wind, and precipitation, were analyzed. The analyses integrated satellite data, remote sensing products, and field measurements from micrometeorological towers. The second study was carried out in the Cerrado, Caatinga, Atlantic Forest, and Pampa biomes, using climate data, soil attributes, and vegetation indicators, combined with geoprocessing tools and multivariate statistical modeling. The results of the first study indicated that heatwaves significantly increased carbon dioxide emissions, mainly due to the increase in microbial respiration in the soil, while the photosynthetic capacity of vegetation remained active and, in some cases, even increased. In the second study, the average annual temperature stood out as the main factor associated with the reduction of soil carbon stocks, highlighting that the advancement of global warming may compromise the ability of Brazilian soils to act as carbon sinks. These findings reinforce the urgent need to adopt mitigation strategies such as sustainable intensification, conservation-oriented soil management, restoration of degraded areas, and the implementation of nature-based solutions, contributing to the resilience of productive systems and the fight against climate change.

Keywords: Climate change; Carbon dioxide emissions; Soil carbon stock; Heatwaves; Mitigation; Climate resilience.

DINÂMICA E CONTROLE DOS CICLOS DE EMISSÃO DE CO_2 DURANTE ONDAS DE CALOR NO NORTE DA EUROPA E NOS DIFERENTES BIOMAS DO BRASIL: MECANISMOS DE RESILIÊNCIA CLIMÁTICA E MITIGAÇÃO

RESUMO: As mudanças climáticas vêm intensificando eventos extremos, como as ondas de calor, que impactam diretamente os ciclos de carbono e a estabilidade dos ecossistemas. Simultaneamente, existe uma crescente preocupação com o aumento da temperatura global e seus efeitos sobre os estoques de carbono no solo, especialmente em regiões tropicais e subtropicais. Diante desse cenário, esta tese teve como objetivo avaliar os efeitos das ondas de calor sobre as emissões de dióxido de carbono em florestas temperadas na Europa e investigar os fatores que controlam os estoques de carbono no solo e as concentrações atmosféricas de dióxido de carbono nos principais biomas do Brasil. O primeiro estudo foi conduzido na região norte da Europa, onde foram analisados dados de concentração atmosférica de dióxido de carbono, fluxos de carbono entre o ecossistema e a atmosfera, variáveis relacionadas ao crescimento da vegetação, umidade e temperatura do solo, além de parâmetros climáticos como temperatura do ar, vento e precipitação. As análises integraram dados de satélites, sensores remotos e medições de campo em torres micrometeorológicas. O segundo estudo foi realizado nos biomas Cerrado, Caatinga, Mata Atlântica e Pampa, utilizando dados climáticos, atributos do solo e indicadores de vegetação, combinados com ferramentas de geoprocessamento e modelagem estatística multivariada. Os resultados do primeiro estudo indicaram que as ondas de calor aumentaram significativamente as emissões de dióxido de carbono, principalmente em função do aumento da respiração microbiana do solo, enquanto a capacidade fotossintética da vegetação permaneceu ativa e, em alguns casos, até aumentou. No segundo estudo, a temperatura média anual se destacou como o principal fator associado à redução dos estoques de carbono no solo, evidenciando que o avanço do aquecimento global pode comprometer a capacidade dos solos brasileiros de atuar como sumidouros de carbono. Os resultados reforçam a necessidade urgente de adoção de estratégias de mitigação, como a intensificação sustentável, o manejo conservacionista do solo, a restauração de áreas degradadas e a implementação de soluções baseadas na natureza, contribuindo para a resiliência dos sistemas produtivos e o enfrentamento das mudanças climáticas.

Palavras-chave: Mudanças climáticas; xCO_2; Estoque de carbono no solo; Ondas de calor; Mitigação; Resiliência climática

LIST OF FIGURES

CHAPTER 1 – GENERAL CONSIDERATIONS

Chapter 1 presented the general structure of this thesis, briefly describing each of the subsequent chapters. In general, this work aims to explore the complexities of climate change, addressing not only its impacts and challenges but also the resilience and mitigation strategies that can be implemented to confront and adapt to these changes. This thesis discusses two major themes related to climate change: heatwaves in Europe and their impact on heterotrophic respiration in temperate ecosystems (1^{rt} article); and controlling variables, resilience, and climate mitigation in four major Brazilian biomes - Cerrado, Caatinga, Atlantic Forest, and Pampa (2^{nd} article).

Chapter 2 is dedicated to the contextualization and literature review of the concepts involved in climate change, its impacts on natural and human ecosystems on Earth, as well as mechanisms for climate mitigation and resilience. In this context, it addresses how human activities - particularly land-use change, deforestation, and agriculture - have contributed to the increase in greenhouse gases in the atmosphere, intensifying the global warming phenomenon. Additionally, resilience and adaptation mechanisms are highlighted as essential to enhance the capacity to absorb shocks and stresses caused by climate change, alongside methods aimed at preventing the intensification of emissions.

Chapter 3 presents the first article proposed in this thesis, entitled: "Heatwaves and the Feedback Cycle with Climate Change: Influence of Heatwaves on CO_2 Emissions in Northern European Forest Ecosystems". Climate feedback is a process in which an initial change in the climate system generates effects that can amplify (positive feedback) or attenuate (negative feedback) that initial change. In the context of the carbon cycle, for example, rising temperatures can intensify soil respiration, releasing more CO_2 into the atmosphere, which in turn contributes to further warming, characterizing positive feedback. Thus, this article analyzes the impact of the 2021 European heatwaves on atmospheric CO_2 concentrations. The results show that these events intensified soil respiration due to the metabolic acceleration of soil microbiota, increasing CO_2 emissions. The hypothesis that thermal stress would reduce plant photosynthesis was rejected, as greater photosynthetic activity was observed during the heatwaves. The analyses compared atmospheric CO_2 concentrations (xCO_2) before and during the heatwaves, using a time series from January 2015 to December 2021, with heatwave-free periods (2015 and 2017) selected as the baseline.

Chapter 4 investigates the main factors influencing CO_2 emissions and soil organic carbon (SOC) stocks, as well as risk zones for SOC under future climate scenarios in the Brazilian biomes of the Atlantic Forest, Cerrado, Caatinga, and Pampa. The analysis used atmospheric CO_2 data from 2015 to 2019 and SOC stocks, applying methods such as Kriging and Stepwise regression. The results highlighted temperature as the most influential variable in atmospheric CO_2 changes across all biomes, revealing its role in both emissions and SOC stabilization. Additionally, an increase of 1.5 °C above pre-industrial temperatures, as projected by the Intergovernmental Panel on Climate Change (IPCC), may lead to significant soil CO_2 release into the atmosphere, impacting national resilience and mitigation efforts. In the studied biomes, a significant portion of the territory is already exposed to high temperatures, emphasizing the urgency of protecting the carbon already sequestered.

Chapter 5 seeks to consolidate the observations developed in the two previous articles, emphasizing the need for actions and public policies to address future climate challenges. This chapter highlights sustainable agricultural practices that promote soil health, such as livestock–forest integration systems, which are strong allies in combating climate change, among other relevant strategies and approaches within this context.

CHAPTER 2 – CLIMATE CHANGE AND GREENHOUSE GAS EMISSIONS: PERSPECTIVES FOR CLIMATE RESILIENCE AND MITIGATION

1. Literature review

1.1. Climate change, impacts on society and control mechanisms

Climate change refers to significant and long-term shifts in global or regional climate patterns (IPCC, 2021). These changes alter global climate averages over time and may redefine climate conditions on smaller, continental, or regional scales (IPCC, 2022a). Widely recognized by the scientific community, climate change is considered one of the most pressing environmental, economic, and social challenges faced by humanity today (IPCC, 2022b).

Although climate shifts can result from natural or anthropogenic factors, human-driven causes are the most concerning, particularly because they are, in theory, under societal control (MASSON-DELMOTTE et al., 2021). The most impactful human activity is the emission of greenhouse gases (GHGs) from the use of non-renewable energy sources, especially fossil fuel combustion (Smith et al., 2008).

Burning coal, oil, and natural gas, along with deforestation and biomass burning for agriculture, releases large amounts of carbon dioxide (CO_2), methane (CH_4), and nitrous oxide (N_2O) into the atmosphere (IPCC, 2017). These gases trap heat, contributing to rising global temperatures (IPCC 2017, 2022a, b).

Before the Industrial Revolution, atmospheric CO_2 concentrations remained relatively stable at around 280 parts per million (ppm) (KEELING et al., 1976; HOWE, 2015). However, industrialization and shifts in agricultural production, particularly during the Green Revolution, led to a sharp increase in these levels (SMITH et al., 2008; RUANE et al., 2018), with current CO_2 concentrations exceeding 415 ppm, levels unseen in millions of years (KEELING et al., 1976; HOWE, 2015).

Future projections under continued emissions scenarios suggest CO_2 levels may reach alarming values by the end of the 21st century (IPCC, 2022b), potentially driving global temperature increases of 1.5 °C or more. Such changes are expected to intensify extreme weather events and pose severe risks to ecosystems, economies, and communities worldwide (SENAPATI et al., 2013; RUANE et al., 2018; ARORA, 2019).

1.2. Nature-based solutions (NBS) and the agriculture paradigm

Over the past decade, atmospheric concentrations of greenhouse gases (GHGs) have reached record levels, with CO_2, CH_4, and N_2O exceeding pre-industrial levels by 144%, 256%, and 121%, respectively (IPCC, 2021). Agriculture significantly contributes to global carbon emissions, accounting for approximately 11% of CO_2, 47% of CH_4, and 58% of N_2O emissions (IPCC, 2021). Additionally, land-use change, and deforestation contribute around 20% of total global emissions.

Unlike sectors such as Waste, Industry, or Energy, Agriculture and Land-Use Change can also be part of Nature-Based Solutions (NBS) - strategies that integrate restoration, protection, and climate resilience actions (BLANCO-CANQUI and LAL, 2004; REICHSTEIN et al., 2013; AZEVEDO et al., 2018; O'HOGAIN and MCCARTON, 2018). According to Seddon et al., (2021), NBS must (1) complement, not replace, the phase-out of fossil fuels; (2) include diverse ecosystems; (3) involve Indigenous Peoples and local communities in their design and implementation; and (4) ensure measurable biodiversity benefits.

NBS aim to reduce GHG emissions and enhance carbon removal and storage by leveraging natural processes. One of the most promising NBS is soil, which can store large amounts of atmospheric CO_2 as soil organic carbon (SOC). BOSSIO et al., (2020) estimate that soil carbon accounts for 25% of the total NBS mitigation potential - around 23.8 Gt CO_2-equivalent per year - 40% from protecting existing soil carbon and 60% from restoring depleted stocks.

In terms of mitigation potential, soil carbon represents 9% in forests, 72% in wetlands, and 47% in agriculture and pasture systems. Therefore, protecting existing SOC and restoring degraded soils is essential for sustainable carbon sequestration and combating land degradation and desertification (BOSSIO et al., 2020; CONCEIÇÃO et al., 2017).

In addition to sustainable land management practices, broader climate mitigation strategies have been developed to support global efforts to reduce greenhouse gas emissions. International agreements such as the Paris Agreement establish frameworks for national commitments to limit global warming and promote carbon neutrality (BRAZIL, 2022). Mechanisms such as carbon markets and the growing corporate participation in initiatives such as the Science Based Targets Initiative (SBTi) demonstrate the private sector's commitment to aligning corporate climate goals with the latest climate science (ZILBER; KOGA, 2011).

In conclusion, agriculture is a key strategy for atmospheric CO_2 sequestration. SOC naturally stores CO_2 and CH_4 and can act as a carbon sink when properly managed (BOSSIO et al., 2020). Protecting and restoring soil organic matter enhances agricultural productivity, resilience, and adaptation, while also providing broad ecological benefits (BOSSIO et al., 2020; CONCEIÇÃO et al., 2017).

1.3. Definition and mechanisms of climate resilience

Historically, most greenhouse gas (GHG) emissions driving climate change have originated from developed countries due to industrialization based on non-renewable energy sources (KEELING et al., 1976; HOWE 2015; KENEA et al., 2021). However, addressing climate change requires global cooperation, as its effects transcend political boundaries (IPCC, 2022b).

To meet the 1.5°C target by the end of the century, an additional reduction of 28 gigatons of CO_2-equivalent emissions per year is needed by 2030, demanding deep transformations in global production systems (JEWELL and CHERP, 2020). Regardless of mitigation success, it is essential to monitor, predict, and manage climate change impacts to minimize environmental and societal harm (ARORA, 2019).

Climate change has increased the frequency and intensity of extreme weather events, including heatwaves, heavy rainfall, and prolonged droughts (IPCC, 2022b, GERDOL et al., 2008). Regional shifts in precipitation patterns are also occurring, especially near the equator (SENAPATI et al., 2013). These trends underscore the importance of adaptation and climate resilience.

Climate resilience refers to the ability of systems - whether communities, ecosystems, economies, or infrastructure - to anticipate, adapt to, and recover from climate-related disturbances. It involves both preventive actions to reduce vulnerability and reactive strategies for rapid recovery, ensuring long-term sustainability (C2ES, 2019; SEDDON et al., 2021).

Agriculture is particularly vulnerable, with temperature and rainfall changes affecting crop yields, pests, and disease dynamics (SENAPATI et al., 2013; ARORA, 2019). Continuous monitoring using satellites, weather stations, and sensors is critical to detect shifts in climate and track extreme events in real time (IPCC, 2022c).

Advanced climate models are vital for forecasting natural disasters and informing early warning systems, which can save lives, reduce economic losses, and guide public policy (IPCC, 2022c). Governments play a key role in implementing climate-resilient policies, long-term adaptation plans, and investments in sustainable infrastructure (JEWELL and CHERP, 2020; IPCC, 2023).

At regional and local levels, communities and governments must tailor these strategies to local needs by identifying vulnerable areas, developing emergency plans, and reinforcing infrastructure - such as drainage systems and levees - to withstand extreme events (JEWELL and CHERP, 2020).

1.4. Definition and mitigation mechanisms for greenhouse gas emissions

To stabilize or reverse climate projections for the end of the 21st century, especially the 1.5 °C target, significant public and private investment is needed to develop and implement technologies that remove carbon dioxide from the atmosphere or reduce emissions from various sectors (IPCC, 2022a). However, carbon removal technologies have not yet reached the scale or cost-effectiveness required for meaningful climate impact (O’HOGAIN and MCCARTON, 2018; JEWELL and CHERP, 2020). This underscores the importance of Nature-Based Solutions (NBS) and the mitigation of emissions from already established processes (SEDDON et al., 2021).

Key sectors in developing countries, such as agriculture, energy, and mining are among the largest GHG emitters while being central to economic growth (JEWELL and CHERP, 2020). Thus, these countries face the challenge of decarbonizing rapidly growing economies without compromising development. Studies indicate that current consumption patterns exceed Earth's natural capacity - if everyone lived like the average American, five planets would be needed to sustain global demand (LIN et al., 2021).

Climate mitigation, therefore, is essential - not only to adapt to but also to prevent further climate deterioration (IPCC, 2022b). Mitigation refers to strategies that reduce or limit GHG emissions, including voluntary carbon markets and regulated emissions targets established under Article 6 of the Paris Agreement.

To date, GHG reduction remains the most effective mitigation strategy. Public, private, and non-governmental institutions are actively implementing mitigation measures in support of countries' Nationally Determined Contributions (NDCs). Environmental policies promoting sustainable agriculture, forest restoration, and regulated carbon markets are critical, especially in countries like Brazil, Colombia, and Costa Rica (ZILBER and KOGA, 2011; CAIADO et al., 2017).

However, developing nations often face financial, technological, and institutional barriers to implementing these policies effectively (CONCEIÇÃO et al., 2017; COSTA et al., 2018). Brazil's NDC under the Paris Agreement commits to reducing total GHG emissions by 37% by 2025 and 43% by 2030 (based on 2005 levels), and aims for net-zero emissions by 2060, potentially anticipating this goal based on global carbon market mechanisms (GIANETTI and FERREIRA FILHO, 2021).

Sustainable land management and conservation practices not only reduce emissions but also strengthen ecosystem and community resilience to climate impacts (BOSSIO et al., 2020; CAMPOS et al., 2022). This study therefore aimed to support the effective design of public policies by identifying vulnerable areas and directing resources towards carbon-rich ecosystems (Chapter 4).

Furthermore, in the global effort toward decarbonization and ecosystem protection, this study highlighted positive feedback loops between European heatwaves and increased CO_2 emissions from temperate ecosystems (Chapter 3). These findings emphasize how climate instability can accelerate soil organic carbon losses, intensifying atmospheric CO_2 levels and reinforcing global warming.

Thus, as a hypothesis, this work understands that the increase in temperature, intensified by extreme events such as heat waves, accelerates biogeochemical processes that increase soil CO_2 emissions and reduce organic carbon stocks, compromising ecosystem resilience and hindering climate mitigation efforts, especially in tropical and subtropical biomes.

Therefore, this research aimed to investigate the effects of climate change on CO_2 emissions and soil organic carbon stocks, considering extreme events (heat waves) in temperate ecosystems and the variables controlling climate resilience in Brazilian biomes, with a view to proposing mitigation and adaptation strategies.

CHAPTER 3 - THE INFLUENCE OF HEAT WAVES ON CO_2 CONCENTRATIONS IN THE NORTHERN EUROPEAN FOREST ECOSYSTEM: THE POSITIVE FEEDBACK CYCLE WITH CLIMATE CHANGE

Abstract: Heat waves in Europe have become common in recent years, in terms of frequency, magnitude and intensity. The objectives of this work are: i) to compare the concentration of CO2 in the atmospheric column (xCO_2), before and during the heat wave in European forest ecosystems, and ii) to understand the vegetative and soil variables that were most impacted by the heat stress period. This study used years 2015 and 2017 as the baseline (non-heatwave period) and the year 2021 as the heatwave period. The most significant result was the statistical confirmation that higher atmospheric CO2 concentrations were observed during the heat wave than in normal times. During the heatwave period, the xCO_2 increased by 1.59 ppm compared to the baseline. Daily variation peaked at +4.3 ppm (July 10) and dipped to –5.0 ppm (July 5), with positive anomalies prevailing between late June and mid-July, the beginning of thermal stress. In contrast, the baseline showed more frequent negative values during the period, indicating greater atmospheric CO_2 removal., Linear regression analyses revealed that xCO_2 responses varied by period. HR exhibited the strongest relationship during the heatwave (R^2 = 0.32), suggesting that increased HR was associated with higher xCO_2 levels. These results reinforce evidence that heat waves intensify the carbon cycle imbalance in terrestrial ecosystems, acting as triggers for positive climate feedbacks. The 1.59 ppm increase in xCO_2 during the heat wave, combined with the predominance of positive values during the period, suggests that such extreme events compromise the capacity of ecosystems to act as carbon sinks, temporarily transforming them into sources of CO_2 to the atmosphere.

Keywords: Heatwave; xCO_2; Carbon NEE; Heterotrophic Respiration; LST Amplitude; Soil Respiration

1. Introduction

The burning of fossil fuels, deforestation, and other industrial practices contribute to the accumulation of greenhouse gases (GHGs) in the atmosphere, particularly carbon dioxide (CO_2), methane (CH4), and nitrous oxide (N2O) (IPCC, 2017, 2021, 2022). These gases trap heat in the atmosphere, causing global warming (IPCC, 2017). According to the Intergovernmental Panel on Climate Change (IPCC), the levels of CO_2, CH4, and N2O have increased by 144%, 256%, and 121% above pre-industrial levels, respectively (IPCC, 2021).

The effects of climate change include more frequent and intense extreme weather events, such as rising sea levels and changes in precipitation patterns (IPCC, 2017). Heat waves may also become more identifiable and frequent in this context of climate instability (AUDET et al., 2017; LHOTKA; KYSELÝ, 2022; RUSSO; SILLMANN; FISCHER, 2015).

In Europe, severe heat waves have been observed 12 times just this century (IBEBUCHI; ABU, 2023; LHOTKA; KYSELÝ, 2022; RUSSO; SILLMANN; FISCHER, 2015). A heat wave is characterized by a prolonged period of exceptionally high temperatures compared to the climatological averages for the region and time of year (LHOTKA; KYSELÝ, 2022). Some authors have highlighted a Positive Climate Feedback effect between climate change and heat waves (KERR; OCHSNER, 2020; YAN et al., 2022).

The stress caused by intense heat waves affects the cycle and emission of GHGs in forests, wetlands, agriculture, and other ecosystems, directly resulting in higher emissions of these gases (GERDOL; BRAGAZZA; BRANCALEONI, 2008; HUMBORG et al., 2019; LHOTKA; KYSELÝ, 2022). Given their proportions, these emissions can increase GHG concentrations in the atmosphere, worsening the current scenario (KERR; OCHSNER, 2020; NEVE; PANNIER; HOFMAN, 1996; WANG et al., 2016).

High temperatures have a considerable impact on the respiration of temperate climate ecosystems, affecting the biogeochemical processes that control the release of CO_2 from the soil to the atmosphere (LIAN et al., 2023; REICHSTEIN et al., 2005, 2013; TANG et al., 2020). In this sense, the soil also plays a crucial role in storing and stabilizing the CO_2 removed from the atmosphere by plant photosynthesis (BALL et al., 1997; CAMPOS; CERRI; SCALA JR, 2022; FIGUEIREDO et al., 2017; MARIA et al., 2023).

The increase in soil respiration caused by intense and prolonged heat accelerates microbial activity in the soil (NEVE; PANNIER; HOFMAN, 1996). The metabolism of microorganisms through the decomposition of organic matter, bacteria, and fungi can transform organic carbon stored in the soil over decades or centuries into a flux of CO_2 to the atmosphere (FIGUEIREDO et al., 2017; NEVE; PANNIER; HOFMAN, 1996).

It is worth noting that this process intensifies as the ecosystem warms, thus increasing soil respiration rates (BLANCO-CANQUI; LAL, 2004; SIERRA, 2001). The stability rate of protected organic carbon in the soil is also impacted (NEVE; PANNIER; HOFMAN, 1996). The exposure of carbon due to different forms of stress results in changes in the quantity and quality of organic residues, making them more available to soil microbiology and consequently accelerating the mineralization of organic matter (GMACH et al., 2020; NEVE; PANNIER; HOFMAN, 1996; WANG; CAJA; GÓMEZ, 2018).

In this context, remote sensing played a key role in this study by providing consistent and spatially integrated data on environmental variables that influence atmospheric CO_2. Satellite-derived indicators allowed the detection of ecosystem responses to heatwaves, supporting the identification of carbon-climate feedbacks that would be difficult to capture with field measurements alone (BÖHNISCH; FELSCHE; LUDWIG, 2023; HAKKARAINEN; IALONGO; TAMMINEN, 2016; KRASNOVA et al., 2022).

Building on this ability of remote sensing to reveal large-scale ecosystem responses, the present study used satellite data to investigate how extreme weather events, particularly heatwaves, affect the carbon cycle. This approach allowed the formulation of a guiding research question focused on quantifying the atmospheric impact of these events over time and space, especially in high-latitude forest ecosystems that play a critical role in global carbon regulation.

This way, recognizing that climate change can lead to more severe heat waves and vice versa, this study sought to quantify the impact of the most severe heat wave of the last 10 years on the Subarctic climate forest of Sweden and Finland (LHOTKA; KYSELÝ, 2022). Thus, the motivating question of this work was: Is it possible to detect, through remote sensing tools, changes in atmospheric CO_2 concentration (xCO_2 ppm) during a severe heat wave in Europe compared to normal times (Baseline)?

As a hypothesis, this work posited that: i) more intense heat waves result in reduced plant photosynthesis, impacting atmospheric CO_2 accumulation; and ii) such events also intensify soil and vegetation respiration, again impacting atmospheric CO_2 accumulation. Therefore, two objectives were established for this study: i) to compare the CO_2 concentration in the atmospheric column (xCO_2) before and during the heat wave in European ecosystems, based on years outside heat waves; and ii) to understand and characterize the control variables for this ecosystem, responsible for removing and supplying CO_2 concentrations to the atmosphere.

2. Materials and Methods

2.1. Study Areas

To determine the study area, the European land use and land cover map was utilized (https://www.copernicus.eu/en), focusing especially on latitudes between 60° and 70°, aiming to isolate homogeneous areas in this region. The selection also aimed to identify regions that had experienced both high incidences of heat waves and periods completely without any interference from these climatic events (LHOTKA; KYSELÝ, 2022). Thus, the forest vegetation of Sweden and Finland was isolated as the study area, as represented in Figure 1.

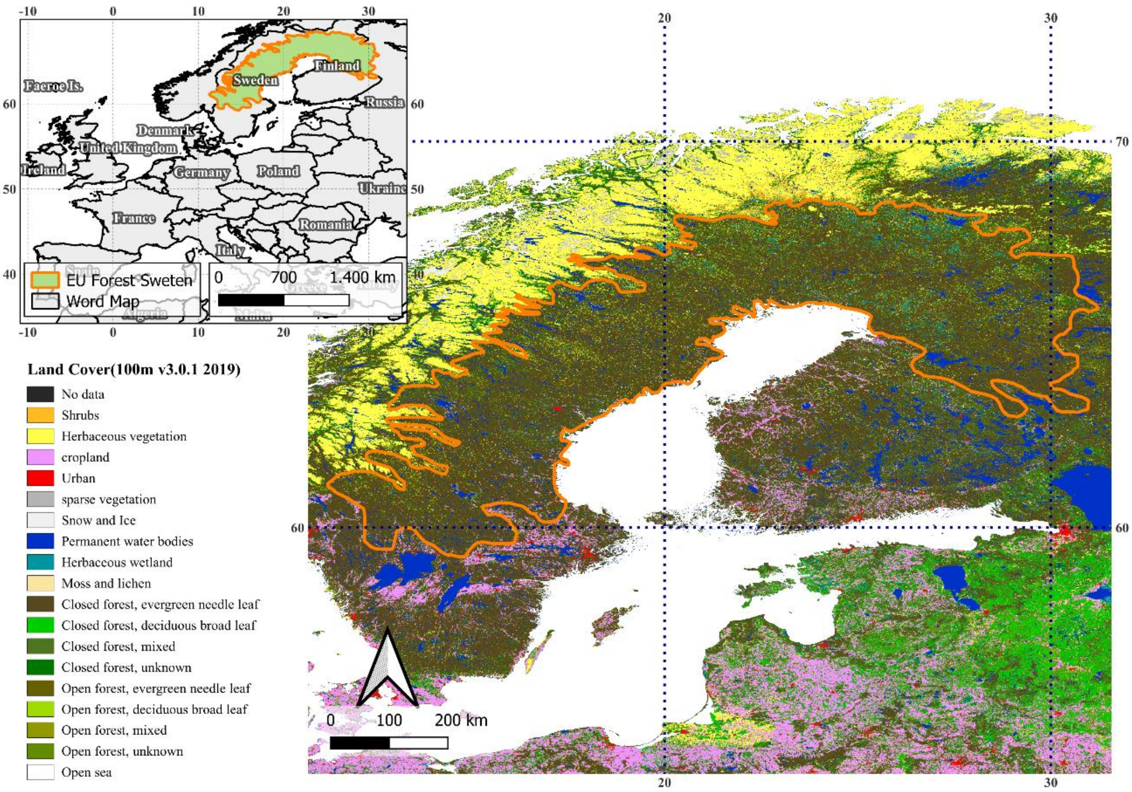

Figure 1: Study area at the European and local level, with land use classified according to Copernicus Global Land Operations "Vegetation and Energy".

The forest vegetation of Sweden and Finland, with around 489.478 km² (49 million hectares), is predominantly characterized by boreal forests. According to the Köppen classification, the region is identified as having a Subarctic climate (Cfc) (CUI; LIANG; WANG, 2021). This climate is characterized by long, cold winters and short, relatively mild summers (CUI; LIANG; WANG, 2021). In general, the predominant climate classification in Sweden and Finland is the cold temperate climate (CUI; LIANG; WANG, 2021).

Regarding the soil in the region, there are predominantly five classes: Podzols, Histosols, Gleysols, Cambisols, and organic soils (HENGL et al., 2017; SOILGRIDS250M2.0, 2022). All the identified soil classes generally contain a high proportion of organic matter in storage and decomposition processes, typically found in wet or waterlogged areas (HENGL et al., 2014; POGGIO et al., 2017).

2.2. Characterizing Heat Waves and Baseline

To enable the comparisons proposed by this study, it was necessary to also separate regions free from periods of heat wave events. Thus, the study sought to compare periods of normal climatic conditions with periods identified with heat waves according to Lhotka and Kyselý (2022). By isolating a region affected by an intense and prolonged heat wave, it became possible to observe the adverse effects of these events on vegetation, which is the objective of this study.

Additionally, it is worth noting that the temporal scope adopted by the study, between 2015 and 2021, was chosen due to the availability of xCO_2 data from NASA's OCO-2, which began being recorded at the end of 2014. Moreover, the year 2021 was selected as the last year of the series as it coincides with the last year characterized by Lhotka and Kyselý (2022).

As illustrated in Figure 2 and described by Lhotka and Kyselý (2022), the years 2015 and 2017 were used as the baseline because the study area did not experience heat waves during these years. On the other hand, the year 2021 was chosen to determine the heat wave period, as it recorded a severe and continuous 60-day heat wave affecting the studied ecosystem (LHOTKA; KYSELÝ, 2022).

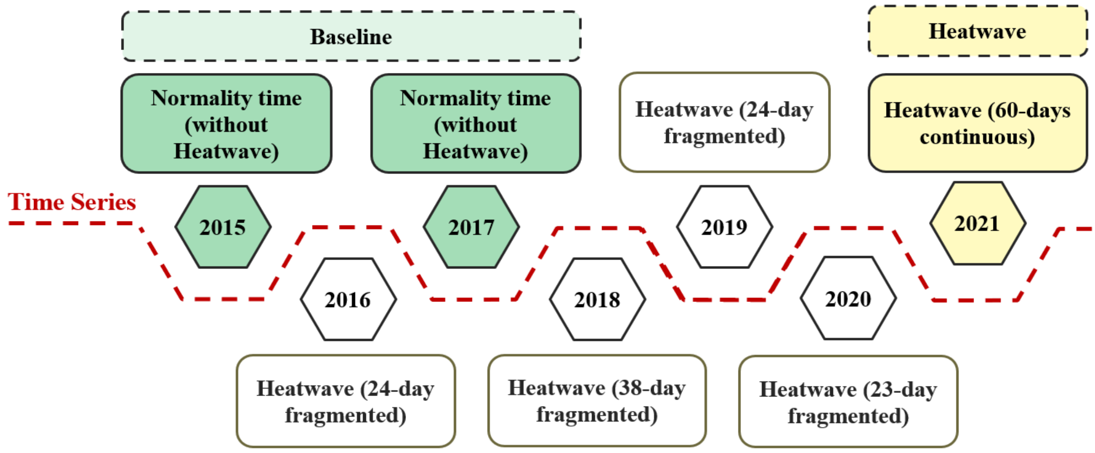

Figure 2: Overview and flow of ideas for determining the Baseline and Heatwave periods, based on Lhotka and Kyselý (2022).

As a criterion for establishing the baseline (times of normality), it was necessary to identify and isolate years in which the region studied here was not impacted by heat waves (LHOTKA; KYSELÝ, 2022). Similarly, to determine the heat wave period, an interval was sought in which the area continuously experienced high-intensity heat).

2.2.1. Definition of Heat Wave for this Study: Heatwave

This work did not seek to determine the period of the heat wave. This study used a heat wave determined according to standards adopted and described by Lhotka and Kyselý (2022), who identified 60 days of heat wave over Europe in the summer of 2021, with persistent hot and dry air masses capable of causing extremely high temperatures over the study region (LHOTKA; KYSELÝ, 2022; RUSSO; SILLMANN; FISCHER, 2015). Therefore, knowing the critical period of this event, this study analyzed the complete historical series characterized as a heat wave that occurred from June 18 to August 19, 2021 (LHOTKA; KYSELÝ, 2022).

Additionally, it is worth noting that after defining 2021 as the heat wave period to be analyzed in this study, it was decided to adopt the 60 days of heat wave that occurred that year as the reference interval to determine the periods completely without heat waves for the study region, understood in this work as the baseline (LHOTKA; KYSELÝ, 2022).

2.2.2. Definition of Baseline for this Study: Baseline

The baseline in this study was established as periods completely without heat wave events, that is, periods of climatic normality. To determine this period, the standard adopted was from June 18 to August 19, 2021, exactly the same days of the year when the heat waves occurred in the study area. Similarly, using the characterization developed by Lhotka and Kyselý (2022), this study determined June 18 to August 19, 2015, and June 18 to August 19, 2017, as the baseline scenarios completely without heat waves, to develop the comparisons proposed by the work.

2.3. Data Collection, Resolution, and Other Attributes

This study sought to collect data capable of explaining the behavior of atmospheric CO_2 and control variables inside and outside heat waves in Europe; thus, the data were classified into four large groups of variables: carbon variables, vegetation, soil, and climate. Table 1 organizes the groups of variables, respective units of measurement, data collection sources and tools, as well as the spatial and temporal resolutions of each studied variable.

Table 1: Studied variables classified into four groups: Carbon, Vegetative, Soil, and Climatic.

Variable	Unit	Sources	Tools	Spatial Resolution (km)	Temporal Resolution (Days)
Carbon					
xCO_2	ppm	NASA	OCO-2	3 x 3	16
Carbon NEE [1]	$gCm^{-2}day^{-1}$	AppEEARS	SPL4CMDL-006	9 x 9	1
HR[2]	$gCm^{-2}day^{-1}$	AppEEARS	SPL4CMDL-006	9 x 9	1
Vegetative					
LAI[3]	$m^2 m^{-2}$	AppEEARS	MCD15A3H-061	0.5 x 0.5	8
Fpar[4]	%	AppEEARS	MCD15A2H-061	0.5 x 0.5	4
Borned Area	Days	AppEEARS	MCD64A1.061	0.5 x 0.5	30
Solo					
SSM[5] at 5 cm depth	$m^3 m^{-3}$	AppEEARS	SPL4SMGP-006	9.0 x 9.0	1
LST[6] Amplitude	°C	AppEEARS	MOD11A1-061	1.0 x 1.0	8
LST[6] Day	°C	AppEEARS	MOD11A1-061	1.0 x 1.0	8
LST[6] Night	°C	AppEEARS	MOD11A1-061	1.0 x 1.0	8
Climáticas					
RH[7]	%	NASA Power	TERRA-2	22,4 x 55,7	1
Precipitation	mm day^{-1}	NASA Power	TERRA-2	22,4 x 55,7	1

Temp.[8] a 2 m	°C	NASA Power	TERRA-2	22,4 x 55,7	1
Max. Temp.[8] at 2 m	°C	NASA Power	TERRA-2	22,4 x 55,7	1
Min. Temp. [8] at 2 m	°C	NASA Power	TERRA-2	22,4 x 55,7	1
Range Temp[8] a 2 m	°C	NASA Power	TERRA-2	22,4 x 55,7	1
Wind at 10 m	m s^{-1}	NASA Power	TERRA-2	22,4 x 55,7	1

1 - Carbon Net Ecosystem Exchange; 2 - Heterotrophic Respiration; 3 - Leaf Area Index; 4 - Fraction Photosynthetically Active Radiation; 5 - Surface Soil Moisture; 6 - Land Surface Temperature; 7 - Relative Humidity; and 8 - Temperature.

Such an organization of variables aimed to facilitate the understanding between variables that seek to directly understand atmospheric CO_2, carbon group variables, and control variables from the vegetation, soil, and climate groups. Vegetative variables are essential because, during photosynthesis, atmospheric CO_2 is captured by plant leaves and used in the synthesis of sugars, which is important for understanding the control variables of atmospheric CO_2.

In order to characterize the chemical and physical attributes of the study area, five random sampling points were selected, representing the two most prevalent soil groups in the region. All details were shown in table 2. The data presented in the table were obtained from the SoilGrids platform, which provides detailed global information on soil properties.

Table 2: Physicochemical Characteristics of the Predominant Soils in the Study Area (30 cm).

Longitude	**Latitude**	**Depth**	**Soil Groups**	**SOC** t/ha	**Clay** g/kg	**Sand** g/kg	**Silt** g/kg	**CEC (at pH 7)** mmol(c)/kg	**pH Water**
25.2182	63.8866			82	121	568	311	181	5.2
24.4464	68.2635			56	108	564	328	216	5
22.7759	68.6754	30 cm	Cambisols	75	71	615	314	213	5.1
14.001	62.2137			58	68	549	383	158	5.1
19.2146	67.0967			77	72	545	383	201	4.9
20.224	64.3431			63	72	577	351	200	4.8
25.0522	65.9035			81	125	542	333	210	4.9
27.310	64.5267	30 cm	Podzols	99	66	686	248	211	5
20.2977	64.6919			65	73	590	337	190	4.8
27.5855	64.6185			62	60	637	303	163	4.8

CEC: Cation exchange capacity
SOC: Soil organic carbon stock

Each point corresponds to the 30 cm depth layer, allowing for a precise comparison of edaphic characteristics. This approach provides a consistent basis for contextualizing the interrelationships between climate, plant, and soil - key aspects for understanding the impacts of heat waves in the region.

2.4. Data Collection and Geospatial Standardization of Data Collection

2.4.1. xCO_2, Average Concentrations of CO_2 in the Atmospheric Column

The variable xCO_2 represents the concentration of carbon dioxide (CO_2) in the atmospheric column, expressed in parts per million (ppm). This data was obtained from NASA's OCO-2 (Orbiting Carbon Observatory-2) mission (O'DELL et al., 2012). The xCO_2 is determined by the satellite using infrared imaging spectrometer sensors capable of detecting infrared radiation emitted by the Sun and reflected by the Earth (Crisp et al., 2012; O'Dell et al., 2012; Saunois et al., 2016). The temporal resolution, or satellite revisit time, provided by OCO-2 is 16 days, and the spatial resolution is approximately 3 x 3 km (O'DELL et al., 2012; SOMKUTI et al., 2021).

It is important to highlight that the xCO_2 variable was determined as a key parameter for collecting control variables data, being responsible for defining the geographic center for collecting other variables. The centroid is the central point of data collection made by the sensor on board the satellite. Therefore, the xCO_2 collection point, i.e. its latitude and longitude, was adopted as the default collection point for all other variables (MARGHANY; HASHIM, 2009).

This approach was necessary to increase the reliability of the data collection process, ensuring that the variables collected subsequently were directly at the same collection location determined by OCO-2 (CAMPOS; CERRI; SCALA JR, 2022). Furthermore, it is important to highlight that the xCO_2 data were corrected from the linear global accumulation trend, allowing a consistent comparison of the 2015 and 2017 concentrations with those recorded in 2021.

Furthermore, to ensure that comparisons between years reflected local ecosystem dynamics rather than the global trend of increasing atmospheric CO_2 concentrations, linear regression was applied to remove the global accumulation signal from the xCO_2 dataset. This allowed for the correction to isolate interannual variability specifically associated with heatwave conditions, enabling a more accurate comparison between the reference years (2015 and 2017) and the heatwave year (2021). The same approach was used in articles such as CAMPOS et al. (2022); da COSTA et al. (2021); MORAIS FILHO et al. (2021); and SOUZA et al. (2025).

2.4.2. Net Ecosystem Exchange of Carbon (Carbon NEE)

The Carbon Net Ecosystem Exchange (NEE) refers to the net exchange of carbon between an ecosystem and the atmosphere (Lian et al., 2023), quantifying the difference between the amount of CO_2 absorbed by the ecosystem through gross primary production (GPP), and the amount released through plant (autotrophic) and non-plant (heterotrophic) respiration, as highlighted in Figure 3A (CHAPIN et al., 2006; HINKO-NAJERA et al., 2017).

The Carbon NEE (Level-4 L4, SPL4CMDL) provides daily global grid estimates of the net CO_2 exchange through a terrestrial carbon flux model based on satellite data (ZHANG et al., 2023). Generally, Carbon NEE is calculated from four main steps: direct measurement of atmospheric CO_2; modeling and simulation; incorporation of meteorological and soil data; and analysis of net carbon exchange (CHAPIN et al., 2006).

Figure 3A was created to schematize the Carbon NEE variable and the factors capable of influencing CO_2 exchange, focusing especially on vertical carbon fluxes. Equation 1 represents the gas exchanges shown in Figure 3. Equation 1 was adapted from Chapin et al., (2006), and Hinko-Najera et al., (2017), considering CO_2 exchanges between the ecosystem and atmosphere, for the interaction between vegetation, soil, and the atmosphere.

$$NEE = GPP - HR - AR \qquad \text{eq.1}$$

Where: NEE is the net ecosystem exchange of carbon; GPP is the Gross Primary Production; HR represents heterotrophic respiration; and AR represents ecosystem autotrophic respiration.

In relation to the CO_2 removals highlighted in Equation 1, GPP (Gross Primary Productivity) refers to the total amount of carbon fixed by plant photosynthesis (ZHANG et al., 2018). Regarding emissions, HR (heterotrophic respiration) refers to the amount of carbon released by the soil due to microbial respiration and the decomposition of organic matter (CHAPIN et al., 2006). For emissions, AR (autotrophic respiration) refers to the respiration of the plants themselves (CHAPIN et al., 2006). The balance between emissions and removals produces Carbon NEE, representing the net carbon exchange between the ecosystem and the atmosphere (GERDOL; BRAGAZZA; BRANCALEONI, 2008).

2.4.3. Heterotrophic Respiration (HR)

The Heterotrophic Respiration (HR) variable represents the amount of CO_2 released by the metabolic processes of heterotrophic organisms, such as microorganisms, fungi, and animals, during their metabolic respiration, particularly in the decomposition of organic matter in the soil (YAN et al., 2022). To calculate this variable, NASA uses computational models, through observational data, temperature, air humidity, soil type, and other factors, to predict heterotrophic respiration on a global scale (KONINGS et al., 2019).

2.4.4. Vegetative Variables

LAI (Leaf Area Index) and FPAR (Fraction of Photosynthetically Active Radiation) are available on NASA's AρρEEARS platform (AρρEEARS, 2022), and are determined from remote sensing data collected by satellites such as MODIS (Moderate Resolution Imaging Spectroradiometer) aboard the Terra and Aqua satellites.

LAI is calculated using a combination of algorithms and models that use the spectral characteristics of vegetation observed in satellite images (REEVES et al., 2003). LAI represents the total leaf surface area per unit of land area, expressed in m^2/m^2 (CLEUGH et al., 2007; MYNENI et al., 2022). The calculations consider the light reflected by the leaves, and after being validated and calibrated with field data, the results are made available (MAJASALMI et al., 2015; REEVES et al., 2003).

FPAR, in turn, is a measure of the amount of photosynthetically active solar radiation absorbed by vegetation in a given area and period (MYNENI et al., 2019). This variable is calculated from reflectances measured in different bands of the red (RED) and near-infrared (NIR) bands (SELLERS et al., 1997; YANG et al., 2006; ZHU et al., 2010). The result is a measure of the fraction of photosynthetically active radiation absorbed by vegetation in a given area (SELLERS et al., 1997).

2.4.5. Soil Variables

The Soil Moisture (SPL4SMGP-006) variable is a product of NASA's Soil Moisture Active Passive (SMAP) mission. Soil moisture represents the amount of water present in the soil, expressed in m^3/m^3 (MARIA et al., 2023). The SPL4SMGP-006 product uses data collected by the SMAP L-band radiometer instrument, which measures microwave radiation emitted by the Earth's surface (MARIA et al., 2023).

The Land Surface Temperature (LST) variable, for day, night, and amplitude, is expressed in °C and calculated from Thermal Infrared Spectral (TIR) measurements (MUTIIBWA; STRACHAN; ALBRIGHT, 2015) taken by MODIS-EARTH (APPEEARS, 2022). The Land Surface Temperature and Emissivity (LSTandE) (APPEEARS, 2022) is obtained in 1 km pixels by the split-window algorithm, and the MOD11A2 product provides land surface temperature and emissivity (https://lpdaac.usgs.gov/products/mod11a2v006/).

The LST Amplitude is the difference between LST for Day and Night, as presented in Equation 2. This equation was developed to describe how the variable was determined and calculated by Campos et al., (2022).

$$\text{LST Amplitude} = \text{LST Day} - \text{LST Night} \qquad \text{eq.2}$$

Where: LST Day is the Land Surface Temperature during the day; and LST Night is the Land Surface Temperature during the night.

In the algorithm, surface emissivity is estimated based on land cover types, air temperature, and water vapor column (WAN, Z., S. HOOK, 2015). For both daytime and nighttime LST, emissivity is retrieved from observations in seven TIR (Thermal Infrared) bands (FREITAS et al., 2013; WAN, Z., S. HOOK, 2015). LST represents the balance between vegetation and bare soil temperatures, also influenced by soil moisture, vegetation cover, and albedo (FREITAS et al., 2013; MUTIIBWA; STRACHAN; ALBRIGHT, 2015; WAN, Z., S. HOOK, 2015).

2.4.6. Climatic Characteristics

The variables determined as Relative Humidity (RH), Precipitation, and Temperature at 2 meters (maximum, minimum, and range) available on the NASA POWER platform are determined through a combination of observational atmospheric data (CHOUDHURY, 1987; HUMPHREY et al., 1996; TODD et al., 2001).

For Relative Humidity and Precipitation, meteorological satellites provide images used to monitor atmospheric moisture and cloud patterns, estimating these variables in different regions of the world. These data are compared and corrected based on data from Ground Meteorological Stations, providing direct measurements of relative humidity and precipitation in specific locations (FAIRALL et al., 2003; HUFFMAN et al., 2007; HUMPHREY et al., 1996; TODD et al., 2001).

Atmospheric temperature data are collected from globally distributed ground meteorological stations (CHOUDHURY, 1987). Besides direct observations, atmospheric models are used to fill gaps in observational data and to provide temperature estimates in locations without meteorological stations (CHOUDHURY, 1987). Temperature estimates are validated using comparisons with independent observational data from meteorological stations (CHOUDHURY, 1987; DA COSTA et al., 2023; DORIGO et al., 2013; MORAIS FILHO et al., 2021).

2.4.7. Wind Speed

The Wind Speed variable at 10 meters from the NASA POWER platform (https://power.larc.nasa.gov/) is calculated using atmospheric models and meteorological observation data (NASA, 2023). This tool uses high-resolution global atmospheric models based on variables such as temperature, pressure, humidity, and air movement (ZHANG et al., 2018). These models are verified and validated using observational data, including data from ground meteorological stations, ocean buoys, weather balloons, and satellites (MORAIS FILHO et al., 2021; NASA, 2023; ZHANG et al., 2018).

2.4.8. Fire Occurrence

The Burned Area product (MCD64A1) from NASA characterizes changes in vegetation structure due to forest fires (APPEEARS, 2022). The MCD64A1 is a product of the MODIS sensor, providing information on the globally burned area. The algorithm analyzes daily changes in surface reflectance to locate rapid changes and detect the approximate date of the fire, mapping the spatial extent of recent fires.

In this study, to help detect the start and end dates of any fire occurrences, the variables 'First_Day' and 'Last_Day' were also used. Therefore, to ensure that the data analyzed in this study were not affected by fires, a survey of the total burned area in the study region during the investigated heat wave period was conducted. It is worth noting that no forest fires were recorded in the study area during the analyzed period.

2.5. Data Treatment and Statistical Analyses

2.5.1. Comparing Atmospheric xCO_2 for Heatwave and Baseline

To develop the analyses characterizing the comparisons proposed by this work between Heatwave and Baseline, Equation 3 was developed, which compares the average normality period (baseline) with the studied heatwave period.

$$xCO_{2\ \text{Delta}} = xCO_{2\ \text{observed (Heatwaves; 2021)}} - xCO_{2\ \text{baseline (daily averages)}} \quad \text{eq.3}$$

Where: xCO_2 Delta refers to the carbon dioxide concentrations in the atmospheric column; xCO_2 Observed represents the values observed during the 60-day period characterized as a heat wave in 2021; and xCO_2 Baseline represents the average of the values observed during the normal periods in 2015 and 2017.

The daily heat wave data minus the average daily baseline data over the studied area were able to demonstrate how much higher the atmospheric CO_2 concentration was during the heat wave compared to normal times. More details about these observations are presented in the results section and discussed in the discussion section.

It is important to note that the environmental variables were not observed simultaneously on all days, and some datasets contained missing values throughout the study period. For the purpose of the time series analysis presented in this section, these missing values were removed to ensure the consistency and reliability of the plotted data.

It is worth highlighting that the innovative aspect of this study lies in the adaptation of a comparative anomaly-based approach, commonly applied in climatological studies, to assess atmospheric CO_2 concentrations (xCO_2) during heatwave events. By constructing a daily delta metric (Δ xCO_2) between the 2021 heatwave and the reference years (2015 and 2017), this method allows a standardized and temporally consistent analysis of xCO_2 dynamics. Although inspired by approaches used in studies of temperature and precipitation anomalies, its application to satellite-derived xCO_2 data represents a novel contribution to climate science.

2.5.2. Descriptive Statistics and Hypothesis Testing: Student's t-test and Wilcoxon-Mann-Whitney Test

Descriptive statistics were calculated for two distinct data groups: Baseline data, represented by the average daily observations from 2015 and 2017, and Heatwave data, consisting of the observations from 2021. The statistical summary included maximum, minimum, median, mean, and the first and third quartiles for each variable in both periods.

Hypothesis tests were applied to assess the significance of differences between the baseline and heat wave periods. Before performing these tests, the normality of the data distribution was assessed using the Shapiro-Wilk test. Based on the results, when normality was confirmed, the Student's t-test was used to compare the means between the two groups. On the other hand, when normality was not observed, the Wilcoxon-Mann-Whitney test was applied as a nonparametric alternative to compare the medians.

This adaptive approach ensured that the appropriate statistical test was used for each variable, depending on the distributional characteristics of the data, thus increasing the robustness and validity of the comparative analysis.

2.5.3. Stepwise Analysis Combined with Principal Component Analysis (PCA)

In this study, Principal Component Analysis (PCA) was used in combination with Stepwise regression analysis to address multicollinearity and optimize the selection of explanatory variables. Multicollinearity occurs when two or more independent variables exhibit strong linear relationships, which can compromise the reliability and interpretability of regression models.

Before performing PCA, all variables were standardized to ensure that the analysis was not biased by differences in units or magnitudes. This transformation allowed a fair comparison between variables expressed on different scales (e.g., °C, ppm, m^2/m^2), preserving the structure of the data and eliminating scale effects.

PCA is a dimensionality reduction technique that transforms the original variables into a smaller set of uncorrelated components, preserving most of the variability of the data. Stepwise regression, in turn, is a variable selection method that iteratively adds or removes predictors based on statistical criteria, identifying the variables that best explain the dependent variable.

After removing highly collinear variables, identified in the PCA by the proximity and orientation of their vectors, the stepwise procedure was applied. This allowed the identification of the climate, vegetation and soil variables most relevant to explaining the behavior of the dependent variable, xCO_2.

3. Results

3.1. Results on Atmospheric xCO_2 for Heatwave and Baseline

The Figure 3 was developed using Equation 3. This analysis aimed to establish a comparative relationship between the atmospheric xCO_2 (ppm) values observed during the heat wave period and the normal period (baseline).

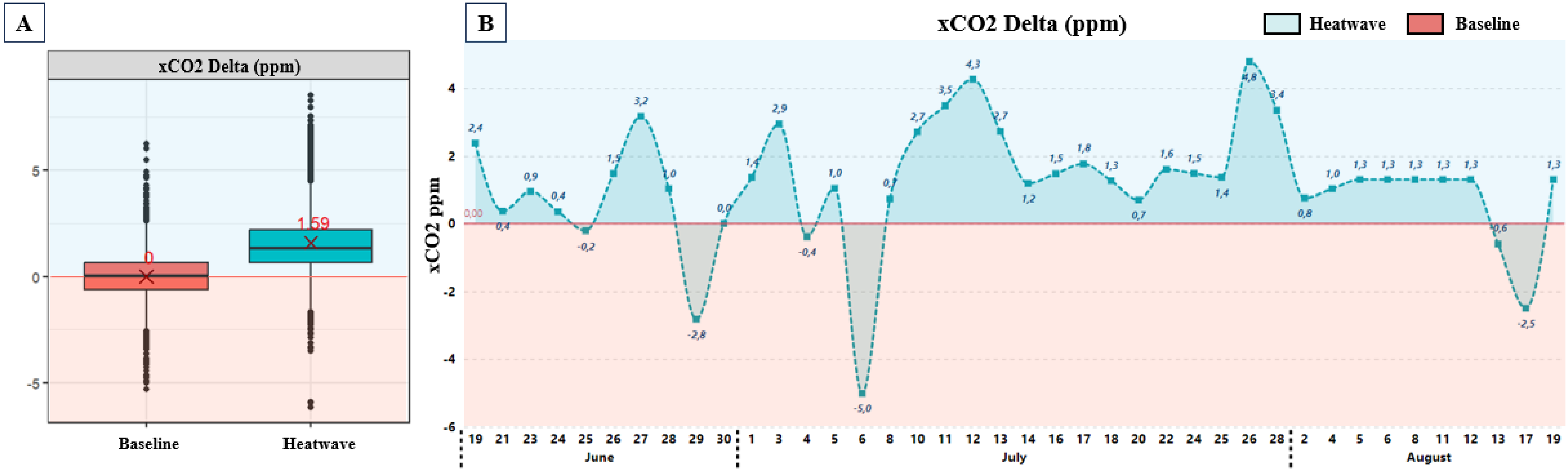

Figure 3: Column CO_2 concentrations in the atmospheric (xCO_2) for Baseline and Heatwave periods, based on the application of Equation 2: where A shows a Boxplot and data distribution; and B shows the temporal distribution of the data during the studied heatwave (2021).

The temporal distribution of the data further highlights the disparity in comparison, as most of the time series values are higher than those of the baseline (Fig. 3 B). Frequent peaks of high xCO_2 concentration can also be observed, with a few moments of lower concentration than the baseline, such as on June 29 and July 6, where the values reached -2.8 ppm and -5.0 ppm, respectively.

3.2. Hypothesis Testing

In this study, Table 3 sought to associate descriptive statistics and hypothesis tests for the pair of variables analyzed. This analysis allowed us to understand the variability of the data and supported the choice of the most appropriate inferential tests. To conduct the hypothesis tests, the normal distribution of the data was assessed using the Shapiro-Wilk test and histogram distribution.

Table 3: Descriptive statistics, data distribution characteristics and hypothesis testing (Student's t-test and Mann-Whitney test) for unprocessed data.

Group and Variables	Unit	Class	Min	Median	Mean	Max	SD	Skew-ness	Kurto-sis	p-value[3,4]
Carbon										
xCO_2	ppm	Bl	396.8	405.8	405.1	412.8	2.63	-0.46	-0.37	t-test
	ppm	Hw	396.7	407.5	407.2	414.6	2.29			
Carbon NEE[1]	$gCm^{-2}day^{-1}$	Bl	-2.88	-0.50	-0.46	2.57	0.78	0.13	-0.54	t-test
	$gCm^{-2}day^{-1}$	Hw	-2.77	-0.43	-0.40	3.15	1.05			
HR[2]	$gCm^{-2}day^{-1}$	Bl	0.59	1.31	1.34	2.15	0.26	0.12	-0.69	t-test
	$gCm^{-2}day^{-1}$	Hw	0.73	1.59	1.58	2.32	0.31			
Vegetation										
LAI	$m^2\ m^{-2}$	Bl	0.10	1.80	1.89	6.90	1.14	0.95	1.43	U test
	$m^2\ m^{-2}$	Hw	0.10	2.20	2.30	6.80	1.17			
Fpar	%	Bl	0.05	0.69	0.66	0.97	0.18	-0.98	1.16	U test
	%	Hw	0.06	0.74	0.72	0.97	0.14			
Soil										
Soil Moisture	$m^3\ m^{-3}$	Bl	0.11	0.32	0.39	0.76	0.18	1.16	-0.35	U test
	$m^3\ m^{-3}$	Hw	0.10	0.31	0.37	0.77	0.18			
LST Amplitude	°C	Bl	-18.74	7.90	7.79	29.10	3.86	-0.16	0.97	t-test
	°C	Hw	-18.04	8.38	8.25	30.32	3.73			
LST Day	°C	Bl	-8.17	17.79	17.63	34.59	3.83	0.09	0.01	t-test
	°C	Hw	-3.89	21.77	21.70	35.09	4.87			

LST Night	°C	Bl	-13.17	9.89	9.84	22.93	3.00	0.08	0.54	t-test
	°C	Hw	-6.19	13.61	13.46	25.73	4.15			
Climate										
RH at 2m	%	Bl	53.65	83.34	82.96	97.72	6.88	-0.21	-0.38	t-test
	%	Hw	53.18	80.53	80.90	98.61	7.52			
Precipitation	mm day^{-1}	Bl	0.00	1.56	3.49	67.83	5.06	3.80	27.03	U test
	mm day^{-1}	Hw	0.00	1.02	3.39	106.37	6.13			
Temperature at 2m	°C	Bl	2.57	12.80	12.73	22.75	2.43	0.41	0.46	t-test
	°C	Hw	5.97	14.95	15.26	24.99	3.45			
Max. Temperature at 2m	°C	Bl	4.58	16.33	16.23	28.23	2.91	0.36	0.42	t-test
	°C	Hw	8.51	18.79	19.07	30.34	4.01			
Min. Temperature at 2m	°C	Bl	0.07	8.70	8.63	18.53	2.47	0.29	0.17	t-test
	°C	Hw	1.29	10.71	10.88	21.13	3.19			
Range Temperature at 2m	°C	Bl	0.76	7.48	7.60	16.54	2.21	0.23	-0.06	t-test
	°C	Hw	1.09	8.12	8.19	17.88	2.40			
Wind at 10m	m s^{-1}	Bl	0.49	1.91	2.00	7.04	0.68	1.09	2.01	p>0.05
	m s^{-1}	Hw	0.62	1.88	2.03	7.42	0.75			

1 - Carbon Net Ecosystem Exchange; 2 - Heterotrophic Respiration; 3 - significant for Student's t-test; 4 -significant for Mann-Whitney test (U test); Bl – Baseline; Hw – Heatwave; SD – Standard Deviation.

Based on these tests, when the data presented a normal distribution, the Student's t-test was used for comparisons between groups; when normality was violated, the Mann-Whitney test (U test) was applied. In addition, for model performance evaluation, an RMSE below 2 gC m^{-2} d^{-1} was considered satisfactory for NEE, while an RMSE below 1 gC m^{-2} d^{-1} was considered satisfactory for RH.

3.3. Temporal and linear regression analyses of atmospheric xCO_2 and control variables for baseline and heatwave

Figure 4 was created to provide a general overview of the data behavior within the studied time series. To facilitate visualization of the maximum and minimum points, a dashed line representing the overall average of the data was added. For xCO_2 during the normal and heatwave periods, the following concentrations were recorded: the maximum values were observed on June 24 (409.7 ppm), June 27 (409.5 ppm), July 1 (409.15 ppm), July 18 (407.26 ppm), and July 24 (406.85 ppm).

Linear regression analysis was used in this work to describe the predictive capacity for the heatwave and baseline periods. As shown in Figure 5, no statistical difference was observed for both periods studied only for the variables: Fpar; LST Amplitude; and temperature range.

Another important factor was the inversion of the regression line trends for the variables: Carbon NEE; HR; LAI; Fpar; LST Temperature; Precipitation; Temperature; maximum temperature and temperature range. However, except for the variable Precipitation, all results showed significance for only one period, either heatwave or baseline. It is worth noting that environmental variables were not observed simultaneously on all days, and some data sets presented missing values throughout the analyzed period. Additionally, the black line (Figure 4), represents the overall mean of the time series, calculated independently of data classification, that is, it reflects the average across both the baseline and heatwave periods.

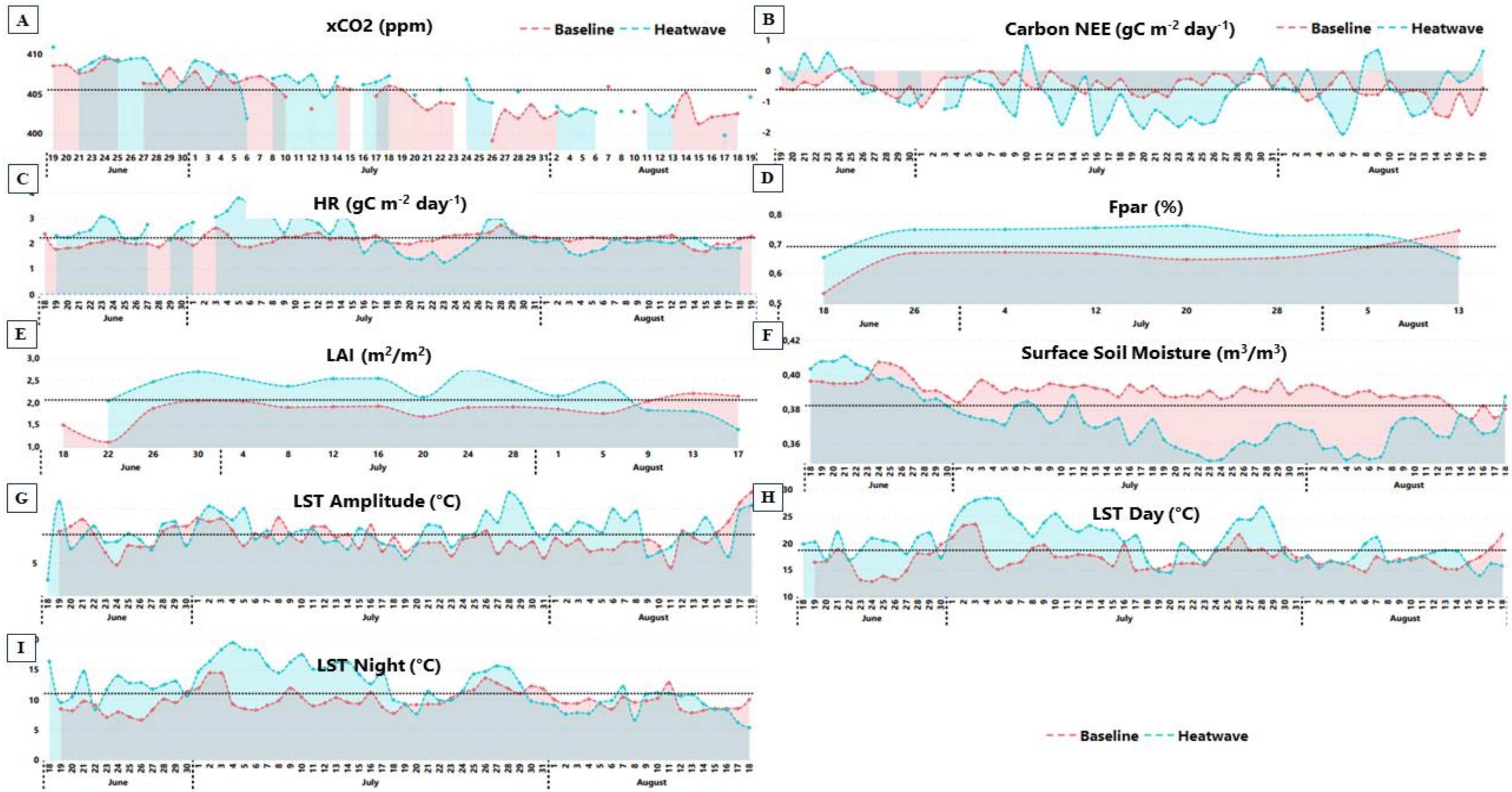

Figure 4: Comparison between the daily mean of baseline (red) and heatwave (blue) time series and the overall mean (black line) for the Carbon, Vegetation and Soil data classes.

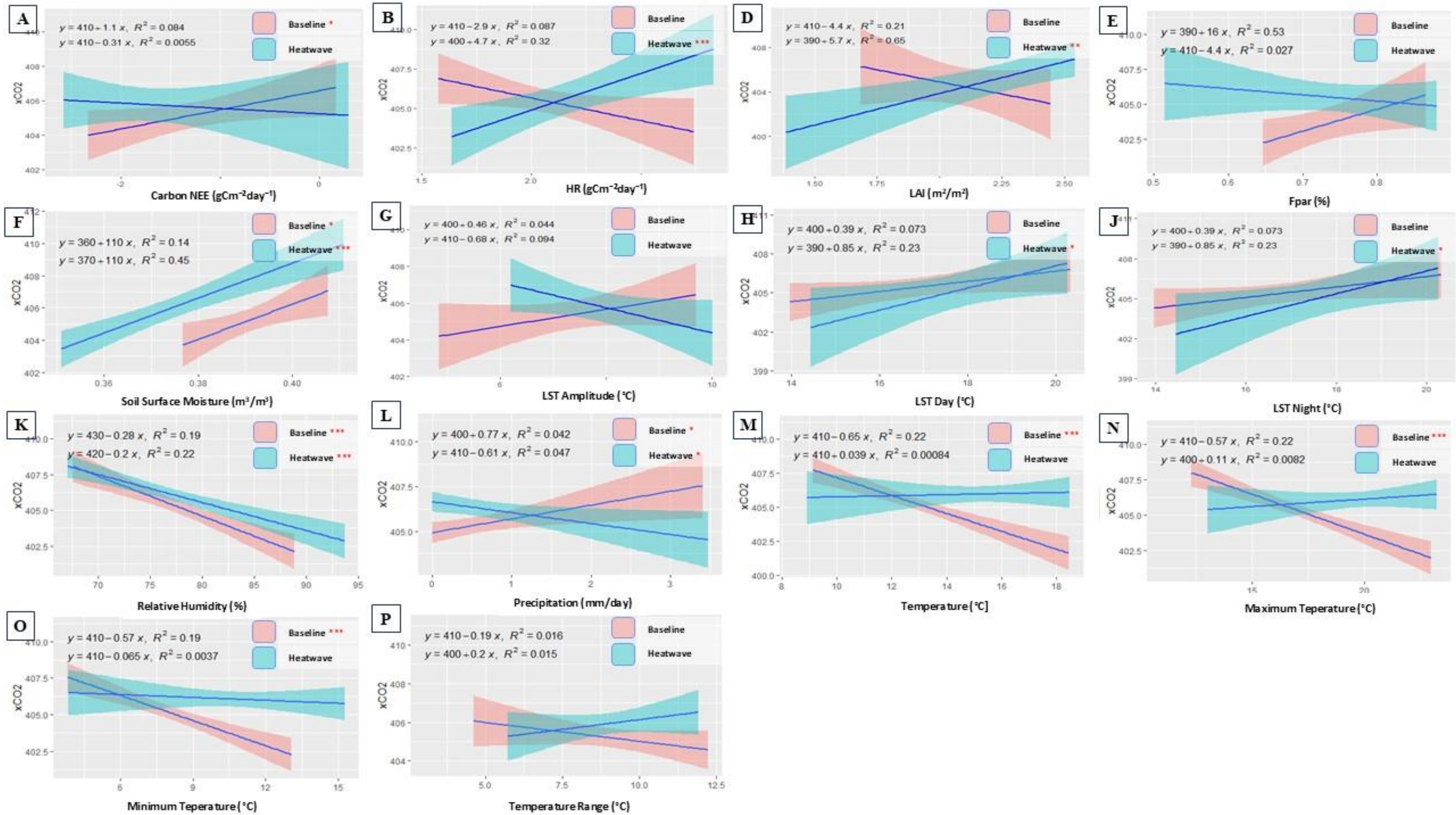

Figure 5: Linear Regression between baseline (Red) and heatwave (Blue) for the data classes of Carbon, Vegetation, Soil, and Climate. Significant at $p < 0.001$ (***), $p < 0.01$ (**), and $p < 0.05$ (*).

The relationship between xCO_2 and Carbon NEE was found to be significant only for the baseline period, indicating a linear growth trend, with a coefficient of determination (R^2) of 0.084 and a p-value of less than 0.01. For the variables HR and LAI during the heatwave, both showed statistical significance and an increasing trend line, with R^2 of 0.32 and $p < 0.001$ for HR, and R^2 of 0.65 and $p < 0.001$ for LAI. Regarding the SSM variable, a negative relationship with xCO_2 was observed for both the baseline and heatwave periods, both statistically significant, with p-values less than 0.01 and 0.001, respectively.

3.4. Stepwise Models for Selecting Variables Capable of Explaining xCO_2 Baseline, and xCO_2 Heatwave

Principal Component Analysis (PCA) was used in this work to exclude variables that present collinearity, in order not to compromise the accuracy of the subsequent Stepwise analysis. The main conclusion of this analysis was to identify the variables xCO_2, LST Day, relative humidity, and Minimum Temperature. These variables were excluded from the set of independent variables for the Stepwise analysis, in order to avoid collinearity. A total explanatory capacity of 61.5% of the data variance, with the first principal component (Dim1) explaining 41.1% of the data variance, while the second (Dim2) explained 20.4%.

Table 4: Best subset regression for the Stepwise model, excluding xCO_2 (ppm), HR, and Carbon NEE as independent variables.

Dependent	Variable Independent	Predictive Parameters		
		Number of Variables	Adj. R^2	MSEP
xCO_2 Baseline	SSM; Precipitation; Fpar	03/11	0.99	0.01
xCO_2 Heatwave	SSM; LST Night; Range Temperature; Fpar	04/11	0.99	0.004

MSEP: Mean Squared Error of Prediction
SSM: Surface Soil Moisture

For modeling xCO_2 behavior during the Baseline, the model used 3 out of 11 independent variables: SSM, Precipitation, and Fpar, with an adjusted R^2 of 0.99, MSEP of 0.01, and FPE of 0.009. Additionally, for xCO_2 during the

Heatwave, the model used 4 out of 11 independent variables, with an R^2 of 0.99, MSEP of 0.004, and FPE of 0.001.

4. Discussion

4.1. How Does Heterotrophic Respiration Explain Higher Atmospheric CO_2 Concentrations During Heatwaves?

To understand the atmospheric CO_2 concentrations during the periods studied, it was important to determine if any fire outbreaks at the location, especially during the heatwave, could have influenced the data. It is noteworthy that no fire outbreaks were observed during the heatwave period studied here, increasing the reliability of the developed relationships.

This verification was crucial because, as demonstrated by Maria et al., (2023) in their study of the influence of fires on atmospheric CH4 (methane) concentration and xCO_2 anomalies, forest and agricultural fires can significantly impact the composition of atmospheric CO_2, as well as other greenhouse gases (GHGs).

Another important verification conducted by the study to enable analyses of the heatwaves' impact on the ecosystem was understanding wind speed during the studied periods, both for normal (baseline) and heatwave periods. Studies by Mousavi and Falahatkar (2020) and Siabi et al., (2019) highlighted the effects of wind on CO_2 concentrations in different land uses in Iran. It is noteworthy that no statistical differences were observed between wind speeds within and outside the heatwave period, increasing the reliability of the relationships developed in this work.

Wind can influence atmospheric xCO_2 values, especially by dispersing CO_2 emitted by the studied ecosystem or bringing gases from other locations (MOUSAVI; FALAHATKAR, 2020). Besides unwanted effects on the data, wind speed also influences gas exchanges between the atmosphere and vegetation, as it can increase the rate of CO_2 exchange between plants and the atmosphere, affecting atmospheric xCO_2 (CAMPOS; CERRI; SCALA JR, 2022).

Campos et al., (2022); da Costa et al., (2021) and Morais Filho et al., (2021), highlighted important statistical mechanisms, also used in this work, as ways to control and reduce wind effects on xCO_2 data. Data volume, comparative time series, and data standardization mechanisms, such as outlier treatment, are important tools for better understanding and accuracy of observed xCO_2 data (CAMPOS; CERRI; SCALA JR, 2022; DA COSTA et al., 2023; MOUSAVI; FALAHATKAR, 2020).

As described at different points in this work, determining periods of normality and heatwaves, and their respective locations of occurrence, was based on the descriptor periods (LHOTKA; KYSELÝ, 2022). This work by Lhotka and Kyselý (2022) is based on a long historical series of climatic parameters to determine heatwave periods. Data such as precipitation, temperature, and maximum temperature, among others, determine two important factors: magnitude and intensity of the heatwave (LHOTKA; KYSELÝ, 2022).

According to the authors, magnitude represents the overall severity of a given heatwave, considering its duration, affected area, and normalized temperature anomaly (LHOTKA; KYSELÝ, 2022). Additionally, the intensity of a heatwave was calculated by the authors as the magnitude divided by the duration of the wave, thus highlighting short-duration events with large positive maximum temperature anomalies (LHOTKA; KYSELÝ, 2022). Moreover, the magnitude of the heatwave was also calculated separately for each of the nine regions studied. Thus, according to Lhotka and Kyselý (2022), the heatwave was attributed to regions where the magnitude was greater than the average calculated across all regions.

In agreement with Lhotka and Kyselý (2022), high temperatures and lower precipitation levels were also observed during heatwave periods compared to normal periods. Even using different databases, the data confirmed the observations made by Lhotka and Kyselý (2022). Additionally, it was possible to observe in the time series and in the statistical hypothesis tests that the climatic variables were significantly higher within the heatwave. These patterns align with past extreme heat events documented in previous studies on heatwaves in Europe (IBEBUCHI; ABU, 2023; LHOTKA; KYSELÝ, 2022; RUSSO; SILLMANN; FISCHER, 2015).

The relationship established from equation 3 allowed us to understand that xCO_2 was higher during the heatwave period compared to the baseline period. The values organized in boxplots show that during the heatwave period, there was an average of 1.59 ppm more CO_2 in the atmosphere. Observing the time series, this assertion becomes even more evident, as during much of the studied period, xCO_2 values were significantly higher compared to the baseline period, with peaks reaching 4.3 ppm and 4.8 ppm on July 11 and July 26, respectively. Significant removal peaks were also observed, such as on June 29 and July 6, when values reached -2.8 ppm and -5.0 ppm, respectively.

One explanation for the observed removal values during the heatwave is the significant capacity of the studied ecosystem to enhance vegetative variables during the heatwave compared to the baseline. According to the hypothesis tests, a difference between the normal and heatwave periods was observed, with higher Fpar and LAI values during the heatwave. This aspect highlights the idea that higher temperatures over the ecosystem during the heatwave produced a positive effect by intensifying vegetation's ability to capture atmospheric CO_2.

An inverse observation was made by da Costa et al., (2021), who found an inversely proportional relationship between higher temperature values and LAI (Leaf Area Index), SIF (Solar-Induced Fluorescence), and consequently xCO_2 in tropical agricultural production systems. Thus, under these conditions, high temperatures negatively impact vegetation's photosynthetic capacity, making it less able to capture CO_2 from the atmosphere; consequently, higher xCO_2 values were observed (DA COSTA et al., 2021; MORAIS FILHO et al., 2021). Therefore, contrary to what was observed in tropical climates, the temperate ecosystem focused on this study demonstrated an enhanced photosynthetic capacity under higher temperatures produced by the heatwave.

The linear regression developed for xCO_2 and LAI for the studied periods showed that, despite being higher for hypothesis tests, the relationship was significant only for the heatwave period, with the highlight of this result being the positive relationship between the variables. In general, as observed in classical studies on the subject (HOWE, 2015; KEELING; BACASTOW; BAINBRIDGE, 1976; KENEA et al., 2021), an increase in leaf area directly impacts the system's photosynthetic capacity to remove CO_2 from the atmosphere, demonstrating a negative relationship. However, for this study, a significant positive relationship was observed for the heat wave, where even with the increase in leaf area, the vegetation did not show a strong impact on xCO_2 values (KEELING; BACASTOW; BAINBRIDGE, 1976; MARIA et al., 2023).

Analyzing the linear regression results between HR and atmospheric xCO_2, significance was observed only during the heatwave period, with a positive trend in the regression line's slope. This indicates that only during the heatwave was there a significant impact of soil respiration on atmospheric CO_2 concentrations, suggesting that an increase in heterotrophic respiration is associated with higher xCO_2 values during the heatwave (KERR; OCHSNER, 2020; NEVE; PANNIER; HOFMAN, 1996; WANG et al., 2016).

These results highlight that, in terms of emission balance, the studied ecosystem became more efficient in removing CO_2 during the heatwave (HINKO-NAJERA et al., 2017; ZHANG et al., 2023). However, this CO_2 capture was not sufficient to result in a negative emission balance, as the system's HR was significantly more intense in emitting CO_2 during the heatwave compared to the baseline (KERR; OCHSNER, 2020; TANG et al., 2020; WANG; CAI; SANTOSO, 2021; YAN et al., 2022).

The variable capable of expanding knowledge regarding this effect is Carbon NEE. For the hypothesis test, Carbon NEE was negative in both study classes, especially because the study period was during the summer, the season responsible for the highest CO_2 removals from the atmosphere (CAMPOS; CERRI; SCALA JR, 2022; HOWE, 2015; KEELING; BACASTOW; BAINBRIDGE, 1976; SMITH et al., 2019). Additionally, statistical significance and a positive relationship between Carbon NEE and xCO_2 were observed; therefore, the more positive NEE is, the higher the atmospheric CO_2 concentration (GOMES; ARAÚJO, 2018; HINKO-NAJERA et al., 2017).

A positive Carbon NEE refers to the net balance of CO_2 exchanges between the ecosystem and the atmosphere over a certain period (HINKO-NAJERA et al., 2017; ZHANG et al., 2023). When Carbon NEE is positive, it means that the ecosystem is releasing more CO_2 into the atmosphere than it is absorbing, acting as a CO_2 source (HINKO-NAJERA et al., 2017; LIAN et al., 2023; REICHSTEIN et al., 2005; ZHANG et al., 2023).

The main indication capable of explaining more positive Carbon NEE values during heatwaves is soil microbial respiration and vegetation autotrophic respiration when not photosynthesizing (REICHSTEIN et al., 2005; TANG et al., 2020). In general, high Carbon NEE values are usually associated with situations where the respiration and organic matter decomposition rate, represented in this work by the HR variable, exceeds the rate of photosynthetic CO_2 capture (CHAPIN et al., 2006; HINKO-NAJERA et al., 2017).

4.2. Positive Feedback and Practical Implications of the Accepted Hypothesis in This Study

The results presented here allow us to reject the first hypothesis of this study, which suggested that the heatwave could: i) cause a reduction in plant photosynthesis due to thermal stress, resulting in higher xCO_2 values in the atmosphere. Thus, this hypothesis was discarded based on the results of statistical analyses and the reviewed scientific literature, as they indicated that vegetation actually increased its photosynthetic capacity, resulting in the removal of CO_2 from the atmosphere.

On the other hand, it is also important to argue the confirmation of the second hypothesis of this study, which posited that the heatwave would: ii) intensify soil respiration due to the metabolic acceleration of its microbiology, resulting in higher xCO_2 values in the atmosphere. Thus, even with the positive response of vegetation during the heatwave, it was possible to observe higher xCO_2 levels compared to normal periods, demonstrating this to be the main factor for understanding atmospheric CO_2 concentrations during heatwave events in temperate natural ecosystems (AUDET et al., 2017; HUMBORG et al., 2019; KWON et al., 2021).

These results highlight a positive feedback effect between the ecosystem under heatwaves and climate change (AN et al., 2022; HUMBORG et al., 2019; KRASNOVA et al., 2022; WOODALL et al., 2012). In terms of emission balance, the studied ecosystem became more efficient in removing CO_2 during the heatwave; however, this CO_2 capture was not greater than the emissions caused by the system's heterotrophic respiration (YAN et al., 2022). Therefore, overall, the atmospheric CO_2 capture driven by higher temperatures was not sufficient to make the net emissions balance negative, especially since the high temperatures also increased CO_2 emissions caused by soil heterotrophic respiration.

Positive feedback is especially concerning for this ecosystem because, as observed in this study, its soils are large carbon organic storage reservoirs (HENGL et al., 2017; SOILGRIDS250M2.0, 2022). According to data from the SoilGrids250m2.0 (2022) platform, the estimated average carbon stocks in the region range between 65 and 95 tons per hectare, values higher than those observed in tropical forests, such as the Amazon, where average estimates range between 40 and 70 tons per hectare (BOSSIO et al., 2020; HENGL et al., 2014, 2017; POGGIO et al., 2017).

These characteristics indicate that in temperate ecosystems, the effect of positive feedback caused by high temperatures can be more compromising for soil organic carbon stocks (DAVIDSON; JANSSENS, 2006; NEVE; PANNIER; HOFMAN, 1996; WANG et al., 2016). Generally, temperate forests tend to have more carbon stocks in the soil than tropical forests, especially due to the recurrent lower temperatures in their formation, which reduce microbial activity in the soil in the long term, producing a slower rate of organic matter decomposition and consequently accumulation (BOSSIO et al., 2020; DAVIDSON; JANSSENS, 2006; LUYSSAERT et al., 2007; METCALF et al., 2011).

In higher carbon stocks, small losses of soil organic carbon can mean significant amounts of CO_2 released into the atmosphere (BOSSIO et al., 2020; DAVIDSON and JANSSENS, 2006). The results of the linear regression between xCO_2 and HR, significant and positive only for the heatwave period, as well as the greater participation of temperature variables in the Stepwise model to explain xCO_2 during the heatwave period, highlight the impacts of high temperatures on this temperate climate ecosystem. Therefore, the impact of heatwaves on the reductions of soil organic carbon stocks in temperate ecosystems with abundant stocks becomes especially concerning (BOSSIO et al., 2020; DAVIDSON; JANSSENS, 2006; LUYSSAERT et al., 2007).

Thus, it is evident that healthy ecosystems can act as carbon sinks, removing CO_2 from the atmosphere, while those affected by climate change can become sources of CO_2, contributing to the increase in atmospheric concentrations of this greenhouse gas and consequently intensifying climate instability (WOODALL et al., 2012). Similarly, the opposite is also true: the more unstable the climate, the more intense and frequent heatwaves will be, resulting in an even more significant loss of ecosystem carbon (WOODALL et al., 2012). This positive feedback between climate change and CO_2 emissions from stressed ecosystems, especially in temperate ecosystems, underscores the importance of mitigation and adaptation measures to address the long-term challenges of climate change (WOODALL et al., 2012; ZEMP et al., 2017).

5. Conclusion

The results of this study offer a clear perspective on the effects of heatwaves on the analyzed ecosystem. Firstly, we statistically confirmed that during the heatwave, there was a notable increase in atmospheric CO_2 concentrations (xCO_2) compared to normal periods. This finding highlights the ecosystem's sensitivity to climate change, especially regarding the intensification of thermal stress.

During the heatwave period, the mean atmospheric CO_2 concentration increased by 1.59 ppm compared to the baseline period. The daily variation of xCO_2 showed marked fluctuations over time, with positive peaks of up to +4.3 ppm (July 10) and decreases of up to –5.0 ppm (July 5). Overall, positive values predominated during the heatwave, especially between late June and mid-July, suggesting higher CO_2 emissions or lower CO_2 sequestration during this period. During the baseline period, values tended to be more negative, indicating a dominance of CO_2 removal processes from the atmosphere.

Linear regression analyses indicated that xCO_2 was highly dependent on the analyzed period. Heterotrophic respiration (HR) showed the strongest relationship during the heatwave ($R^2 = 0.32$), indicating that increases in RH were associated with higher atmospheric xCO_2 concentrations.

Despite the significant increase in photosynthetic activity and leaf area, as indicated by LAI and Fpar during the heatwave, the data revealed a negative carbon balance, with CO_2 emissions exceeding atmospheric uptake. This finding suggests a positive feedback mechanism in which thermal stress enhances heterotrophic respiration and limits carbon sequestration efficiency, contributing to elevated atmospheric CO_2 concentrations and amplifying climatic instability.

It is noteworthy that, due to the large carbon reserves stored in the soil of these ecosystems and the high rate of heterotrophic respiration observed during the heatwave, temperate forest ecosystems may be even more vulnerable to the effects of increasing temperature than other types of ecosystems. This finding highlights the importance of a deep understanding of the interactions between climate, soil, and vegetation under these conditions.

Ultimately, the central conclusion of this study is that, while heatwaves can trigger adaptive physiological responses in plants, such as increased photosynthetic activity, they also exacerbate imbalances in the carbon cycle, resulting in net emissions that are higher than absorptions. This emphasizes the critical importance of understanding and mitigating the effects of climate change on this ecosystem to minimize negative impacts on the atmosphere and global atmospheric carbon balance.

6. References

AN, Z.; BORK, E. W.; OLEFELDT, D.; CARLYLE, C. N.; CHANG, S. X. Simulated heat wave events increase CO2 and N2O emissions from cropland and forest soils in an incubation experiment. **Biology and Fertility of Soils**, [s. l.], v. 58, n. 7, p. 789–802, 2022.

AUDET, J.; NEIF, É. M.; CAO, Y.; HOFFMANN, C. C.; LAURIDSEN, T. L.; LARSEN, S. E.; SØNDERGAARD, M.; JEPPESEN, E.; DAVIDSON, T. A. Heat-wave effects on greenhouse gas emissions from shallow lake mesocosms. **Freshwater Biology**, [s. l.], v. 62, n. 7, p. 1130–1142, 2017.

APPEEARS. **AρρEEARS**. 2022. Disponível em: <https://appeears.earthdatacloud.nasa.gov/>. Acesso em: 6 jul. 2022.

BALL, B. C.; DOBBIE, K. E.; PARKER, J. P.; SMITH, K. A. The influence of gas transport and porosity on methane oxidation in soils. **Journal of Geophysical Research Atmospheres**, [s. l.], v. 102, n. 19, p. 23301–23308, 1997.

BLANCO-CANQUI, H.; LAL, R. **Mechanisms of carbon sequestration in soil aggregates**, 2004.

BÖHNISCH, A.; FELSCHE, E.; LUDWIG, R. European heatwave tracks: using causal discovery to detect recurring pathways in a single-regional climate model large ensemble. **Environmental Research Letters**, [s. l.], v. 18, n. 1, 2023.

BOSSIO, D. A.; COOK-PATTON, S. C.; ELLIS, P. W.; FARGIONE, J.; SANDERMAN, J.; SMITH, P.; WOOD, S.; ZOMER, R. J.; VON UNGER, M.; EMMER, I. M.; GRISCOM, B. W. The role of soil carbon in natural climate solutions. **Nature Sustainability**, [s. l.], v. 3, n. 5, p. 391–398, 2020. Disponível em: <http://dx.doi.org/10.1038/s41893-020-0491-z>

BRAZIL. Paris Agreement: Nationally Determined Contribution (NDC). **Intended Nationally Determined Contribution**, [s. l.], n. 8.5.2017, p. 2003–2005, 2022. Disponível em: <https://unfccc.int/sites/default/files/NDC/2022-06/Updated - First NDC - FINAL - PDF.pdf>

C2ES. **WHAT IS CLIMATE RESILIENCE AND WHY DOES IT MATTER?** [s.l: s.n.].

CAMPOS, M. O. De; CERRI, C. E. P.; SCALA JR, N. La. Atmospheric CO2 , soil carbon stock and control variables in managed and degraded pastures in central Brazil. **Remote Sensing Applications: Society and Environment**, [s. l.], v. 28, n. August, p. 100848, 2022. Disponível em: <https://doi.org/10.1016/j.rsase.2022.100848>

CHAPIN, F. S.; WOODWELL, G. M.; RANDERSON, J. T.; RASTETTER, E. B.; LOVETT, G. M.; BALDOCCHI, D. D.; CLARK, D. A.; HARMON, M. E.; SCHIMEL, D. S.; VALENTINI, R.; WIRTH, C.; ABER, J. D.; COLE, J. J.; GOULDEN, M. L.; HARDEN, J. W.; HEIMANN, M.; HOWARTH, R. W.; MATSON, P. A.; MCGUIRE, A. D.; MELILLO, J. M.; MOONEY, H. A.; NEFF, J. C.; HOUGHTON, R. A.; PACE, M. L.; RYAN, M. G.; RUNNING, S. W.; SALA, O. E.; SCHLESINGER, W. H.; SCHULZE, E. D. **Reconciling carbon-cycle concepts, terminology, and methods**, 2006.

CHOUDHURY, B. J. **Relationships Between Vegetation Indices, Radiation Absorption, and Net Photosynthesis Evaluated by a Sensitivity AnalysisREMOTE SENSING OF ENVIRONMENT**. [s.l: s.n.].

CLEUGH, H. A.; LEUNING, R.; MU, Q.; RUNNING, S. W. Regional evaporation estimates from flux tower and MODIS satellite data. **Remote Sensing of Environment**, [s. l.], v. 106, n. 3, p. 285–304, 2007.

CUI, D.; LIANG, S.; WANG, D. Observed and projected changes in global climate zones based on Köppen climate classification. **Wiley Interdisciplinary Reviews: Climate Change**, [s. l.], v. 12, n. 3, p. 1–28, 2021.

DA COSTA, L. M.; DE ARAÚJO SANTOS, G. A.; DE MENDONÇA, G. C.; MORAIS FILHO, L. F. F.; DE MENESES, K. C.; DE SOUZA ROLIM, G.; LA SCALA, N. Spatiotemporal variability of atmospheric CO2 concentration and controlling factors over sugarcane cultivation areas in southern Brazil. **Environment, Development and Sustainability**, [s. l.], n. 0123456789, 2021. Disponível em: <https://doi.org/10.1007/s10668-021-01677-6>

DA COSTA, L. M.; DE MENDONÇA, G. C.; ARAÚJO SANTOS, G. A. De; MORAES, J. R. da S. C. De; COLOMBO, R.; PANOSSO, A. R.; LA SCALA, N. High spatial resolution solar-induced chlorophyll fluorescence and its relation to rainfall precipitation across Brazilian ecosystems. **Environmental Research**, [s. l.], v. 218, n. November 2022, 2023.

DAVIDSON, E. A.; JANSSENS, I. A. **Temperature sensitivity of soil carbon decomposition and feedbacks to climate change**, 2006.

DORIGO, W. A.; XAVER, A.; VREUGDENHIL, M.; GRUBER, A.; HEGYIOVÁ, A.; SANCHIS-DUFAU, A. D.; ZAMOJSKI, D.; CORDES, C.; WAGNER, W.; DRUSCH, M. Global Automated Quality Control of In Situ Soil Moisture Data from the International Soil Moisture Network. **Vadose Zone Journal**, [s. l.], v. 12, n. 3, p. 1–21, 2013. Disponível em: <https://onlinelibrary.wiley.com/doi/full/10.2136/vzj2012.0097>. Acesso em: 23 fev. 2024.

FAIRALL, C. W.; BRADLEY, E. F.; HARE, J. E.; GRACHEV, A. A.; EDSON, J. B. **Bulk Parameterization of Air-Sea Fluxes: Updates and Verification for the COARE Algorithm**. [s.l: s.n.].

FIGUEIREDO, E. B.; PANOSSO, A. R.; BORDONAL, R. de O.; TEIXEIRA, D. D. B.; BERCHIELLI, T. T.; LA SCALA, N. Soil CO2–C Emissions and Correlations with Soil Properties in Degraded and Managed Pastures in Southern Brazil. **Land Degradation and Development**, [s. l.], v. 28, n. 4, p. 1263–1273, 2017.

FREITAS, S. C.; TRIGO, I.; MACEDO, J.; BARROSO, C.; SILVA, R.; PERDIGAO, R. Land Surface Temperature from multiple geostationary satellites. **International Journal of Remote Sensing**, [s. l.], v. Vol 34, n. 9–10, 2013.

GERDOL, R.; BRAGAZZA, L.; BRANCALEONI, L. Heatwave 2003: High summer temperature, rather than experimental fertilization, affects vegetation and CO2 exchange in an alpine bog. **New Phytologist**, [s. l.], v. 179, n. 1, p. 142–154, 2008.

GMACH, M. R.; CHERUBIN, M. R.; KAISER, K.; CERRI, C. E. P. **Processes that influence dissolved organic matter in the soil: A review**, Scientia Agricola, 2020.

GOMES, V. E. de V.; ARAÚJO, R. C. P. De. Análise dos fatores determinantes do valor dos contratos do Programa Agricultura de Baixo Carbono (ABC) no Brasil no ano safra 2014/15. **Revista de Ciências Agroambientais**, [s. l.], v. 16, n. 1, p. 39–53, 2018.

HAKKARAINEN, J.; IALONGO, I.; TAMMINEN, J. Direct space-based observations of anthropogenic CO2 emission areas from OCO-2. **Geophysical Research Letters**, [s. l.], v. 43, n. 21, p. 11,400-11,406, 2016.

HENGL, O.; JESUS, J. M. De; MACMILLAN, R. A.; BATJES, N. H.; HEUVELINK, G. B. M.; RIBEIRO, E.; SAMUEL-ROSA, A.; KEMPEN, B.; LEENAARS, J. G. B.; WALSH, M. G.; GONZALEZ, M. R. **SoilGrids1km — Global Soil Information Based onAutomated Mapping**, 2014. Disponível em:

<https://journals.plos.org/plosone/article?id=10.1371/journal.pone.0105992>

HENGL, T.; DE JESUS, J. M.; HEUVELINK, G. B. M.; GONZALEZ, M. R.; KILIBARDA, M.; BLAGOTIĆ, A.; SHANGGUAN, W.; WRIGHT, M. N.; GENG, X.; BAUER-MARSCHALLINGER, B.; GUEVARA, M. A.; VARGAS, R.; MACMILLAN, R. A.; BATJES, N. H.; LEENAARS, J. G. B.; RIBEIRO, E.; WHEELER, I.; MANTEL, S.; KEMPEN, B. **SoilGrids250m: Global gridded soil information based on machine learning**. [s.l: s.n.]. v. 12 Disponível em: <http://www.isric.org/content/isric- releases-upgraded-soilgrids-system-two-times- improved-accuracy-predictions>

HINKO-NAJERA, N.; ISAAC, P.; BERINGER, J.; VAN GORSEL, E.; EWENZ, C.; MCHUGH, I.; EXBRAYAT, J. F.; LIVESLEY, S. J.; ARNDT, S. K. Net ecosystem carbon exchange of a dry temperate eucalypt forest. **Biogeosciences**, [s. l.], v. 14, n. 16, p. 3781–3800, 2017.

HOWE, J. P. This is nature; This is un-nature: Reading the keeling curve. **Environmental History**, [s. l.], v. 20, n. 2, p. 286–293, 2015.

HUFFMAN, G. J.; ADLER, R. F.; BOLVIN, D. T.; GU, G.; NELKIN, E. J.; BOWMAN, K. P.; HONG, Y.; STOCKER, E. F.; WOLFF, D. B. The TRMM Multisatellite Precipitation Analysis (TMPA): Quasi-global, multiyear, combined-sensor precipitation estimates at fine scales. **Journal of Hydrometeorology**, [s. l.], v. 8, n. 1, p. 38–55, 2007.

HUMBORG, C.; GEIBEL, M. C.; SUN, X.; MCCRACKIN, M.; MÖRTH, C. M.; STRANNE, C.; JAKOBSSON, M.; GUSTAFSSON, B.; SOKOLOV, A.; NORKKO, A.; NORKKO, J. High emissions of carbon dioxide and methane from the coastal Baltic Sea at the end of a summer heat wave. **Frontiers in Marine Science**, [s. l.], v. 6, n. JUL, 2019.

HUMPHREY, M. D.; ISTOK, J. D.; LEE, J. Y.; HEVESI, J. A.; FLINT, A. L. **A New Method for Automated Dynamic Calibration of Tipping-Bucket Rain Gauges**. [s.l: s.n.].

IBEBUCHI, C. C.; ABU, I. O. Characterization of temperature regimes in Western Europe, as regards the summer 2022 Western European heat wave. **Climate Dynamics**, [s. l.], v. 61, n. 7–8, p. 3707–3720, 2023.

IPCC. Climate Change and Land Ice; IPCC Special Report on climate change, desertification, land degradation, sustainable land management, food security, and greenhouse gas fluxes in terrestrial ecosystems; Summary for Policymakers. **Ipcc**, [s. l.], p. 1–15, 2017.

IPCC. **Climate Change 2021: The Physical Science Basis. Contribution of Working Group I to the Sixth Assessment Report of the Intergovernmental Panel on Climate Change [Masson-Delmotte, V., P. Zhai, A. Pirani, S.L. Connors, C. Péan, S. Berger, N. Caud, Y. Chen,**. 2021.

IPCC. **Global Warming of 1.5°C**. [s.l.] : Cambridge University Press, 2022.

KEELING, C. D.; BACASTOW, R. B.; BAINBRIDGE, A. E. Atmospheric carbon dioxide variations at Mauna Loa Observatory, Hawaii. **Tellus**, [s. l.], v. 28, n. 6, p. 538–551, 1976.

KENEA, S.-T.; LEE, H.-Y.; JOO, S.-W.; LI, S.-L.; LABZOVSKII, L. D.; CHUNG, C.-Y.; KIM, Y.-H. Interannual Variability of Atmospheric CH4 and Its Driver Over South Korea Captured by Integrated Data in 2019. **Remote Sensing**, [s. l.], v. 13, n. 12, 2021.

KERR, D. D.; OCHSNER, T. E. Soil organic carbon more strongly related to soil moisture than soil temperature in temperate grasslands. **Soil Science Society of America Journal**, [s. l.], v. 84, n. 2, p. 587–596, 2020.

KONINGS, A. G.; ANTHONY BLOOM, A.; LIU, J.; PARAZOO, N. C.; SCHIMEL, D. S.;

BOWMAN, K. W. Global satellite-driven estimates of heterotrophic respiration. **Biogeosciences**, [s. l.], v. 16, n. 11, p. 2269–2284, 2019.

KRASNOVA, A.; MANDER; NOE, S. M.; URI, V.; KRASNOV, D.; SOOSAAR, K. Hemiboreal forests' CO2 fluxes response to the European 2018 heatwave. **Agricultural and Forest Meteorology**, [s. l.], v. 323, 2022.

KWON, M. J.; BALLANTYNE, A.; CIAIS, P.; BASTOS, A.; CHEVALLIER, F.; LIU, Z.; GREEN, J. K.; QIU, C.; KIMBALL, J. S. Siberian 2020 heatwave increased spring CO2uptake but not annual CO2uptake. **Environmental Research Letters**, [s. l.], v. 16, n. 12, 2021.

LHOTKA, O.; KYSELÝ, J. The 2021 European Heat Wave in the Context of Past Major Heat Waves. **Earth and Space Science**, [s. l.], v. 9, n. 11, 2022.

LIAN, Y.; LI, H.; RENYANG, Q.; LIU, L.; DONG, J.; LIU, X.; QU, Z.; LEE, L. C.; CHEN, L.; WANG, D.; ZHANG, H. **Mapping the net ecosystem exchange of CO2 of global terrestrial systems**, Elsevier B.V., 2023.

LUYSSAERT, S. et al. CO2 balance of boreal, temperate, and tropical forests derived from a global database. **Global Change Biology**, [s. l.], v. 13, n. 12, p. 2509–2537, 2007.

MAJASALMI, T.; RAUTIAINEN, M.; STENBERG, P.; MANNINEN, T. Validation of MODIS and GEOV1 fPAR products in a boreal forest site in Finland. **Remote Sensing**, [s. l.], v. 7, n. 2, p. 1359–1379, 2015.

MARGHANY, M.; HASHIM, M. Robust of Doppler Centroid for Mapping Sea Surface Current by Using Radar Satellite Data. **American Journal of Engineering and Applied Sciences**, [s. l.], v. 2, n. 4, p. 781–788, 2009.

MARIA, L. de S.; ROSSI, F. S.; COSTA, L. M. Da; CAMPOS, M. O.; BLAS, J. C. G.; PANOSSO, A. R.; SILVA, J. L. Della; SILVA JUNIOR, C. A. Da; LA SCALA, N. Spatiotemporal analysis of atmospheric XCH4 as related to fires in the Amazon biome during 2015–2020. **Remote Sensing Applications: Society and Environment**, [s. l.], v. 30, n. March, p. 100967, 2023. Disponível em: <https://doi.org/10.1016/j.rsase.2023.100967>

METCALF, C. J. E.; GRAHAM, A. L.; HUIJBEN, S.; BARCLAY, V. C.; LONG, G. H.; GRENFELL, B. T.; READ, A. F.; BJØRNSTAD, O. N. Partitioning regulatory mechanisms of within-host malaria dynamics using the effective propagation number. **Science**, [s. l.], v. 333, n. 6045, p. 984–988, 2011.

MORAIS FILHO, L. F. F.; MENESES, K. C. De; SANTOS, G. A. de A.; BICALHO, E. da S.; ROLIM, G. de S.; LA SCALA, N. xCO2 temporal variability above Brazilian agroecosystems: A remote sensing approach. **Journal of Environmental Management**, [s. l.], v. 288, n. February, 2021.

MOUSAVI, S. M.; FALAHATKAR, S. Spatiotemporal distribution patterns of atmospheric methane using GOSAT data in Iran. **Environment, Development and Sustainability**, [s. l.], v. 22, n. 5, p. 4191–4207, 2020.

MUTIIBWA, D.; STRACHAN, S.; ALBRIGHT, T. Land Surface Temperature and Surface Air Temperature in Complex Terrain. **IEEE Journal of Selected Topics in Applied Earth Observations and Remote Sensing**, [s. l.], v. 8, n. 10, p. 4762–4774, 2015.

MYNENI, R. B.; HALL, F. G.; SELLERS, P. J.; MARSHAK, A. L. The interpretation of spectral vegetation indexes. **IEEE Transactions on Geoscience and Remote Sensing**, [s. l.], v. 33, n. 2, p. 481–486, 2019.

MYNENI, R. B.; HOFFMAN, S.; KNYAZIKHIN, Y.; PRIVETTE, J. L.; GLASSY, J.; TIAN, Y.; WANG, Y.; SONG, X.; ZHANG, Y.; SMITH, G. R.; LOTSCH, A.; FRIEDL, M.; MORISETTE, J. T.; VOTAVA, P.; NEMANI, R. R.; RUNNING, S. W. Global products of vegetation leaf area and fraction absorbed PAR from year one of MODIS data. **Remote Sensing of Environment**, [s. l.], 2022. Disponível em: <www.elsevier.com/locate/rse>

NASA, P. **NASA POWER**. 2023. Disponível em: <https://power.larc.nasa.gov/>. Acesso em: 1 maio. 2023.

NEVE, S. De; PANNIER, J.; HOFMAN, G. **Temperature effects on C-and N-mineralization from vegetable crop residuesPlant and Soil**. [s.l: s.n.].

O'DELL, C. W.; CONNOR, B.; BÖSCH, H.; O'BRIEN, D.; FRANKENBERG, C.; CASTANO, R.; CHRISTI, M.; ELDERING, D.; FISHER, B.; GUNSON, M.; MCDUFFIE, J.; MILLER, C. E.; NATRAJ, V.; OYAFUSO, F.; POLONSKY, I.; SMYTH, M.; TAYLOR, T.; TOON, G. C.; WENNBERG, P. O.; WUNCH, D. The ACOS CO₂ retrieval algorithm – Part 1: Description and validation against synthetic observations. **Atmospheric Measurement Techniques**, [s. l.], v. 5, n. 1, p. 99–121, 2012.

POGGIO, L.; DE SOUSA, L. M.; BATJES, N. H.; HEUVELINK, G. B. M.; KEMPEN, B.; RIBEIRO, E.; ROSSITER, D. SoilGrids 2.0: Producing soil information for the globe with quantified spatial uncertainty. **Soil**, [s. l.], v. 7, n. 1, p. 217–240, 2017.

REEVES, G. D.; MCADAMS, K. L.; FRIEDEL, R. H. W.; O'BRIEN, T. P. Acceleration and loss of relativistic electrons during geomagnetic storms. **Geophysical Research Letters**, [s. l.], v. 30, n. 10, 2003.

REICHSTEIN, M.; BAHN, M.; CIAIS, P.; FRANK, D.; MAHECHA, M. D.; SENEVIRATNE, S. I.; ZSCHEISCHLER, J.; BEER, C.; BUCHMANN, N.; FRANK, D. C.; PAPALE, D.; RAMMIG, A.; SMITH, P.; THONICKE, K.; VAN DER VELDE, M.; VICCA, S.; WALZ, A.; WATTENBACH, M. **Climate extremes and the carbon cycle**, 2013.

REICHSTEIN, M.; FALGE, E.; BALDOCCHI, D.; PAPALE, D.; AUBINET, M.; BERBIGIER, P.; BERNHOFER, C.; BUCHMANN, N.; GILMANOV, T.; GRANIER, A.; GRÜNWALD, T.; HAVRÁNKOVÁ, K.; ILVESNIEMI, H.; JANOUS, D.; KNOHL, A.; LAURILA, T.; LOHILA, A.; LOUSTAU, D.; MATTEUCCI, G.; MEYERS, T.; MIGLIETTA, F.; OURCIVAL, J. M.; PUMPANEN, J.; RAMBAL, S.; ROTENBERG, E.; SANZ, M.; TENHUNEN, J.; SEUFERT, G.; VACCARI, F.; VESALA, T.; YAKIR, D.; VALENTINI, R. **On the separation of net ecosystem exchange into assimilation and ecosystem respiration: Review and improved algorithm**, 2005.

RUSSO, S.; SILLMANN, J.; FISCHER, E. M. Top ten European heatwaves since 1950 and their occurrence in the coming decades. **Environmental Research Letters**, [s. l.], v. 10, n. 12, 2015.

SEDDON, N.; SMITH, A.; SMITH, P.; KEY, I.; CHAUSSON, A.; GIRARDIN, C.; HOUSE, J.; SRIVASTAVA, S.; TURNER, B. Getting the message right on nature-based solutions to climate change. **Global Change Biology**, [s. l.], v. 27, n. 8, p. 1518–1546, 2021. Disponível em: <https://onlinelibrary.wiley.com/doi/full/10.1111/gcb.15513>. Acesso em: 21 maio. 2024.

SELLERS, P. J.; DICKINSON, R. E.; RANDALL, D. A.; BETTS, A. K.; HALL, F. G.; BERRY, J. A.; COLLATZ, G. J.; DENNING, A. S.; MOONEY, H. A.; NOBRE, C. A.; SATO, N.; FIELD, C. B.; HENDERSON-SELLERS, A. Modeling the Exchanges of Energy, Water, and Carbon Between Continents and the Atmosphere. **Science**, [s. l.], v. 275, n. 5299, p. 502–509, 1997. Disponível em: <https://www.science.org/doi/10.1126/science.275.5299.502>. Acesso em: 22 fev. 2024.

SIABI, Z.; FALAHATKAR, S.; ALAVI, S. J. Spatial distribution of XCO2 using OCO-2 data in growing seasons. **Journal of Environmental Management**, [s. l.], v. 244, n. January, p. 110–118, 2019.

SIERRA, J. **Nitrogen mineralization and nitrification in a tropical soil: effects of fluctuating temperature conditions**. [s.l: s.n.]. Disponível em: <www.elsevier.com/locate/soilbio>.

SMITH, P.; ADAMS, J.; BEERLING, D. J.; BERINGER, T.; CALVIN, K. V; FUSS, S.; GRISCOM, B.; HAGEMANN, N.; KAMMANN, C.; KRAXNER, F.; MINX, J. C.; POPP, A.; RENFORTH, P.; VICENTE, J. L. Land-Management Options for Greenhouse Gas Removal and Their Impacts on Ecosystem Services and the Sustainable Development Goals. **Annual Review ofEnvironment and Resources**, [s. l.], 2019.

SOILGRIDS250M2.0. **SoilGrids250m 2.0**. 2022. Disponível em: <https://soilgrids.org/>. Acesso em: 5 ago. 2022.

SOMKUTI, P.; O'DELL, C. W.; CROWELL, S.; KÖHLER, P.; MCGARRAGH, G. R.; CRONK, H. Q.; BURGH, E. B. Solar-induced chlorophyll fluorescence from the Geostationary Carbon Cycle Observatory (GeoCarb): An extensive simulation study. **Remote Sensing of Environment**, [s. l.], v. 263, n. June, 2021.

SOUZA, L. De; SARAGOSA, F.; MIGUEL, L.; ODORIZZI, M.; RODRIGO, A.; ANTONIO, C.; LA, N.; JR, S. ScienceDirect Atmospheric concentrations of CH 4 in central-western areas of Brazil for 2009 – 2019 using GOSAT satellite. **Advances in Space Research**, [s. l.], n. xxxx, 2025. Disponível em: <https://doi.org/10.1016/j.asr.2025.01.058>

TANG, X.; PEI, X.; LEI, N.; LUO, X.; LIU, L.; SHI, L.; CHEN, G.; LIANG, J. Global patterns of soil autotrophic respiration and its relation to climate, soil and vegetation characteristics. **Geoderma**, [s. l.], v. 369, 2020.

TODD, M. C.; KIDD, C.; KNIVETON, D.; BELLERBY, T. J. A Combined Satellite Infrared and Passive Microwave Technique for Estimation of Small-Scale Rainfall. **JOURNAL OF ATMOSPHERIC AND OCEANIC TECHNOLOGY**, [s. l.], 2001.

WAN, Z., S. HOOK, G. H. **MOD11A2 MODIS/Terra Land Surface Temperature/Emissivity 8-Day L3 Global 1km SIN Grid V006. 2015, distributed by NASA EOSDIS Land Processes DAAC**. 2015.

WANG, C.; CAJA, J.; GÓMEZ, E. Comparison of methods for outlier identification in surface characterization. **Measurement: Journal of the International Measurement Confederation**, [s. l.], v. 117, n. December 2017, p. 312–325, 2018. Disponível em: <https://doi.org/10.1016/j.measurement.2017.12.015>

WANG, G.; CAI, W.; SANTOSO, A. Simulated Thermocline Tilt Over the Tropical Indian Ocean and Its Influence on Future Sea Surface Temperature Variability. **Geophysical Research Letters**, [s. l.], v. 48, n. 6, 2021.

WANG, Y.; GAO, S.; LI, C.; ZHANG, J.; WANG, L. Effects of temperature on soil organic carbon fractions contents, aggregate stability and structural characteristics of humic substances in a Mollisol. **Journal of Soils and Sediments**, [s. l.], v. 16, n. 7, p. 1849–1857, 2016.

WOODALL, C. W.; DOMKE, G. M.; MACFARLANE, D. W.; OSWALT, C. M. Forests and climate change: forcings, feedbacks, and the climate benefits of forests. **Forestry - Institute of Foresters of Great Britain.**, [s. l.], v. 85, n. 1, p. 1444–1449, 2012.

YAN, Y.; WANG, J.; TIAN, D.; ZHANG, R.; SONG, L.; LI, Z.; NIU, S. Heterotrophic respiration and its proportion to total soil respiration decrease with warming but increase with clipping. **Catena**, [s. l.], v. 215, 2022.

YANG, W.; TAN, B.; HUANG, D.; RAUTIAINEN, M.; SHABANOV, N. V.; WANG, Y.; PRIVETTE, J. L.; HUEMMRICH, K. F.; FENSHOLT, R.; SANDHOLT, I.; WEISS, M.; AHL, D. E.; GOWER, S. T.; NEMANI, R. R.; KNYAZIKHIN, Y.; MYNENI, R. B. MODIS leaf area index products: From validation to algorithm improvement. **IEEE Transactions on Geoscience and Remote Sensing**, [s. l.], v. 44, n. 7, p. 1885–1896, 2006.

ZEMP, D. C.; SCHLEUSSNER, C. F.; BARBOSA, H. M. J.; HIROTA, M.; MONTADE, V.; SAMPAIO, G.; STAAL, A.; WANG-ERLANDSSON, L.; RAMMIG, A. Self-amplified Amazon forest loss due to vegetation-atmosphere feedbacks. **Nature Communications**, [s. l.], v. 8, 2017.

ZHANG, W.; LUO, G.; YUAN, X.; LI, C.; XIE, M.; WANG, Y.; MA, X.; SHI, H.; HAMDI, R.; HELLWICH, O.; MA, X.; TERMONIA, P.; DE MAEYER, P. New data-driven method for estimation of net ecosystem carbon exchange at meteorological stations effectively increases the global carbon flux data. **Methods in Ecology and Evolution**, [s. l.], v. 14, n. 9, p. 2449–2463, 2023.

ZHANG, Z.; ZIMMERMANN, N. E.; CALLE, L.; HURTT, G.; CHATTERJEE, A.; POULTER, B. Enhanced response of global wetland methane emissions to the 2015-2016 El Niño-Southern Oscillation event. **Environmental Research Letters**, [s. l.], v. 13, n. 7, 2018.

ZHU, X.; CHEN, J.; GAO, F.; CHEN, X.; MASEK, J. G. An enhanced spatial and temporal adaptive reflectance fusion model for complex heterogeneous regions. **Remote Sensing of Environment**, [s. l.], v. 114, n. 11, p. 2610–2623, 2010.

ZILBER, S. N.; KOGA, E. The carbon credits market in Brazil and the role of intermediary agents: challenges and opportunities. **Organizações Rurais e Agroindustriais**, [s. l.], v. 13, n. 1, p. 139–153, 2011.

CHAPTER 4 – SPATIAL VARIABILITY OF ATMOSPHERIC CO_2, SOIL CARBON STOCKS AND CONTROL VARIABLES IN THE CERRADO, ATLANTIC FOREST, CAATINGA AND PAMPA BIOMES OF BRAZIL

Abstract: Agriculture, land-use change, and deforestation are responsible for over 70% of CO_2-equivalent emissions in Brazil. Agriculture holds an ambiguous position in the context of climate change: while it is impacted by climate-related events, it also has the potential to act as a mitigation mechanism through carbon sequestration. This study aimed to: (i) identify the main factors influencing atmospheric CO_2 emissions and soil organic carbon (SOC) stocks in Brazilian biomes - Atlantic Forest, Cerrado, Caatinga, and Pampa; and (ii) map priority areas for emission control and mitigation, as well as for climate resilience strategies. Time series data (2015–2019) of xCO_2 and environmental variables were analyzed. Results indicated that temperature was the primary factor associated with xCO_2 variations across all biomes. Surface temperature amplitude, influenced by temperature and land use, was also relevant, especially in the Cerrado. Considering the projected 1.5 °C increase in global average temperature, the results enabled the identification of carbon risk zones in soils already storing carbon, encompassing approximately 35% of the Caatinga, 24% of the Cerrado, 15.9% of the Atlantic Forest, and 20.3% of the Pampa. These risk zones concentrate between 15% and 26.5% of the total carbon stored in the studied biomes. These findings highlight the urgent need for strategies to protect already sequestered carbon and to strengthen regional climate resilience, preventing soil organic carbon from being released into the atmosphere as CO_2.

Keywords: Emissions mitigation; Climate resilience; Sustainable agriculture; Decarbonization; Carbon capture

1. Introduction

Global greenhouse gas (GHG) emissions continue to rise rapidly, reaching 36.3 billion tons of CO_2 in 2022 (FRIEDLINGSTEIN et al., 2022; IPCC, 2022, 2021). These emissions drive global warming and lead to extreme events and biodiversity loss (GERDOL et al., 2008; IPCC, 2017; SESSO et al., 2023). Although agriculture is vulnerable to climate change, it can also play a mitigating role (HOWE, 2015; KEELING et al., 1976) through atmospheric CO_2 capture and sustainable soil management.

Practices such as crop rotation, no-till farming, and regenerative agriculture contribute to reducing CH_4 and N_2O emissions (CAMPOS et al., 2022; WEBB et al., 2016; TUNNICLIFFE et al., 2020), while also promoting soil carbon stabilization, the main terrestrial carbon reservoir (BAUMGÄRTNER et al., 2021; GHELLER et al., 2019). On the other hand, unsustainable agricultural practices accelerate the mineralization of organic matter and the release of stored soil organic carbon as CO_2 into the atmosphere (NEVE et al., 1996; FIGUEIREDO et al., 2017).

Given the vastness and ecological diversity of Brazilian biomes, remote sensing emerges as a strategic tool to map vulnerabilities and opportunities related to land use, vegetation, and soil carbon across the country (CAMPOS et al., 2022; MARIA et al., 2023). Combined with statistical tools, it allows the identification of spatial and temporal patterns of carbon sequestration and emission, offering scientific support for mitigation and adaptation policies to climate change (MOUSAVI et al., 2017; YU et al., 2019).

Thus, the guiding question of this study was: which are the key climate variables and soil characteristics, evaluated at a large scale for each biome, that most influence atmospheric CO_2 concentrations and soil organic carbon stocks?

As working hypotheses, this study proposed: (i) to identify and describe the behavior of important environmental variables that control atmospheric CO_2 concentrations and SOC stocks in the studied biomes; and (ii) to visualize and characterize spatial patterns of climate, vegetation and soil within the biomes, providing valuable insights to map areas of greater climate vulnerability.

Therefore, the objectives of this study were: (i) to investigate the main drivers of atmospheric CO_2 emissions and soil carbon stocks in the Atlantic Forest, Cerrado, Caatinga, and Pampa biomes; and (ii) to map and identify potential zones of climate vulnerability, as well as priority areas for mitigation and climate resilience strategies.

2. Materials and Methods

2.1. Study Area

Brazil has different biomes, each with particular characteristics of vegetation, climate, soil and biodiversity. Figure 6 sought to highlight the entire Brazilian territory and its political division into states, also highlighting the four biomes focused on in this work: Cerrado, Caatinga, Atlantic Forest and Pampa.

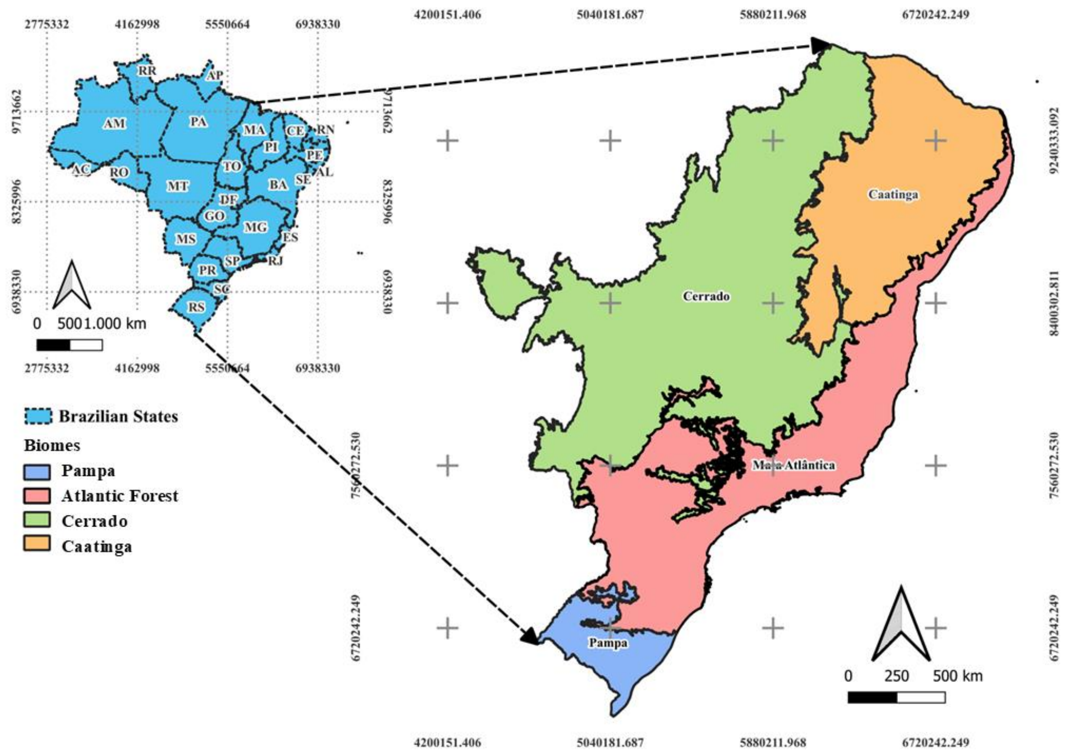

Figure 6: Brazil and the respective biomes studied: Atlantic Forest, Cerrado, Caatinga and Pampa.

According to the Köppen classification, the Cerrado has a seasonal tropical climate, with a rainy season between November and April and a dry season from May to October, and average annual temperatures above 22°C (ALVARES et al., 2013; BECK et al., 2018; MACENA et al., 2008; NASCIMENTO et al., 2021). The Caatinga has a semi-arid climate, with scarce and irregular rainfall, a prolonged dry season, and average temperatures above 25°C (ALVARES et al., 2013; FRANCISCO et al., 2020).

The Atlantic Forest has humid tropical and subtropical climates, with rainfall well distributed throughout the year and temperatures generally above 20°C, varying according to latitude and altitude (ALVARES et al., 2013; CARDOSO, 2016; BUYSSE et al., 2013). The Pampa has a humid subtropical climate, with well-defined seasons, mild summers (~22°C) and cold winters, with averages below 18°C (ALVARES et al., 2013; BECK et al., 2018; IBGE, 2020).

2.2. Data collection and variables studied

2.2.1. Determination of Carbon variables: xCO_2 ppm and Soil Organic Carbon (mean of 0 - 30cm t ha^{-1})

The variable xCO_2 (ppm) represents the average column concentrations of atmospheric CO_2, collected in this study over a complete 5-year time series, from January 2015 to December 2019. The xCO_2 data were obtained from NASA's OCO-2 (Orbiting Carbon Observatory-2) satellite (CRISP et al., 2012; O'DELL et al., 2012), available through the platform: https://search.earthdata.nasa.gov/Search. The data were corrected for the global trend of increasing CO_2, and the spatial distribution maps were generated using geo-statistical Kriging analysis based on pixel-specific values.

Soil carbon stock (mean 0–30 cm, t ha^{-1}) was obtained from the SoilGrids250m 2.0 platform (https://soilgrids.org/). The data are provided as maps with a spatial resolution of 250 meters (SOILGRIDS250m2.0, 2022). According to Poggio et al., (2017), these maps were developed using machine learning models, primarily Logistic Regression and Random Forest (HENGL et al., 2017).

The input data used by researchers to train these models are based on real-world datasets published by the scientific community over time, consisting of approximately 110.000 field observations collected globally (COOPER et al., 2005; HENGL et al., 2014; POGGIO et al., 2017).

2.2.2. Determination of vegetative variables: SIF (Wm^{-2} sr^{-1} μm^{-1}), NDVI, and LAI (m^2 m^{-2})

The SIF (Solar-Induced Fluorescence) variable is a measure of the radiation emitted by chlorophyll in plants during photosynthesis (YU et al., 2019). This variable was collected from the NASA OCO-2 service (SIABI et al., 2019). The algorithm used to determine this variable takes into account the intensity and spectral distribution of incident solar radiation, and spectral characteristics of radiation reflected by the Earth's surface (SHEKHAR et al., 2020; SIABI et al., 2019; YU et al., 2019).

In this work, the SIF (W m^{-2} sr^{-1} μm^{-1}) was processed from the removal of negative values, and subsequently the correction analysis, equation 4, proposed by Yu et al., (2019), was Applied:

$$SIF = \frac{SIF757 + 1.5\,SIF771}{2} \qquad \text{eq.4}$$

Where: SIF (W m^{-2} sr^{-1} μm^{-1}) represents the Solar-Induced Chlorophyll Fluorescence; SIF 757 refers to the solar-induced chlorophyll fluorescence at 757 nm; and SIF 771 refers to the solar-induced chlorophyll fluorescence at 771 nm.

The Normalized Difference Vegetation Index (NDVI) and Leaf Area Index (LAI) were obtained from NASA's AρρEEARS platform (APPEEARS, 2022), and are derived from remote sensing data collected by satellites such as MODIS (Moderate Resolution Imaging Spectroradiometer) onboard the Terra and Aqua satellites (HOTT et al., 2019; HUETE et al., 2002; MURADYAN et al., 2019; YANG et al., 2006).

NDVI is calculated using the red and near-infrared (NIR) spectral bands from the MODIS sensor (NAGLER et al., 2007). NDVI values range from -1 to 1, where values close to 1 indicate areas with high densities of healthy vegetation, and values near 0 indicate bare soil or sparse vegetation cover (HOTT et al., 2019).

LAI is calculated from spectral characteristics of vegetation captured by satellite imagery, representing the total leaf surface area per unit of ground area (CLEUGH et al., 2007; MYNENI et al., 2019). The algorithms account for light absorption by leaves, canopy geometry, and light interaction with the land surface, and are later validated using field data collected from multiple regions around the world (HOTT et al., 2019; HUETE et al., 2002; MURADYAN et al., 2019; YANG et al., 2006).

2.2.3. Determination of Climate Variables

For the Climatic variable group, precipitation (mean/annual) and 2-meter air temperature (mean/annual) were obtained from the NASA POWER platform ("NASA POWER," 2023), and were determined based on a combination of observational data and atmospheric models (CHOUDHURY, 1987; HUMPHREY et al., 1996; TODD et al., 2001).

Soil variables, including Soil Moisture Active Passive (SMAP) and Land Surface Temperature Amplitude (LST Amplitude), were collected from NASA's AρρEEARS platform (APPEEARS, 2022). These variables provide estimates of surface soil moisture on a global grid (DORIGO et al., 2013; MARIA et al., 2023) and soil thermal amplitude, calculated based on land surface temperature during the day (LST Day) and night (LST Night) (CAMPOS et al., 2022; FREITAS et al., 2013; MUTIIBWA et al., 2015).

LST Amplitude (°C) is derived from measurements made by Infrared Spectral Thermometers (IST) (MUTIIBWA et al., 2015), based on MODIS-EARTH data (APPEEARS, 2022). For its calculation, land surface temperatures during the day (LST Day) and night (LST Night) were recorded (ZHANG et al., 2014), and processed using the equation proposed by CAMPOS et al., (2022).

$$LST_{\,Amplitude}\ C° = (LST_{\,Day\ C°} - LST_{\,Night\ C°}) / n \quad \text{eq.5}$$

Onde: LST Day é a Temperatura da Superfície Terrestre durante a; LST Night é a Temperatura da Superfície Terrestre durante a noite; e n é o número de coletas mensais.

Such processing made it possible to obtain an average for each data collection point throughout the entire time series, capturing the variation in local soil temperature while summarizing the measurements over time (CAMPOS et al., 2022).

2.2.4. Standardization procedures for variables: First Group (spatiotemporal) and Second Group (only spatial)

The variables, along with their respective sources and characteristics, are summarized in Table 5. In general, this study employed two distinct groups of variables: the first group included variables with both spatial and temporal resolution, represented by vegetative, climatic, and soil variables, while the second group was composed of a single variable with only spatial resolution, namely the soil carbon stock data provided by the SoilGrids250m2.0 platform (SOILGRIDS250M2.0, 2022).

The spatial resolution of satellite data (latitude and longitude) for the xCO_2 variable was used as the standard reference for collecting all other variables from the first group. This procedure was adopted to standardize the different spatial resolutions among the variables analyzed (CAMPOS et al., 2022).

The first group of variables was processed to convert its spatio-temporal characteristics into a dataset with purely spatial dimensions. This transformation involved processing xCO_2, climate, vegetation, and soil data into annual means for each satellite-derived latitude and longitude coordinate, which were then processed using kriging.

These annual means were used to summarize the 5-year time series into annual averages at each satellite sampling point, while the kriging interpolation was used to homogenize the data into uniformly sized pixels. As a result, all variables, both from the first and second groups, were standardized in terms of their spatial dimension.

Table 5: Source, Temporal and spatial resolution of the variables studied: Carbon, Climate and Vegetation variables

Variables	Group	Data	Source	Spatial Resolution (km^2)	Temporal Resolution (days)
Carbon					
	1	xCO_2 (ppm)	NASA OCO-2	1.0 x 2.25	16
	2	Stock organic carbon (t ha^{-1} 0 -30cm)	SoilGrids250m	0.25 x 0.29	-
Vegetative					
	1	SIF (Wm^{-2} sr^{-1} m^{-1})	OCO-2	1.0 x 2.25	16
	1	NDVI	AρρEEARS	0.5 x 0.5	16
	1	LAI (m^2 m^{-2})	AρρEEARS	0.5 x 0.5	8
Climate					
	1	Temperature (°C)	NASA Power	1.1 x 1.1	30
	1	Precipitation (mm)	NASA Power	1.1 x 1.1	30
Soil					
	1	LST Amplitude (°C)	AρρEEARS	1.0 x 1.0	8
	1	SMAP (m^3 m^{-3})	NASA Power	9.0 x 9.0	30

Figure 7 illustrates the data processing workflow used for generating the kriging maps and subsequently collecting standardized data. Group 1, consisting of spatio-temporal variables, included SMAP, LST Amplitude, precipitation, temperature, LAI, NDVI, and SIF. In contrast, Group 2, containing a purely spatial variable, includes data on soil organic carbon stock from SOILGRIDS 250M 2.0.

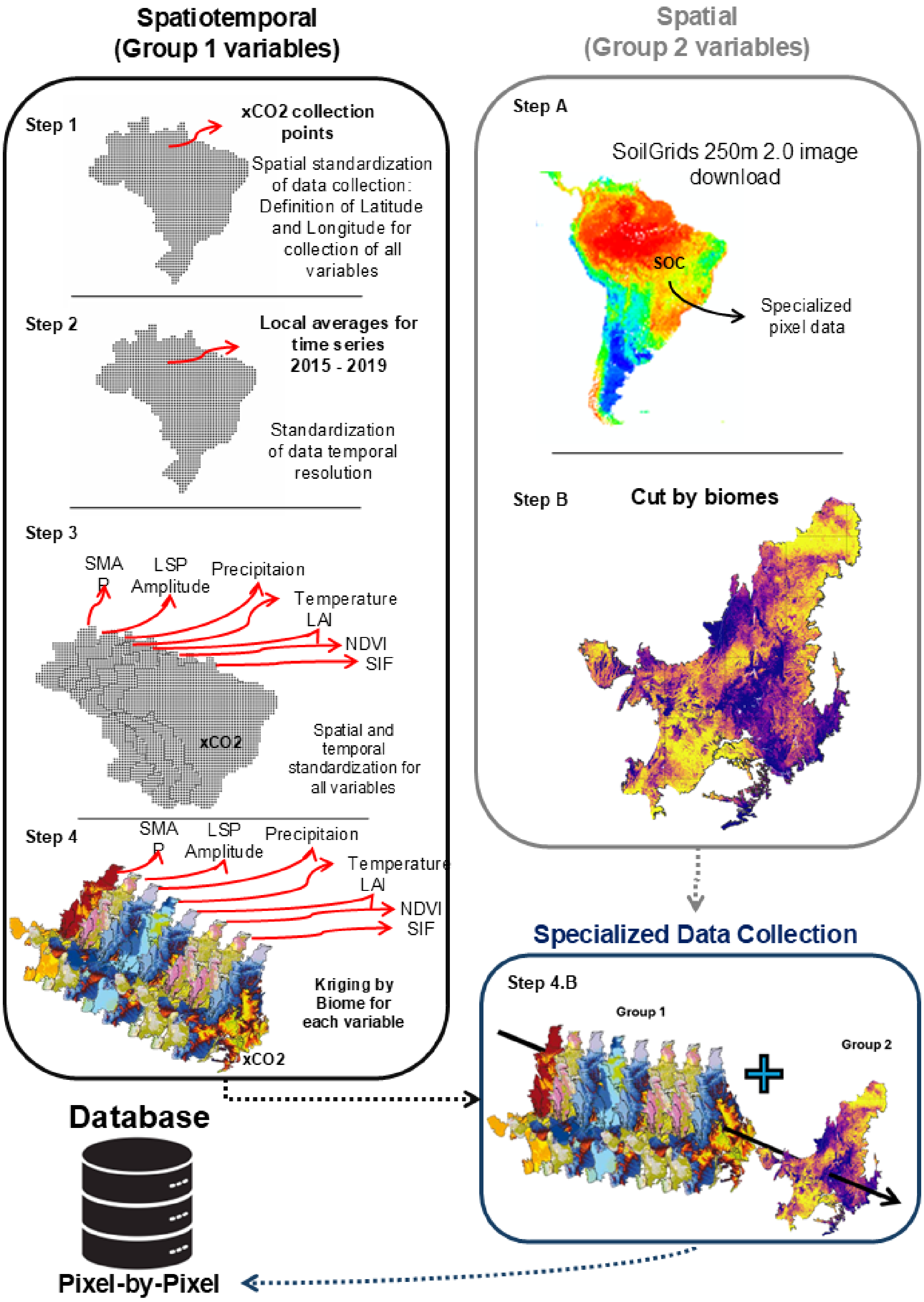

Figure 7: Data processing flow and pairing of Group 1 and 2 maps.

Before conducting the statistical analyses, the assumptions of normality, homoscedasticity and skewness were tested to ensure the reliability of the results.

2.2.5. Flowchart and Statistical Data Analysis

To analyze xCO_2 and all other variables, normality tests, homoscedasticity tests, and histogram evaluations were performed for all variables studied (CAMPOS et al., 2008; MCNAMARA, 2019; WANG et al., 2018). Data analysis and geoprocessing were conducted using R software version 4.0.4 (MCNAMARA, 2019) and QGIS 3.26.1 (QGIS 3.26.1, 2022), respectively.

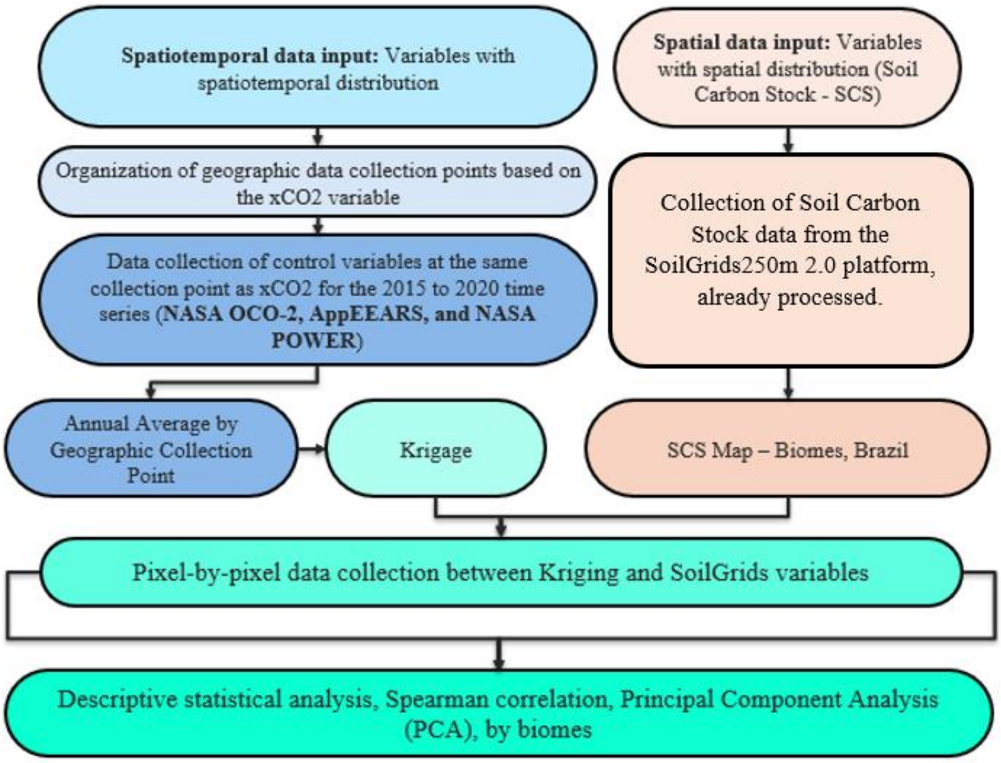

Figure 8: Flowchart for data collection and processing: approaches, preparation, treatment and statistical manipulation

Regarding data processing, outliers were suspended for the development of kriging in order to preserve the spatial integrity of the original information. However, for Spearman's statistical analysis, these extreme values were excluded using the interquartile range (IGR) identification method to ensure the robustness of the statistical analyses (WANG et al., 2018).

2.3. Geostatistical Analysis Using Ordinary Kriging

In this study, ordinary kriging, a geostatistical regression method, was employed to analyze the spatial dependence of environmental variables in the

Cerrado, Atlantic Forest, and administrative regions of Minas Gerais biomes. Ordinary kriging is a spatial interpolation technique that estimates unknown values at unsampled locations based on the spatial correlation structure of the observed data (PEREIRA et al., 2004).

To model spatial dependence, we constructed experimental semivariograms (CAMPOS et al., 2008; VIEIRA et al., 1983). The degree of spatial dependence (SD) was classified according to the criteria proposed by Cambardella et al. (1994): strong (0–25%), moderate (25–75%) and weak (75–100%).

Three theoretical semivariogram models, spherical, exponential and Gaussian, were tested and fitted to the data, allowing an accurate spatial representation and interpretation of the underlying spatial structure (CAMBARDELLA et al., 1994; CAMPOS et al., 2008; PEREIRA et al., 2004; SILVA et al., 2007).

2.4. 2.5.3. Stepwise Analysis Combined with Principal Component Analysis (PCA)

Principal Component Analysis (PCA) was used in combination with Stepwise regression analysis to address multicollinearity and optimize the selection of explanatory variables. Multicollinearity occurs when two or more independent variables present strong linear relationships, which can compromise the reliability and interpretability of regression models. Before performing PCA, all variables were standardized to ensure that the analysis was not biased by differences in units or magnitudes.

After removing highly collinear variables, identified in PCA by the proximity and orientation of their vectors, it was possible to identify the most relevant climate, vegetation and soil variables to explain the behavior of the dependent variable, xCO_2 and SOC.

Stepwise regression, in turn, is a variable selection method that iteratively adds or removes predictors based on statistical criteria, allowing the identification of the variables that best explain the dependent variable of interest for this work.

2.5. Determining Soil Carbon Risk Zones in Future Scenarios of Global +1.5°C Mean Rise

According to the Sixth Assessment Report of the IPCC (Working Group I), global warming of +1.5 °C is projected to be reached or exceeded within the next two decades, anticipating the impacts of climate change (IPCC, 2022b). In this context, mapping areas with high soil organic carbon (SOC) stocks that are already exposed to elevated temperatures is strategic for guiding resilience, adaptation, and climate mitigation actions.

The scenarios were defined based on the interaction among environmental variables selected through Stepwise regression and Spearman correlation analyses, which showed significant direct or inverse relationships with SOC stocks.

Thus, for each biome, risk zones were defined as the set of pixels considering: (i) variables selected by Stepwise that are directly proportional to SOC with values above the fourth quartile; and (ii) variables selected by Stepwise that are inversely proportional to SOC with values below the second quartile. Simultaneously, to simulate the warming projected by the IPCC, mean temperature was included as an additional risk criterion whenever its values exceeded the fourth quartile, regardless of the direction of its correlation with SOC.

In this way, the risk zones represent regions where environmental conditions significantly favor the persistence of soil organic carbon, but which are already subjected to high temperatures within the context of each biome. Considering the projected average warming of +1.5 °C, these areas are likely to experience even greater thermal pressure, potentially compromising the stability of the currently stored SOC.

For each biome, the SOC was treated as a dependent variable, and its relationship with the main independent environmental variables. The direction of the correlation (direct or inverse) between the SOC and each variable was established based on Sperman correlation analysis.

To define the risk thresholds, a classification based on quantiles was applied. Variables positively correlated with the SOC were considered at risk when below the 2nd quartile, while variables negatively correlated with the SOC were considered critical when projected above the 4th quartile in the warming scenario. Each simulation reflects the climatic thresholds under which the stability of the SOC may be compromised for each biome.

On the other hand, in the case of air temperature, although the correlation with soil organic carbon (SOC) was inversely proportional, meaning that higher temperatures tend to be associated with lower SOC stocks, it was decided to simulate its impact using values above the 4th quartile. This methodological decision was made to reflect worst-case scenario projections, consistent with a +1.5°C increase in global mean temperature, as indicated by the IPCC.

Thus, it was possible to identify areas with high concentrations of SOC, which coexist side by side with environmental indicators capable of helping to preserve the amount of carbon already present in the soil, but which have also been experiencing temperatures above the 4th quartile. Therefore, in conditions of +1.5°C, these areas will be directly impacted, as their exposure to even higher temperatures will increase even further.

3. Results

3.1. Geostatistical analysis by Kriging on the Cerrado, Caatinga, Atlantic Forest and Pampa

Table 6 presents descriptive statistics for the variables studied, prior to the geostatistical Kriging processing. Such analyses allow us to summarize and describe the main characteristics of a set of data studied in each biome.

Table 6: *Descriptive statistics of the studied variables segmented according to the biomes studied, before the geostatistical Kriging processing.*

Variable	Unit	mean	SD[1]	SE[2]	Median	Man[3]	Max[4]
				Pampa			
xCO_2	ppm	400,11	3,30	0,050	400,60	367,85	413,14
SIF	$Wm^{-2}\ sr^{-1}\ \mu m^{-1}$	0,79	0,83	0,014	0,58	0,00	10,43
NDVI	-	0,63	0,14	0,002	0,65	0,00	0,94
LAI	$m^2\ m^{-2}$	1,51	1,11	0,018	1,32	0,00	6,75
Temp.	°C	18,79	0,85	0,111	18,79	17,42	20,76
Precip.	mm	121,74	12,40	1,610	123,24	97,86	144,70
LSTAmp.	°C	14,51	1,53	0,064	14,31	11,53	19,49
SMAP	$m^3\ m^{-3}$	0,72	0,05	0,006	0,74	0,58	0,79
				Caatinga			

xCO_2	ppm	401,25	2,63	0,020	401,40	379,42	415,32
SIF	$Wm^{-2}\ sr^{-1}\ \mu m^{-1}$	0,57	0,52	0,004	0,45	0,00	20,81
NDVI	-	0,48	0,18	0,001	0,45	0,00	0,92
LAI	$m^2\ m^{-2}$	1,27	0,80	0,006	1,05	0,00	6,40
Temp.	°C	26,60	1,43	0,093	26,91	22,01	29,13
Precip.	mm	46,42	11,62	0,759	44,48	21,08	79,25
LSTAmp.	°C	22,04	1,70	0,033	22,08	14,33	27,28
SMAP	$m^3\ m^{-3}$	0,53	0,08	0,005	0,54	0,25	0,65
		Mata Atlântica					
xCO_2	ppm	399,95	3,97	0,031	400,59	361,82	416,96
SIF	$Wm^{-2}\ sr^{-1}\ \mu m^{-1}$	0,92	1,08	0,008	0,67	0,00	36,34
NDVI	-	0,66	0,15	0,001	0,69	0,00	0,93
LAI	$m^2\ m^{-2}$	2,23	1,51	0,011	1,82	0,00	6,92
Temp.	°C	21,81	2,44	0,131	22,03	15,81	26,58
Precip.	mm	99,98	23,35	1,260	97,47	44,75	147,58
LSTAmp.	°C	10,41	3,69	0,029	9,94	0,00	35,60
SMAP	$m^3\ m^{-3}$	0,64	0,08	0,004	0,65	0,44	0,82
		Cerrado					
xCO_2	ppm	401,26	3,05	0,017	401,63	354,64	415,82
SIF	$Wm^{-2}\ sr^{-1}\ \mu m^{-1}$	0,73	0,82	0,005	0,56	0,00	32,02
NDVI	-	0,61	0,09	0,001	0,61	0,05	0,91
LAI	$m^2\ m^{-2}$	1,72	0,94	0,005	1,55	0,00	6,70
Temp.	°C	25,80	2,02	0,082	25,66	19,58	29,28
Precip.	mm	82,66	15,07	0,612	85,11	40,31	127,04
LSTAmp.	°C	12,50	4,75	0,027	11,77	0,00	41,37
SMAP	$m^3\ m^{-3}$	0,54	0,11	0,004	0,56	0,30	0,72

1 - Standard Deviation; 2 – Standard Error; 3 – Minimum; 4 – Maximum

Table 7 presents the results obtained from semivariogram modeling for Kriging analysis and also shows the spatial dependence of the variables within each biome. In Kriging analysis, the Nugget/Sill ratio indicates the proportion between the minimum spatial variation (Nugget) and the total variance (Sill), representing the fraction of spatial variation not explained by the model (CAMBARDELLA et al., 1994). A high ratio therefore suggests a poor model fit to the data, while a low ratio indicates a good fit (CAMBARDELLA et al., 1994).

Table 7: Kriging analysis for xCO_2 (ppm) and other control variables, based on georeferenced averages of the collected data.

Variable	Nugget (C_0)	Contribution (C1)	Level (C_0+C1)	Sweep (km)	Nugget % $C_0/(C_0+C_1)$	SD[1]	Model
			Pampa				
xCO_2	1,50	0,50	2,00	150	75%	Low	Exp.

SIF	0,60	0,10	0,70	500	86%	Low	Exp.
NDVI	0,01	0,01	0,02	500	59%	Moderate	Exp.
LAI	0,80	0,40	1,20	100	67%	Moderate	Exp.
Temp.	0,10	0,20	0,30	200	33%	Moderate	Gau.
Precip.	5,00	150,00	200,00	120	25%	Hight	Sph.
LSTAmp	0,70	1,00	1,70	90	41%	Moderate	Exp.
SMAP	0,001	0,001	0,002	150	33%	Moderate	Gau.
			Caatinga				
xCO_2	6,00	1,00	7,00	100	86%	Low	Exp.
SIF	0,25	0,05	0,30	200	83%	Low	Exp.
NDVI	0,03	0,01	0,03	200	83%	Low	Sph
LAI	0,50	0,10	0,60	100	83%	Low	Exp.
Temp.	0,20	1,00	1,20	200	17%	Hight	Gau
Precip.	20,00	130,00	150,00	200	13%	Hight	Sph.
LSTAmp.	1,40	1,60	3,00	200	47%	Moderate	Exp.
SMAP	0,002	0,004	0,006	200	33%	Moderate	Sph.
			Mata Atlântica				
xCO_2	15,00	1,00	16,00	500	94%	Low	Sph.
SIF	1,00	0,50	1,50	150	67%	Moderate	sph
NDVI	0,02	0,01	0,02	500	75%	Low	Exp.
LAI	1,50	1,00	2,50	500	60%	Moderate	Gau
Temp.	0,50	1,50	2,00	500	25%	Hight	Exp.
Precip.	10,00	140,00	150,00	500	07%	Hight	Exp.
LSTAmp.	10,00	5,00	15,00	900	67%	Moderate	Sph.
SMAP	0,001	0,003	0,004	500	25%	Hight	Sph.
			Cerrado				
xCO_2	8,00	1,00	9,00	500	89%	Low	Sph.
SIF	0,60	0,20	0,80	100	75%	Low	Gau.
NDVI	0,01	0,00	0,01	200	80%	Low	Exp.
LAI	0,60	0,20	0,80	250	75%	Low	Exp.
Temp.	0,20	1,00	1,20	400	17%	Hight	Sph.
Precip.	20,00	130,00	150,00	500	13%	Hight	Sph.
LSTAmp.	20,00	5,00	25,00	150	80%	Low	Exp.
SMAP	0,002	0,008	0,010	500	20%	Hight	Sph

1 - Spatial Dependency

Figures 8 show maps generated by kriging. The colors represent interquartile ranges of xCO_2 concentration and the other variables studied. For xCO_2, the minimum class (dark blue) indicated values below 397 ppm, while the maximum class (dark red) presented values above 403 ppm.

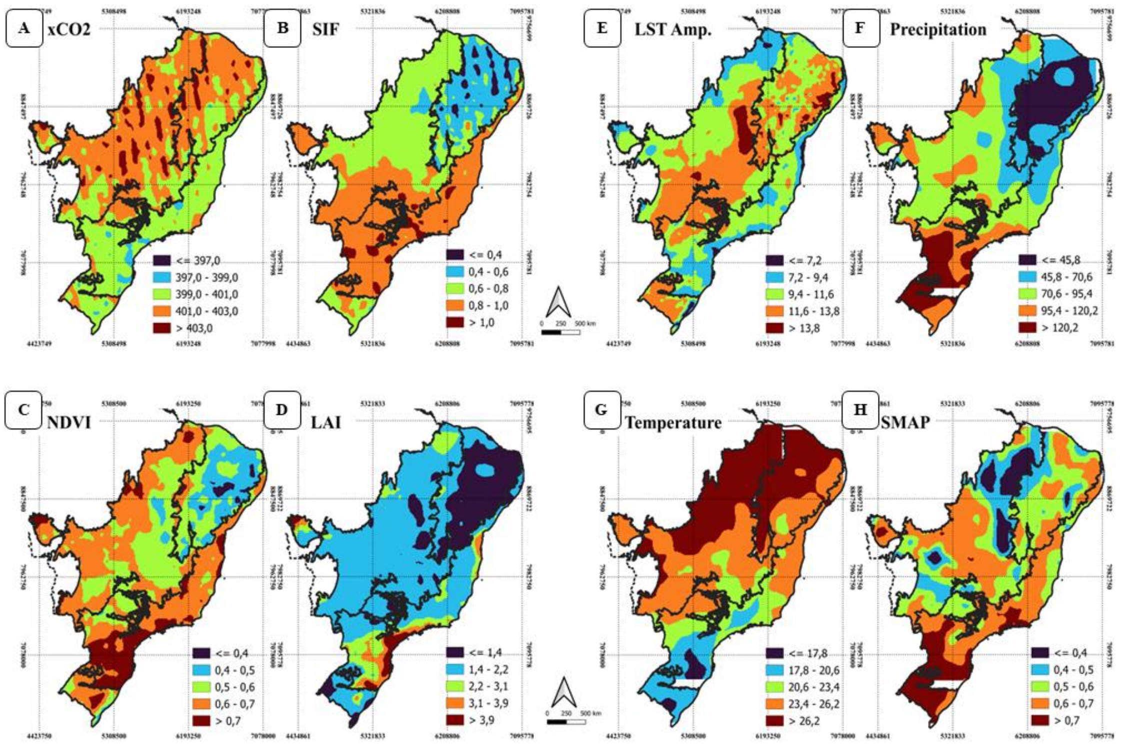

Figure 8. Maps generated from the interpolation of mean values of xCO_2 (ppm), SIF (Wm^{-2} sr^{-1} μm^{-1}), NDVI, LAI (m^2 m^{-2}), LST Amplitude (°C), Precipitation (mm), Temperature (°C), and SMAP (m^3 m^{-3}).

Figures 8 show the spatial variation of environmental variables. For SIF, NDVI, and LAI, the lowest classes (dark blue) had mean values below 0.4 Wm^{-2} sr^{-1} μm^{-1}, 0.4, and 1.4 m^2/m^2, respectively, while the highest classes (dark red) exceeded 1.0, 0.7, and 3.9. LST Amplitude ranged from less than 7.2°C to more than 13.8°C; precipitation from less than 45.8 mm to more than 120.2 mm; temperature from less than 17.8°C to more than 26.2°C; and SMAP from less than 0.4 m^3/m^3 to more than 0.7 m^3/m^3.

Figures 9 were developed to individually represent the statistical spatialization derived from Kriging for all variables and biomes analyzed. These maps were created to visualize the specific nuances of each biome. To achieve this, a color classification method based on interquartile differences was adopted.

In the Caatinga biome, xCO_2 values ranged from 400.72 to 402.39 ppm. SIF fluctuated from <0.43 to >0.62 Wm^{-2} sr^{-1} μm^{-1}, NDVI from <0.45 to >0.55, and LAI from <1.08 to >1.51. LST Amplitude ranged between 10.56°C and

12.65°C, while temperature varied from 37.14°C to 51.82°C. Precipitation ranged from 25.35 to 27.58 mm, and SMAP from 0.47 to 0.59 m³/m³.

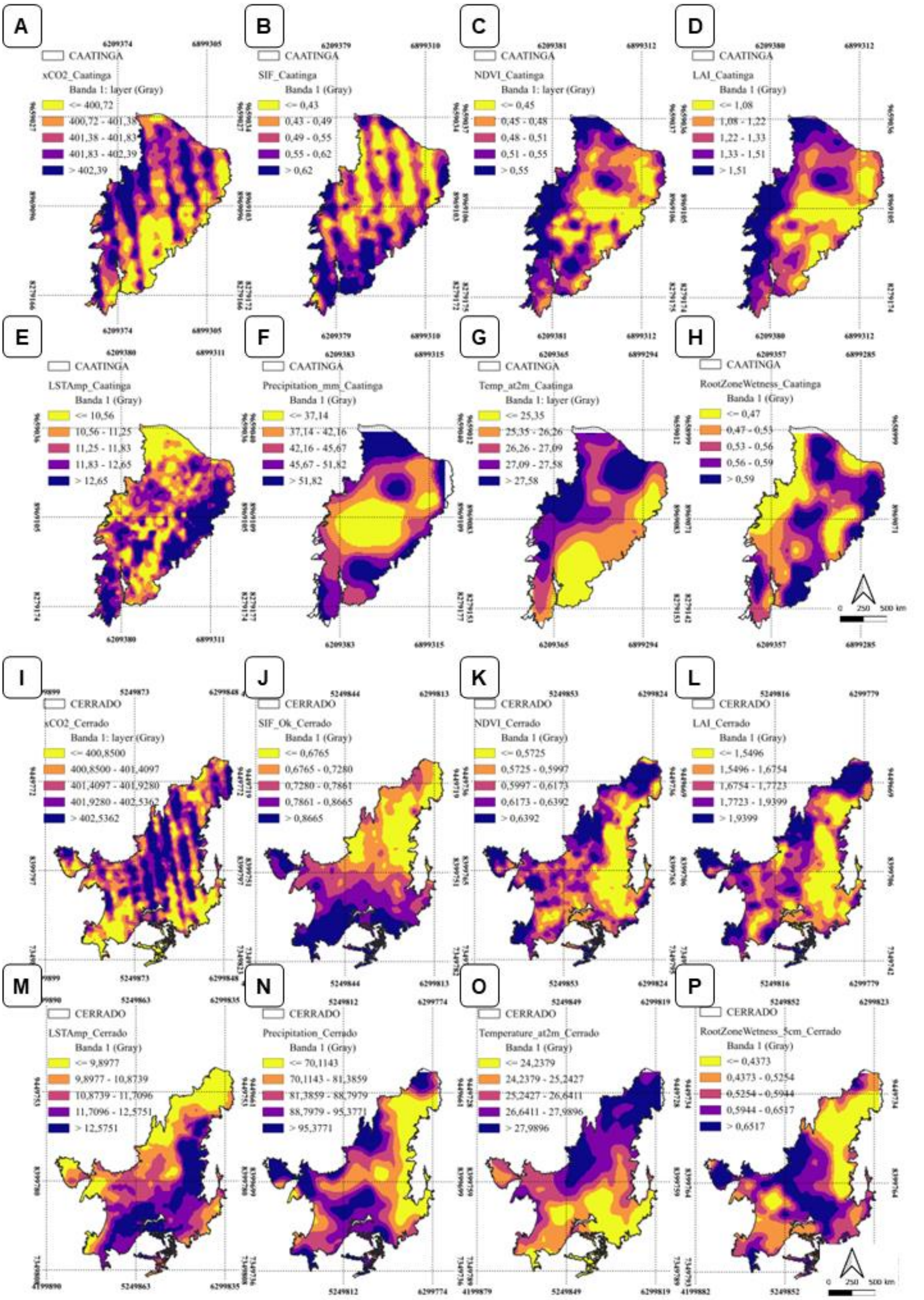

Figure 9: Geospatialization by Kriging for mean values per satellite collection point, for the Caatinga and Cerrado Biomes. For the Caatinga biome: (A) xCO_2, (B) SIF (Solar-Induced Fluorescence), (C) NDVI (Normalized Difference Vegetation Index), (D) LAI (Leaf Area Index), (E) LST Amplitude (Land Surface Temperature Amplitude), (F) Precipitation, (G) Temperature at

2 meters, and (H) Root Zone Wetness. For the Cerrado biome: (I) xCO_2, (J) SIF (Solar-Induced Fluorescence), (K) NDVI, (L) LAI, (M) LST Amplitude, (N) Precipitation, (O) Temperature at 2 meters, and (P) Root Zone Wetness.

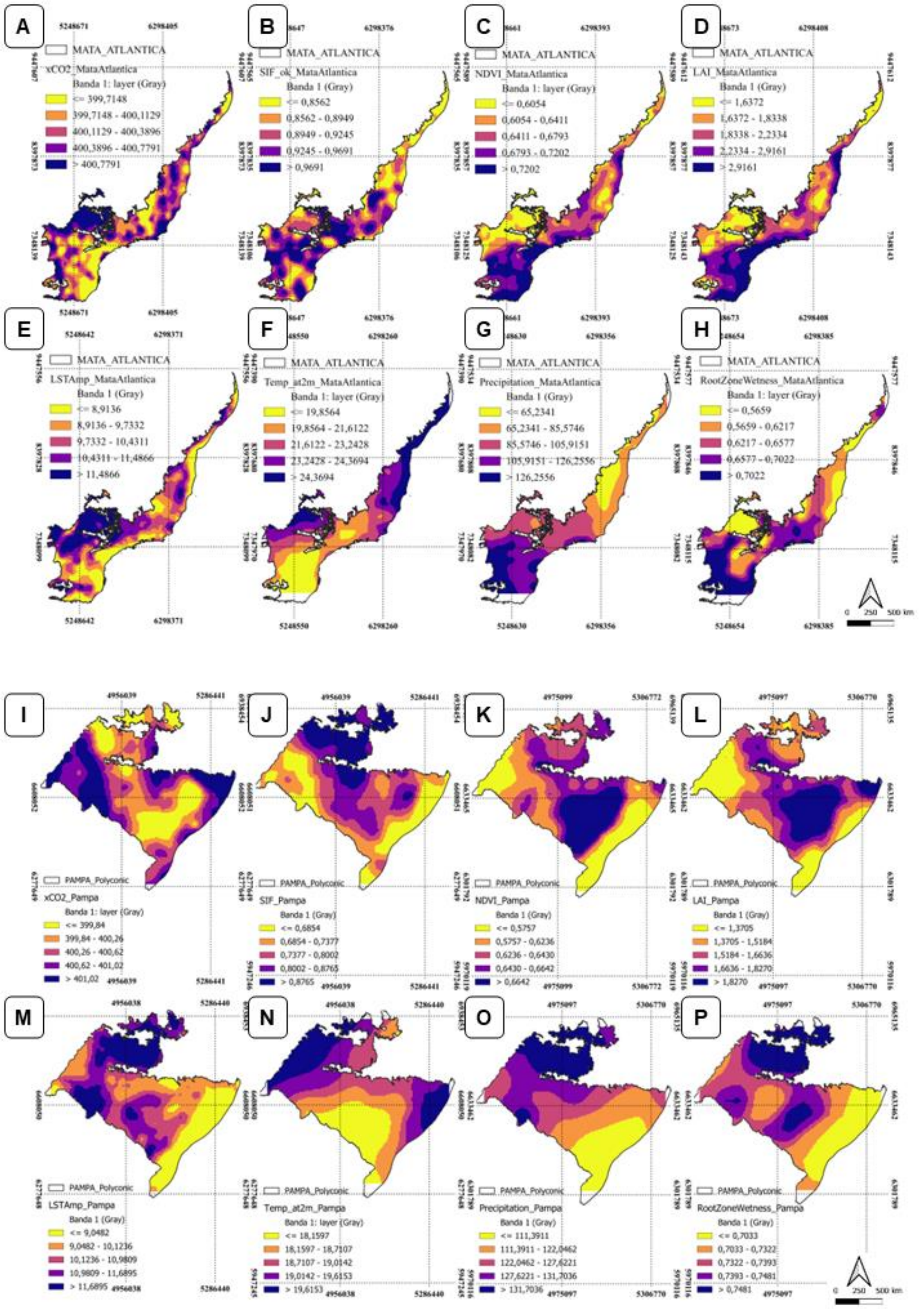

Figure10: Geospatialization by Kriging for mean values per satellite collection point, for the Atlantic Forest and Pampa Biomes. For the Atlantic Forest biome: (A) xCO_2, (B) SIF (Solar-Induced Fluorescence), (C) NDVI (Normalized Difference Vegetation

Index), (D) LAI (Leaf Area Index), (E) LST Amplitude (Land Surface Temperature Amplitude), (F) Temperature at 2m, (G) Precipitation, and (H) Root Zone Wetness. For the Pampa biome: (I) xCO_2, (J) SIF, (K) NDVI, (L) LAI, (M) LST Amplitude, (N) Temperature at 2m, (O) Precipitation, and (P) Root Zone Wetness.

In the Cerrado biome, xCO_2 values ranged from <400.85 to >402.36 ppm. SIF fluctuated between 0.67 and >0.86 Wm^{-2} sr^{-1} μm^{-1}, NDVI from <0.57 to >0.64, and LAI from <1.55 to >1.84 m^2/m^2. LST Amplitude varied from 9.89°C to 12.57°C, and temperature from 70.11°C to 95.37°C. Precipitation ranged from 24.23 to 27.98 mm, and SMAP from 0.43 to 0.56 m^3/m^3.

In the Atlantic Forest biome, xCO_2 ranged from <399.71 to >400.78 ppm. SIF fluctuated between <0.85 and >0.96 Wm^{-2} sr^{-1} μm^{-1}, NDVI from <0.60 to >0.72, and LAI from <1.63 to >2.91 m^2/m^2. LST Amplitude varied from 8.91°C to 11.48°C, while temperature ranged from 19.85°C to 24.36°C. Precipitation ranged from 65.23 to 126.25 mm, and SMAP from 0.56 to 0.70 m^3/m^3.

In the Pampa biome, xCO_2 ranged from <399.84 to >401.02 ppm. SIF fluctuated between 0.68 and >0.87 Wm^{-2} sr^{-1} μm^{-1}, NDVI from <0.57 to >0.66, and LAI from <1.37 to >1.82 m^2/m^2. LST Amplitude varied from 9.04°C to 11.68°C, while temperature ranged from 18.15°C to 19.61°C. Precipitation varied from 111.39 to 127.30 mm, and SMAP from 0.703 to 0.748 m^3/m^3.

Figure 11 was developed to assist in visualizing the amounts of soil organic carbon stocks, color-coded and classified according to each biome. The data aimed to map the spatial variation of carbon stocks across the Cerrado, Caatinga, Atlantic Forest, and Pampa biomes in Brazil.

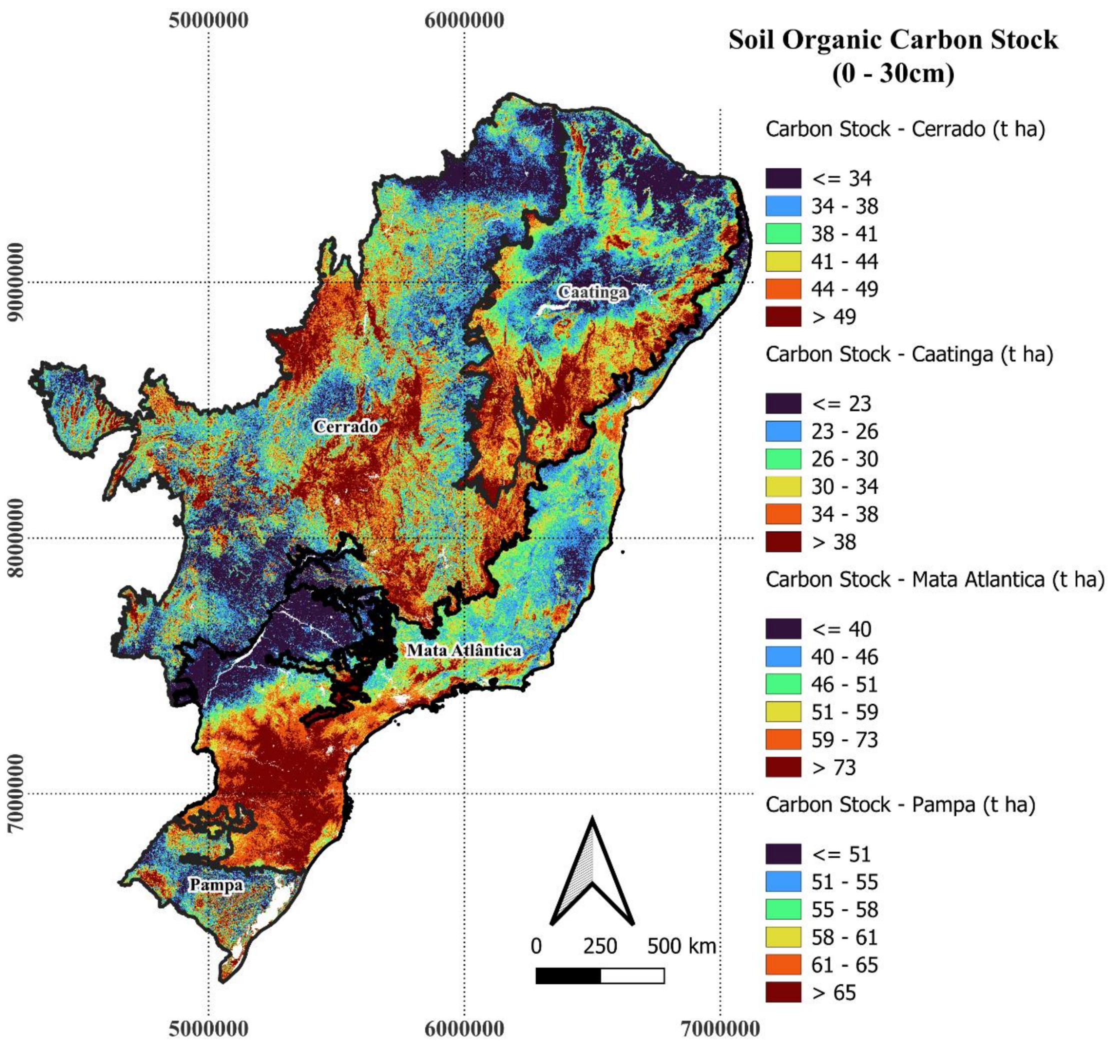

Figure 11: *Soil carbon stock map, organized by colors according to the difference between quarts, for data provided by the platform (SoilGrids250m2.0, 2022).*

Soil carbon stocks varied among biomes, with the Atlantic Forest standing out for presenting the greatest range between classes (40 to 73 t ha^{-1}; 33 t ha^{-1}), and the Pampa showing the smallest variation (51 to 65 t ha^{-1}; 14 t ha^{-1}), but with the highest absolute values. In the Cerrado, stocks ranged from 34 to 49 t ha^{-1}, while in the Caatinga, they ranged from 23 to 38 t ha^{-1}.

The correlation analysis was performed using pixel-level data generated after the geospatialization of the variables. The results are shown in Figure 10, aiming to identify whether there is an association between the variables, as well as the direction and strength of this association. xCO_2 showed a moderate negative correlation with SMAP (–0.37), SIF (–0.54), and precipitation (–0.36). Temperature exhibited a strong positive correlation with xCO_2 (0.62), suggesting that increased temperatures favor higher atmospheric CO_2 concentrations.

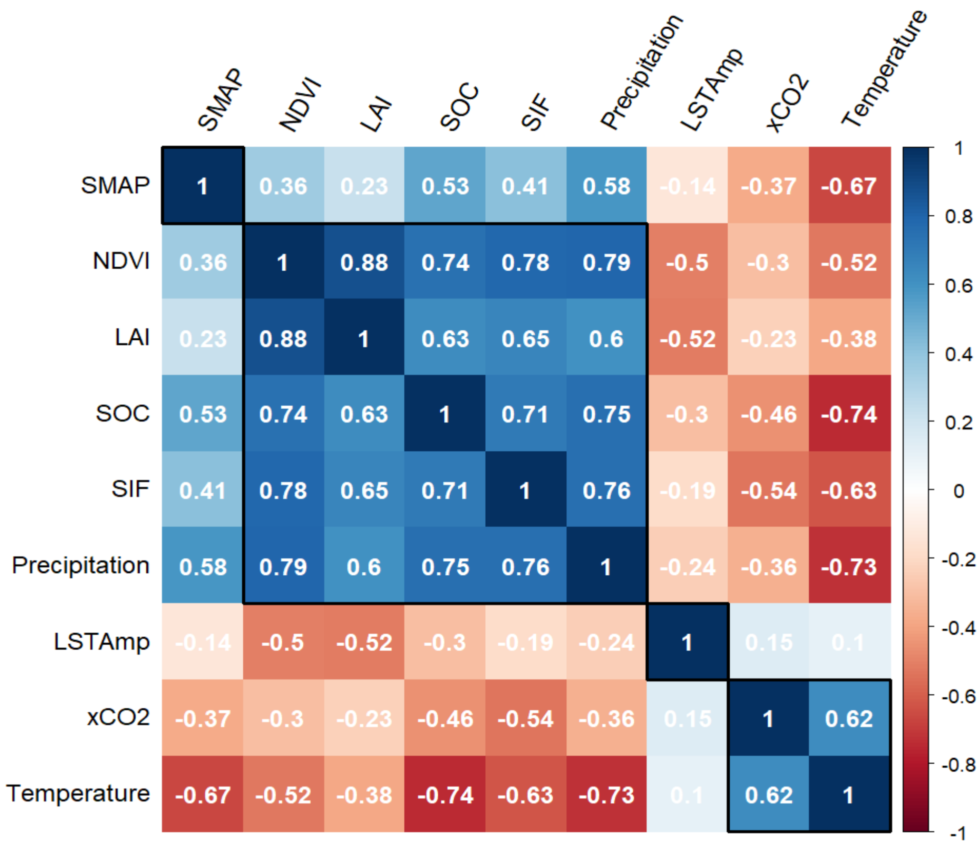

Figure 92: Spearman correlation analysis, developed with the pixel values produced from the spatialization of the variables studied.

SOC showed a strong negative correlation with temperature (–0.76) and a positive correlation with precipitation (0.76). Vegetation-related variables were also positively correlated with SOC, such as SIF (0.68) and LAI (0.60). xCO_2 had a moderate negative correlation (–0.46). Among the soil-related variables, SMAP showed a moderate positive correlation (0.54), while LST Amplitude had a moderate negative correlation (–0.34).

Figure 13 shows the results of the Principal Component Analysis (PCA), which was used to assess multicollinearity among variables and improve the Stepwise model fitting. The first two components explained 69.0% of the total data variance, with 54.3% attributed to Dim1 and 14.7% to Dim2, adequately representing the data structure in two dimensions.

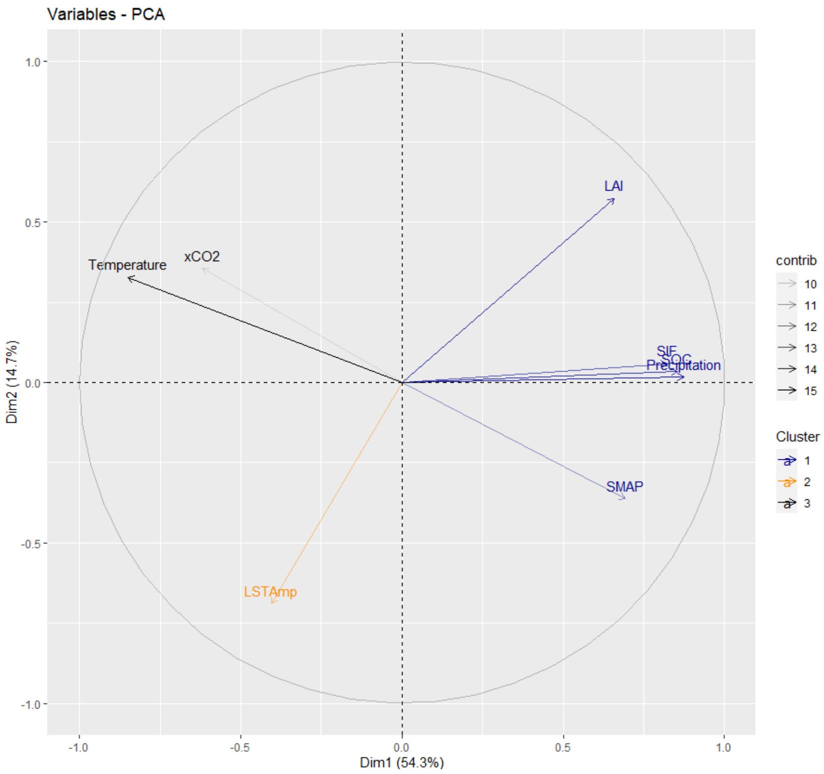

Figure 13: Principal Component Analysis with data after Kriging.

The PCA analysis, combined with Spearman correlation, indicated collinearity among SIF, SOC, and precipitation. To avoid interference in the Stepwise regression, SIF and precipitation were excluded from the model, while SOC was retained as it is the central variable of interest in this study.

Stepwise analysis was used to identify, for each biome, the most relevant independent variables in explaining the dependent variables xCO_2 and SOC, allowing for the selection of predictors with greater statistical effectiveness.

Table 8: Results of the Stepwise analysis for each biome studied, as well as the set.

Variables		Parameters			
Dependent	**Independent**	**N° Variables**	**R^2**	**Adj. R^2**	**AIC**
	All biomes				
xCO_2	Temperature; LSTAmp; SMAP	3/5	0.40	0,4	0.60
SOC	Temperature; SMAP; LAI	3/5	0.69	0.69	0.30
	Cerrado				
xCO_2	Temperature; LSTAmp;	2/5	0.39	0.39	0.60
SOC	Temperature; LSTAmp; SMAP; LAI	4/5	0.69	0.69	0.30
	Caatinga				

xCO_2	Temperature; LSTAmp; SMAP	3/5	0.40	0.40	0.60
SOC	Temperature; SMAP; LAI	3/5	0.70	0.70	0.30
	Atlantic Forest				
xCO_2	Temperature	1/5	0.39	0.39	0.60
SOC	Temperature; LAI	2/5	0.68	0.68	0.31
	Pampa				
xCO_2	Temperature; LSTAmp	2/5	0.39	0.39	0.60
SOC	Temperature; SMAP; LAI	3/5	0.69	0.69	0.30

SMAP – Soil Moisture Accounting Procedure; LAI - Leaf Area Index; LSTAmp – Land Surface Temperature Amplitude.

In the combined analysis of all biomes (Brazil), xCO_2 was best explained by three variables (Temperature, LST Amplitude, and SMAP), with R^2 = 0.40. For SOC, the model included Temperature, SMAP, and LAI, with R^2 = 0.69. In the Cerrado, xCO_2 was explained by Temperature and LST Amplitude (R^2 = 0.39), while SOC required four variables (Temperature, LST Amplitude, SMAP, and LAI), maintaining R^2 = 0.69.

In the Caatinga, xCO_2 was modeled by three variables (Temperature, LST Amplitude, and SMAP), with R^2 = 0.40, and SOC by Temperature, SMAP, and LAI (R^2 = 0.70). In the Atlantic Forest, xCO_2 had Temperature as the sole predictor (R^2 = 0.39), and SOC was explained by Temperature and LAI (R^2 = 0.68). Finally, in the Pampa, xCO_2 was explained by Temperature and LST Amplitude (R^2 = 0.39), while SOC was modeled by Temperature, SMAP, and LAI (R^2 = 0.69), a pattern similar to that observed in the other biomes.

3.2. Determining Soil Carbon Risk Zones in Future Scenarios of Global +1.5°C Mean Rise

Table 8 was developed to characterize the scenarios projected by the IPCC involving a +1.5°C temperature increase. These scenarios, in turn, indicate areas potentially vulnerable to climate change, with a focus on soil organic carbon in the 0–30 cm layer.

Table 9: Soil Carbon Risk Zones under Future Scenarios of +1.5°C Global Mean Rise.

Variable		Correlation trend	Selection reference quartile (Q)	Simulation	Unit
Dependent	Independent				
		Cerrado			
SOC	Temperature;	Inversely proportional	+ 1.5 °C (IPCC)	> 26,64	°C
	LSTAmp;	Inversely proportional	< 2° Q	< 9,89	°C
	SMAP;	Directly proportional	> 4° Q	> 0,59	$m^3\ m^{-3}$
	LAI	Directly proportional	> 4° Q	> 1,77	$m^2\ m^{-2}$
		Caatinga			
SOC	Temperature;	Inversely proportional	+ 1.5 °C (IPCC)	> 27,09	°C
	SMAP;	Directly proportional	> 4° Q	> 0,56	$m^3\ m^{-3}$
	LAI	Directly proportional	> 4° Q	> 1,08	$m^2\ m^{-2}$
		Atlantic Forest			
SOC	Temperature;	Inversely proportional	+ 1.5 °C (IPCC)	> 23,24	°C
	LAI	Directly proportional	> 4° Q	> 2.23	$m^2\ m^{-2}$
		Pampa			
SOC	Temperature;	Inversely proportional	+ 1.5 °C (IPCC)	> 19,01	°C
	SMAP;	Directly proportional	> 4° Q	> 0,70	$m^3\ m^{-3}$
	LAI	Directly proportional	> 4° Q	> 1,66	$m^2\ m^{-2}$

SMAP – Soil Moisture Accounting Procedure; LAI - Leaf Area Index; LSTAmp – Land Surface Temperature Amplitude.

The risk zone was therefore defined by the overlap of these criteria, reflecting areas with high carbon stocks and favorable conditions for carbon preservation, but that are currently exposed to high temperatures and are likely to face even more adverse thermal conditions in the near future.

4. Discussion

4.1. What are the main variables responsible for coordinating atmospheric CO_2 concentrations (xCO_2 ppm) and carbon stocks in the edaphoclimatic particularities of each biome in Brazil?

This study investigated the main factors influencing average atmospheric CO_2 concentrations (xCO_2) and soil organic carbon stocks (SOC, 0–30 cm) across four Brazilian biomes: Atlantic Forest, Cerrado, Caatinga, and Pampa. The analysis integrated remote sensing data and statistical methods (Spearman correlation, PCA, and Stepwise regression) to identify the key environmental drivers of these variables.

Temperature emerged as the most relevant factor, showing a negative correlation with SOC (–0.74) and a positive correlation with xCO_2 (0.62), reinforcing its influence on carbon emission and sequestration processes (DAVIDSON and JANSSENS, 2006; CHEN et al., 2021). LST Amplitude also stood out, particularly in the Cerrado, indicating that thermal variations in the soil directly affect the stability of organic carbon by influencing microbial activity and soil respiration (CAMPOS et al., 2022; YOUNESZADEH et al., 2015).

Vegetative variables such as SIF, NDVI, and LAI showed negative correlations with xCO_2, suggesting that increased photosynthetic activity helps reduce atmospheric CO_2 concentrations (SHEKHAR et al., 2020; ZHANG et al., 2016). This pattern is consistent with the seasonal dynamics of CO_2 described by KEELING et al., (1976), with higher carbon sequestration during the summer.

Soil moisture (SMAP) and precipitation also correlated positively with SOC and negatively with xCO_2, emphasizing the role of water in regulating photosynthesis and soil respiration (KONINGS et al., 2019; YAN et al., 2022). However, CO_2 emissions from soil respiration did not exceed plant carbon uptake, particularly under tropical conditions, as reported by CAMPOS et al., (2022) and MORAIS FILHO et al., (2021).

Stepwise analysis revealed temperature as the most effective variable in explaining both xCO_2 and SOC across all biomes. LST Amplitude also emerged as an important predictor in all biomes except the Atlantic Forest, where temperature alone explained 40% of the xCO_2 variation (R^2 = 0.40). These findings highlight the central role of temperature in carbon dynamics in tropical ecosystems (NEVE et al., 1996; WANG et al., 2016).

High SOC values were associated with lower soil thermal amplitudes, indicating that carbon-rich soils function as natural thermal insulators, retaining more moisture and stabilizing temperature (ACERO and GONZÁLEZ-ASENSIO, 2018; AMOOH et al., 2015). Additionally, the high specific heat of water retained in soils with higher carbon content contributes to reducing thermal fluctuations (GOMES and CLAVICO, 2005; MALONE et al., 2009).

The positive relationship between SOC and SMAP, and the negative relationship between SMAP and LST Amplitude, further reinforce the role of soil carbon in maintaining moisture and protecting against thermal stress (CHENG et al., 2021). This contributes to the stability of soil aggregates, reducing the availability of carbon for microbial decomposition (CHAPLOT and COOPER, 2015; CHENG et al., 2021).

Vegetation also plays a crucial role in both CO_2 capture and soil protection. Systems with high vegetation density promote shading, reduce evaporation, and enhance soil water and thermal retention (FREITAS et al., 2013; ANKENBAUER and LOHEIDE, 2017). Soils with higher SOC provide better physical and chemical conditions, supporting plant growth and consequently atmospheric CO_2 sequestration (AMOOH et al., 2015; MORARU and TEODOR, 2005).

These mechanisms are reflected in the inverse correlation between SOC and xCO_2 (–0.46), suggesting that areas with higher soil carbon stocks also have greater capacity to remove CO_2 from the atmosphere (MOITINHO et al., 2015; CAMPOS et al., 2022). Moreover, integrated agricultural systems and healthy forests can enhance this effect by promoting shading, reducing thermal stress, and lowering soil respiration (CONCEIÇÃO et al., 2017; GIL et al., 2016).

In summary, temperature emerged as the main controlling variable for xCO_2 and SOC across all analyzed biomes, underscoring its critical influence on carbon emission and sequestration processes. These results highlight the importance of sustainable management strategies, soil and vegetation conservation, and the use of remote sensing for environmental monitoring and national-scale planning.

Given IPCC (2022b) projections indicating a +1.5 °C temperature increase in the coming decades, identifying areas with high SOC under thermal risk becomes essential., Regions already exhibiting temperatures above the fourth quartile, combined with high carbon stocks, should be prioritized for climate mitigation and resilience actions (ZEMP et al., 2017; WOODALL et al., 2012).

4.2. Priority areas for resilience mechanisms, CO_2 emissions mitigation and soil carbon stock protection

Based on the PCA, Stepwise, and Spearman correlation analyses, regions with high potential for soil organic carbon accumulation were identified, yet already exposed to elevated temperatures. This suggests an increasing climate risk under the +1.5 °C scenario projected by the IPCC (2022b, 2022c, 2023). Figure 15 illustrates zones with favorable conditions for the accumulation and maintenance of soil carbon stocks, but which are already experiencing high temperatures.

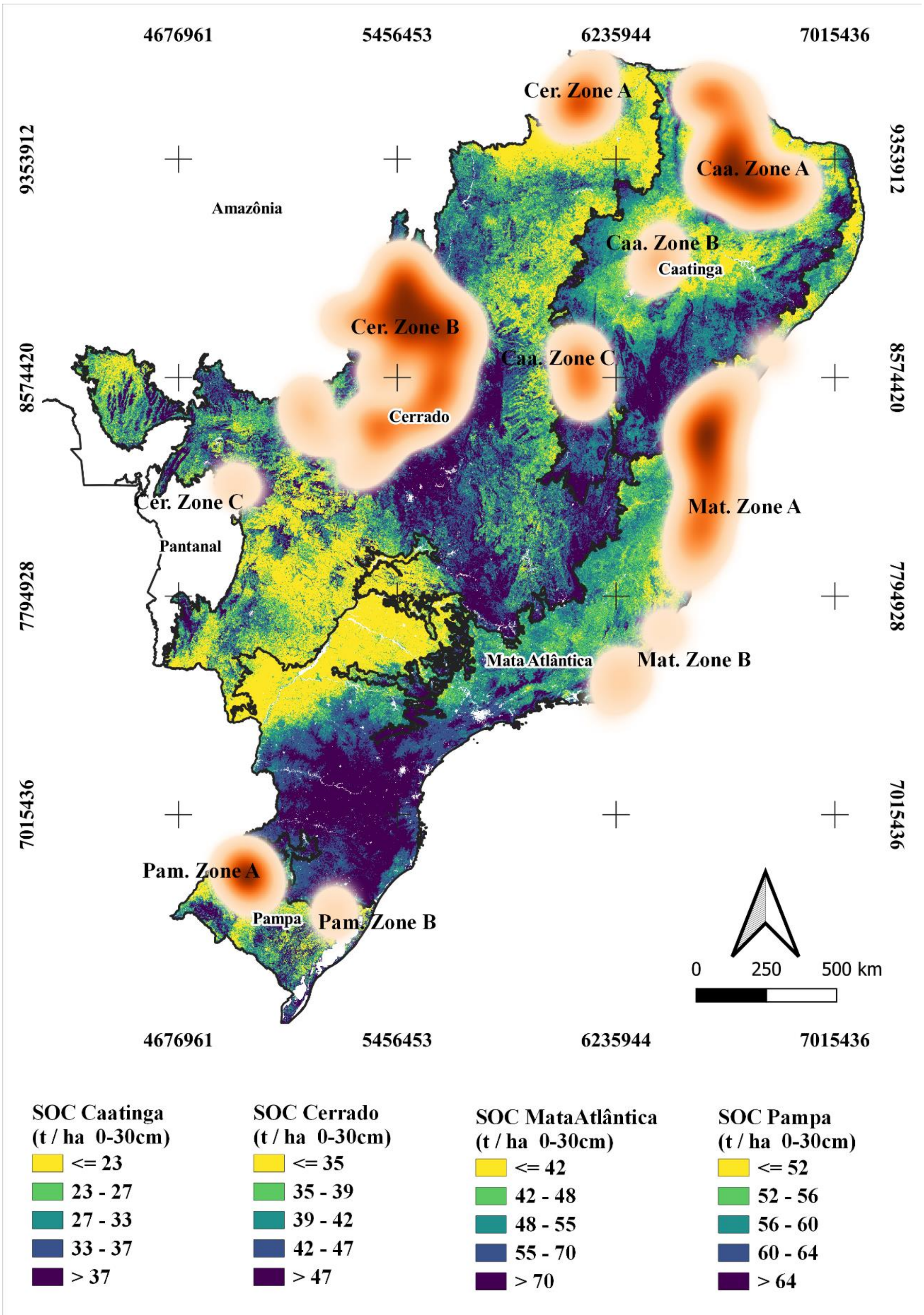

Figure 10: Soil carbon stock map (Soilgrids 250m 2.0), and in light red priority zones in each biome for adaptation and mitigation strategies.

The preservation of areas with high SOC is strategic, as carbon-rich soils contribute to thermal stability, water retention, and improved vegetative performance (AMOOH et al., 2015; MALONE et al., 2009), thereby enhancing photosynthesis and atmospheric CO_2 removal (SHEKHAR et al., 2020). However, if these same areas are exposed to high temperatures, they may lose their carbon stocks to the atmosphere as CO_2 through various mechanisms (IPCC, 2022a, 2022b).

Global warming directly impacts agriculture by reducing productivity, increasing evaporation, and intensifying pests and diseases (RUANE et al.,2018; IPCC, 2022b). C3 crops are particularly vulnerable to heat stress, whereas C4 crops tend to be more resilient (SILVEIRA and PEREZ, 2014). Moreover, soil degradation and aggregate instability, both intensified by high temperatures, compromise SOC stability (GMACH et al., 2020; WANG et al., 2016).

Climate resilience refers to the capacity to absorb, adapt, and transform in response to the impacts of climate change. Mitigation strategies include both emission reductions (e.g., sustainable land management, fire control) and carbon removals through vegetation and soil sequestration (ARORA, 2019; IPCC, 2022c). This study provides technical insights to support public policies and local actions aimed at promoting the sustainability of Brazilian biomes in the face of global climate change.

Table 9 presents a comparison of soil organic carbon stocks (t ha^{-1}, mean 0–30 cm) obtained from the SoilGrids250m 2.0 platform, between Brazilian biomes and the risk zones identified in the analysis developed in this study. Table 10 supported the quantification of SOC in tons per hectare, providing a clear overview of each biome's and each risk zone's capacity to sequester carbon.

Table 10: Characterization of risk zones compared to the carbon stock potential of each biome (Soilgrids250m 2.0).

Biomes and Risk Zone	Stock Organic Carbon t ha^{-1} (Mean 0 - 30cm)						Area	
	Min	Median	Mean	Max	Sum (million tons)	Carbon %	km²	%
Caatinga	10	30	30.63	111	419,7	100	844,453	100
Zone A	10	25	25.55	111	69,9	16.7	201,555	23.9
Zone B	16	23	23.6	46	12,3	2.9	44,846	5.3
Zone C	21	39	39.08	82	25,9	6.2	49,126	5.8
Total Zone					108,2	25.8	295,528	35.0
Pampa	30	58	58.31	130	159,8	100	176,496	100.0
Zone A	30	58	57.63	85	32,2	20.2	28,534	16.2

Zone B	41	54	55.43	91	7,7	4.8	7,249	4.1
Total Zone					39,9	25.0	35,782	20.3
Cerrado	13	41	41.35	158	1.279,4	100	2,036,448	100.0
Zone A	21	35	35.16	72	43,9	3.4	78,197	3.8
Zone B	22	43	44.22	123	277,9	21.7	392,794	19.3
Zone C	20	43	44.48	85	16,7	1.3	23,581	1.2
Total Zone					338,6	26.5	494,572	24.3
Atlantic Forest	14	51	55.20	221	934,1	100	1,110,182	100
Zone A	22	47	48.56	116	102,3	11.0	131,795	11.9
Zone B	27	49	51.82	121	37,5	4.0	45,245	4.1
Total Zone					139,9	15.0	177,040	15.9

Soil organic carbon accounts for approximately 25% of the potential of nature-based climate solutions, with an estimated mitigation potential of 23.8 $GtCO_2eq$/year, 40% through the protection of existing stocks and 60% through the restoration of degraded soils (BOSSIO et al., 2020). Its importance is especially notable in agricultural and pasture lands (47%) and wetlands (72%). Protecting current stocks and preventing their loss is essential for climate change mitigation (DAVIDSON and JANSSENS, 2006; FIGUEIREDO et al., 2017).

In this study, the Pampa biome presented the highest average SOC concentration (58.3 t ha^{-1}), followed by the Atlantic Forest (55.2 t ha^{-1}), Cerrado (41.3 t ha^{-1}), and Caatinga (30.6 t ha^{-1}), consistent with MAPBIOMAS (2022) data. In the Cerrado, about 22% of the total SOC (278 Mt C) is located in thermal risk zones, which could represent a potential release of 1.2 $GtCO_2eq$ if lost. In the Caatinga, 17% of its SOC is at risk, which could result in emissions of up to 397 $MtCO_2eq$. The Atlantic Forest and Pampa, with 11% and 20% of their stocks at risk, could release between 515 and 147 $MtCO_2eq$, respectively, if 10% of SOC in those areas were to be mineralized.

These potential losses are significant, considering that the land-use change and agriculture sectors are already the largest contributors to emissions in Brazil, accounting for 46% and 26% of total emissions, respectively (SEEG, 2022). Furthermore, the advancement of desertification in regions such as northern Cerrado and Caatinga exacerbates the risk of degradation

(TOMASELLA et al., 2018), compromising the ability of these ecosystems to function as carbon sinks.

Therefore, the zones mapped in this study require urgent attention for soil conservation, degradation prevention, and climate adaptation strategies to ensure the stability of carbon stocks and the resilience of Brazilian biomes in the face of climate change (AMOOH et al., 2015; CAMPOS et al., 2022; CHIA and LIM, 2022).

5. Conclusion

5.1. xCO_2 (ppm) and SOC (t ha-1 mean 0-30cm) and control variables for Brazilian biomes.

Temperature was the main explanatory variable for xCO_2 variations across all biomes, reinforcing its central role in carbon dynamics. Higher vegetation indices (SIF, NDVI, and LAI) were also associated with lower atmospheric CO_2 concentrations, highlighting the importance of vegetation in capturing this greenhouse gas.

LST Amplitude stood out in the Cerrado, revealing that soils with high carbon content exhibit lower thermal variation and greater moisture retention, key factors for climate resilience. This study underscores the need for integrated management strategies, such as the conservation of vegetated areas and the adoption of integrated agricultural systems.

5.2. Risk zones and climate resilience and mitigation mechanisms

According to the IPCC, a 1.5 °C increase in global average temperature poses a significant risk of releasing SOC as CO_2. In the Caatinga, 35% of the territory, where 25.8% of the SOC is concentrated, already experiences temperatures above the fourth quartile. In the Cerrado, this condition affects 24% of the area, which holds 26.5% of the stored carbon. In the Atlantic Forest, 15.9% of the territory (15% of SOC), and in the Pampa, 20.3% of the area (25% of SOC), are also under elevated thermal risk.

These data highlight the urgency of biome-specific strategies focused on SOC conservation, sustainable soil and vegetation management, and public policies that integrate both adaptation and mitigation. Such measures are essential to preserve biodiversity, maintain agricultural productivity, and prevent CO_2 emissions, thereby safeguarding climate resilience and the country's carbon footprint.

1. References

ABRAHÃO, R.; CARVALHO, M.; CAUSAPÉ, J. Carbon and water footprints of irrigated corn and non-irrigated wheat in Northeast Spain. **Environmental Science and Pollution Research**, v. 24, p. 5647-5653, 2017. DOI: https://doi.org/10.1007/s11356-016-8322-5.

ACERO, J. A.; GONZÁLEZ-ASENSIO, B. Influence of vegetation on the morning land surface temperature in a tropical humid urban area. **Urban Climate**, v. 26, p. 231-243, 2018. DOI: https://doi.org/10.1016/j.uclim.2018.09.004.

ALVARES, C. A.; STAPE, J. L.; SENTELHAS, P. C.; DE MORAES GONÇALVES, J. L.; SPAROVEK, G. Köppen's climate classification map for Brazil. **Meteorologische Zeitschrift**, v. 22, p. 711-728, 2013. DOI: https://doi.org/10.1127/0941-2948/2013/0507.

AMOOH, M.; AMOOH, M. K.; BONSU, M. Effects of soil texture and organic matter on evaporative loss of soil moisture. **Journal of Global Agriculture and Ecology**, 2015.

AN, Z.; BORK, E. W.; OLEFELDT, D.; CARLYLE, C. N.; CHANG, S. X. Simulated heat wave events increase CO_2 and N_2O emissions from cropland and forest soils in an incubation experiment. **Biology and Fertility of Soils**, v. 58, p. 789-802, 2022. DOI: https://doi.org/10.1007/s00374-022-01661-w.

ANKENBAUER, K. J.; LOHEIDE, S. P. The effects of soil organic matter on soil water retention and plant water use in a meadow of the Sierra Nevada, CA. **Hydrological Processes**, v. 31, p. 891-901, 2017. DOI: https://doi.org/10.1002/hyp.11070.

ARANTES CAMARGO, L.; MARQUES JÚNIOR, J.; TADEU PEREIRA, G.; ALVES HORVAT, R. Variabilidade espacial de atributos mineralógicos de um Latossolo sob diferentes formas do relevo. II - Correlação espacial entre mineralogia e agregados. [S. l.]: [s. n.], [s. d.].

ARORA, N. K. Impact of climate change on agriculture production and its sustainable solutions. **Environmental Sustainability**, v. 2, p. 95-96, 2019. DOI: https://doi.org/10.1007/s42398-019-00078-w.

ARTURSSON, T.; EKLÖV, T.; LUNDSTRÖM, I.; MÅRTENSSON, P.; SJÖSTRÖM, M.; HOLMBERG, M. Drift correction for gas sensors using multivariate methods. **Journal of Chemometrics**, v. 14, p. 711-723, 2000. DOI: https://doi.org/10.1002/1099-128X(200009/12)14:5/6<711::AID-CEM607>3.0.CO;2-4.

NASA. AppEEARS. Disponível em: https://appeears.earthdatacloud.nasa.gov/. Acesso em: 5 jul. 2022.

BALBINO, L. C.; CORDEIRO, L. A. M.; OLIVEIRA, P.; KLUTHCOUSKI, J.; GALERANI, P. R.; VILELA, L. Agricultura sustentável por meio da integração lavoura-pecuária-floresta (iLPF). Piracicaba: International Plant Nutrition Institute - Brasil, 2012.

BALL, B. C.; DOBBIE, K. E.; PARKER, J. P.; SMITH, K. A. The influence of gas transport and porosity on methane oxidation in soils. **Journal of Geophysical Research Atmospheres**, v. 102, p. 23301-23308, 1997. DOI: https://doi.org/10.1029/97jd00870.

BARRACHINA, M.; CRISTÓBAL, J.; TULLA, A. F. Estimating above-ground biomass on mountain meadows and pastures through remote sensing. **International Journal of Applied Earth Observation and Geoinformation**, v. 38, p. 184-192, 2015. DOI: https://doi.org/10.1016/j.jag.2014.12.002.

BECK, H. E.; ZIMMERMANN, N. E.; MCVICAR, T. R.; VERGOPOLAN, N.; BERG, A.; WOOD, E. F. Present and future Köppen-Geiger climate classification maps at 1-km resolution. **Scientific Data**, v. 5, p. 1-12, 2018. DOI: https://doi.org/10.1038/sdata.2018.214.

BLANCO-CANQUI, H.; LAL, R. Mechanisms of carbon sequestration in soil aggregates. **Critical Reviews in Plant Sciences**, v. 23, n. 6, p. 481-504, 2004. DOI: https://doi.org/10.1080/07352680490886842.

BOSSIO, D. A.; COOK-PATTON, S. C.; ELLIS, P. W.; FARGIONE, J.; SANDERMAN, J.; SMITH, P.; WOOD, S.; ZOMER, R. J.; VON UNGER, M.; EMMER, I. M.; GRISCOM, B. W. The role of soil carbon in natural climate solutions. **Nature Sustainability**, v. 3, p. 391-398, 2020. DOI: https://doi.org/10.1038/s41893-020-0491-z.

BRANDANI, C. B.; ABBRUZZINI, T. F.; CONANT, R. T.; CERRI, C. E. P. Soil organic and organomineral fractions as indicators of the effects of land management in conventional and organic sugar cane systems. **Soil Research**, v. 55, p. 145-161, 2017. DOI: https://doi.org/10.1071/SR15322.

BUNCE, J. A. Effects of humidity on photosynthesis. **Journal of Experimental Botany**, v. 35, n. 8, p. 1245-1251, 1984.

BUYSSE, P.; GOFFIN, S.; CARNOL, M.; MALCHAIR, S.; DEBACQ, A.; LONGDOZ, B.; AUBINET, M. Short-term temperature impact on soil heterotrophic respiration in limed agricultural soil samples. **Biogeochemistry**, v. 112, p. 441-455, 2013. DOI: https://doi.org/10.1007/s10533-012-9739-7.

CAMBARDELLA, C. A.; MOORMAN, T. B.; NOVAK, J. M.; PARKIN, T. B.; KARLEN, D. L.; TURCO, R. F.; KONOPKA, A. E. Field-scale variability of soil properties in Central Iowa soils. **Soil Science Society of America Journal**, v. 58, p. 1501-1511, 1994. DOI: https://doi.org/10.2136/sssaj1994.03615995005800050033x.

CAMPOS, M. O.; CERRI, C. E. P.; LA SCALA JÚNIOR, N. Atmospheric CO_2, soil carbon stock and control variables in managed and degraded pastures in central Brazil. **Remote Sensing Applications**, v. 28, 100848, 2022. DOI: https://doi.org/10.1016/j.rsase.2022.100848.

CARDOSO, J. T. A Mata Atlântica e sua conservação. [S. l.], 2016.

CENCI, D. R.; LORENZO, C. A mudança climática e o impacto na produção de alimentos: alguns elementos de análise da realidade brasileira e argentina. **Revista Direito em Debate**, v. 29, p. 32-43, 2020. DOI: https://doi.org/10.21527/2176-6622.2020.54.32-43.

CHAPIN, F. S.; WOODWELL, G. M.; RANDERSON, J. T.; RASTETTER, E. B.; LOVETT, G. M.; BALDOCCHI, D. D.; CLARK, D. A.; HARMON, M. E.; SCHIMEL, D. S.; VALENTINI, R.; WIRTH, C.; ABER, J. D.; COLE, J. J.; GOULDEN, M. L.; HARDEN, J.

W.; HEIMANN, M.; HOWARTH, R. W.; MATSON, P. A.; MCGUIRE, A. D.; MELILLO, J. M.; MOONEY, H. A.; NEFF, J. C.; HOUGHTON, R. A.; PACE, M. L.; RYAN, M. G.; RUNNING, S. W.; SALA, O. E.; SCHLESINGER, W. H.; SCHULZE, E. D. Reconciling carbon-cycle concepts, terminology, and methods. **Ecosystems**, v. 9, p. 1041-1050, 2006. DOI: https://doi.org/10.1007/s10021-005-0105-7.

CHAPLOT, V.; COOPER, M. Soil aggregate stability to predict organic carbon outputs from soils. **Geoderma**, v. 243-244, p. 205-213, 2015. DOI: https://doi.org/10.1016/j.geoderma.2014.12.013.

CHEN, Z.; LIU, J.; HENZE, D. K.; HUNTZINGER, D. N.; WELLS, K. C.; SITCH, S.; FRIEDLINGSTEIN, P.; JOETZJER, E.; BASTRIKOV, V.; GOLL, D. S.; HAVERD, V.; JAIN, A. K.; KATO, E.; LIENERT, S.; LOMBARDOZZI, D. L.; MCGUIRE, P. C.; MELTON, J. R.; NABEL, J. E. M. S.; POULTER, B.; TIAN, H.; WILTSHIRE, A. J.; ZAEHLE, S.; MILLER, S. M. Linking global terrestrial CO_2 fluxes and environmental drivers: inferences from the Orbiting Carbon Observatory 2 satellite and terrestrial biospheric models. **Atmospheric Chemistry and Physics**, v. 21, p. 6663-6680, 2021. DOI: https://doi.org/10.5194/acp-21-6663-2021.

CHENG, J.; YANG, Y.; YUAN, M. M.; GAO, Q.; WU, L.; QIN, Z.; SHI, Z. J.; SCHUUR, E. A. G.; COLE, J. R.; TIEDJE, J. M.; ZHOU, J. Winter warming rapidly increases carbon degradation capacities of fungal communities in tundra soil: potential consequences on carbon stability. **Molecular Ecology**, v. 30, p. 926-937, 2021. DOI: https://doi.org/10.1111/mec.15773.

CHIA, S. Y.; LIM, M. W. A critical review on the influence of humidity for plant growth forecasting. **IOP Conference Series: Materials Science and Engineering**, v. 1257, 012001, 2022. DOI: https://doi.org/10.1088/1757-899x/1257/1/012001.

CHOUDHURY, B. J. Relationships between vegetation indices, radiation absorption, and net photosynthesis evaluated by a sensitivity analysis. **Remote Sensing of Environment**, v. 22, n. 2, p. 139-155, 1987.

CLEUGH, H. A.; LEUNING, R.; MU, Q.; RUNNING, S. W. Regional evaporation estimates from flux tower and MODIS satellite data. **Remote Sensing of Environment**, v. 106, p. 285-304, 2007. DOI: https://doi.org/10.1016/j.rse.2006.07.007.

CONCEIÇÃO, M. C. G.; MATOS, E. S.; BIDONE, E. D.; RODRIGUES, R. A. R.; CORDEIRO, R. C. Changes in soil carbon stocks under integrated crop-livestock-forest system in the Brazilian Amazon region. **Agricultural Sciences**, v. 8, p. 904-913, 2017. DOI: https://doi.org/10.4236/as.2017.89066.

COSTA, N. B.; BALDISSERA, T. C.; PINTO, C. E.; GARAGORRY, F. C.; MORAES, A.; CARVALHO, P. C. F. Public policies for low carbon emission agriculture foster beef cattle production in southern Brazil. **Land Use Policy**, v. 80, p. 269-273, 2019. DOI: https://doi.org/10.1016/j.landusepol.2018.10.014.

COSTA, M. P.; SCHOENEBOOM, J. C.; OLIVEIRA, S. A.; VIÑAS, R. S.; MEDEIROS, G. A. A socio-eco-efficiency analysis of integrated and non-integrated crop-livestock-forestry systems in the Brazilian Cerrado based on LCA. **Journal of Cleaner Production**, v. 171, p. 1460-1471, 2018. DOI: https://doi.org/10.1016/j.jclepro.2017.10.063.

CRISP, D.; FISHER, B. M.; O'DELL, C.; FRANKENBERG, C.; BASILIO, R.; BÖSCH, H.; BROWN, L. R.; CASTANO, R.; CONNOR, B.; DEUTSCHER, N. M.; ELDERING, A.;

GRIFFITH, D.; GUNSON, M.; KUZE, A.; MANDRAKE, L.; MCDUFFIE, J.; MESSERSCHMIDT, J.; MILLER, C. E.; MORINO, I.; NATRAJ, V.; NOTHOLT, J.; O'BRIEN, D. M.; OYAFUSO, F.; POLONSKY, I.; ROBINSON, J.; SALAWITCH, R.; SHERLOCK, V.; SMYTH, M.; SUTO, H.; TAYLOR, T. E.; THOMPSON, D. R.; WENNBERG, P. O.; WUNCH, D.; YUNG, Y. L. The ACOS CO_2 retrieval algorithm – Part II: global XCO_2 data characterization. **Atmospheric Measurement Techniques**, v. 5, p. 687-707, 2012. DOI: https://doi.org/10.5194/amt-5-687-2012.

BAUMGÄRTNER, L. C.; CORDEIRO, R. C.; RODRIGUES, R. A. R.; MAGALHÃES, C. S.; MATOS, E. S. Estoque e mecanismo de proteção física do carbono no solo em manejos agrícolas. [S. l.], 2021.

DA COSTA, L. M.; DE ARAÚJO SANTOS, G. A.; DE MENDONÇA, G. C.; MORAIS FILHO, L. F. F.; DE MENESES, K. C.; DE SOUZA ROLIM, G.; LA SCALA, N. Spatiotemporal variability of atmospheric CO_2 concentration and controlling factors over sugarcane cultivation areas in southern Brazil. **Environment, Development and Sustainability**, 2021. DOI: https://doi.org/10.1007/s10668-021-01677-6.

DA COSTA, L. M.; DE MENDONÇA, G. C.; DE ARAÚJO SANTOS, G. A.; DE MORAES, J. R. S. C.; COLOMBO, R.; PANOSSO, A. R.; LA SCALA, N. High spatial resolution solar-induced chlorophyll fluorescence and its relation to rainfall precipitation across Brazilian ecosystems. **Environmental Research**, v. 218, 2023. DOI: https://doi.org/10.1016/j.envres.2022.114991.

DAVIDSON, E. A.; JANSSENS, I. A. Temperature sensitivity of soil carbon decomposition and feedbacks to climate change. **Nature**, v. 440, p. 165-173, 2006. DOI: https://doi.org/10.1038/nature04514.

DE FIGUEIREDO, E. B.; JAYASUNDARA, S.; DE OLIVEIRA BORDONAL, R.; BERCHIELLI, T. T.; REIS, R. A.; WAGNER-RIDDLE, C.; LA SCALA, N. Greenhouse gas balance and carbon footprint of beef cattle in three contrasting pasture-management systems in Brazil. **Journal of Cleaner Production**, v. 142, p. 420-431, 2017. DOI: https://doi.org/10.1016/j.jclepro.2016.03.132.

DE OLIVEIRA BORDONAL, R.; DE FIGUEIREDO, E. B.; AGUIAR, D. A.; ADAMI, M.; RUDORFF, B. F. T.; LA SCALA, N. Greenhouse gas mitigation potential from green harvested sugarcane scenarios in São Paulo State, Brazil. **Biomass and Bioenergy**, v. 59, p. 195-207, 2013. DOI: https://doi.org/10.1016/j.biombioe.2013.08.040.

DE, P. L. O.; MACHADO, A. Carbono do solo e a mitigação da mudança climática global. **Química Nova**, v. 28, n. 6, p. 1038-1045, 2005.

DORIGO, W. A.; XAVER, A.; VREUGDENHIL, M.; GRUBER, A.; HEGYIOVÁ, A.; SANCHIS-DUFAU, A. D.; ZAMOJSKI, D.; CORDES, C.; WAGNER, W.; DRUSCH, M. Global automated quality control of in situ soil moisture data from the International Soil Moisture Network. **Vadose Zone Journal**, v. 12, p. 1-21, 2013. DOI: https://doi.org/10.2136/VZJ2012.0097.

FAIRALL, C. W.; BRADLEY, E. F.; HARE, J. E.; GRACHEV, A. A.; EDSON, J. B. Bulk parameterization of air-sea fluxes: updates and verification for the COARE algorithm. **Journal of Climate**, v. 16, p. 571-591, 2003.

FIGUEIREDO, E. B.; PANOSSO, A. R.; BORDONAL, R. DE O.; TEIXEIRA, D. D. B.; BERCHIELLI, T. T.; LA SCALA, N. Soil CO_2–C emissions and correlations with soil properties in degraded and managed pastures in southern Brazil. **Land Degradation & Development**, v. 28, p. 1263-1273, 2017. DOI: https://doi.org/10.1002/ldr.2524.

FRANCISCO, P. R. M.; CHAVES, I. DE B.; CHAVES, L. H. G. Bioma caatinga e degradação: modelo de mapeamento. [S. l.], 2020.

FRANCO, A. L. C.; CHERUBIN, M. R.; PAVINATO, P. S.; CERRI, C. E. P.; SIX, J.; DAVIES, C. A.; CERRI, C. C. Soil carbon, nitrogen and phosphorus changes under sugarcane expansion in Brazil. **Science of the Total Environment**, v. 515-516, p. 30-38, 2015. DOI: https://doi.org/10.1016/j.scitotenv.2015.02.025.

FRANKENBERG, C.; POLLOCK, R.; LEE, R. A. M.; ROSENBERG, R.; BLAVIER, J.-F.; CRISP, D.; O'DELL, C. W.; OSTERMAN, G. B.; ROEHL, C.; WENNBERG, P. O.; WUNCH, D. The Orbiting Carbon Observatory (OCO-2): spectrometer performance evaluation using pre-launch direct sun measurements. **Atmospheric Measurement Techniques**, v. 8, p. 301-313, 2015. DOI: https://doi.org/10.5194/amt-8-301-2015.

FREITAS, S. C.; TRIGO, I.; MACEDO, J.; BARROSO, C.; SILVA, R.; PERDIGÃO, R. Land surface temperature from multiple geostationary satellites. **International Journal of Remote Sensing**, v. 34, n. 9-10, p. 3051-3068, 2013. DOI: https://doi.org/10.1080/01431161.2012.716543.

FRIEDLINGSTEIN, P. et al. Global carbon budget 2022. **Earth System Science Data**, v. 14, p. 4811-4900, 2022. DOI: https://doi.org/10.5194/essd-14-4811-2022.

GERDOL, R.; BRAGAZZA, L.; BRANCALEONI, L. Heatwave 2003: High summer temperature, rather than experimental fertilization, affects vegetation and CO_2 exchange in an alpine bog. **New Phytologist**, v. 179, p. 142-154, 2008. DOI: https://doi.org/10.1111/j.1469-8137.2008.02429.x.

GHELLER, D. G.; GAZOLLA, M.; MARINI, M. J. Gases de efeito estufa na agricultura. **Revista Brasileira de Agricultura Irrigada**, v. 13, p. 93-111, 2019.

GIL, J. D. B.; GARRETT, R.; BERGER, T. Determinants of crop-livestock integration in Brazil: evidence from the household and regional levels. **Land Use Policy**, v. 59, p. 557-568, 2016. DOI: https://doi.org/10.1016/j.landusepol.2016.09.022.

GMACH, M. R.; CHERUBIN, M. R.; KAISER, K.; CERRI, C. E. P. Processes that influence dissolved organic matter in the soil: a review. **Scientia Agricola**, v. 77, e20180164, 2020. DOI: https://doi.org/10.1590/1678-992x-2018-0164.

GONÇALVES, A. S. F. Emissões de gases de efeito estufa e estoque de carbono em função da calagem e do preparo do solo na cana-de-açúcar. **Revista Brasileira de Ciência do Solo**, v. 44, p. 1689-1699, 2020.

HENGL, O. et al. SoilGrids1km – global soil information based on automated mapping. **PLoS ONE**, v. 9, e105992, 2014. DOI: https://doi.org/10.1371/journal.pone.0105992.

HENGL, T. et al. SoilGrids250m: global gridded soil information based on machine learning. **PLoS ONE**, v. 12, e0169748, 2017. DOI: https://doi.org/10.1371/journal.pone.0169748.

HINKO-NAJERA, N.; ISAAC, P.; BERINGER, J.; VAN GORSEL, E.; EWENZ, C.; MCHUGH, I.; EXBRAYAT, J. F.; LIVESLEY, S. J.; ARNDT, S. K. Net ecosystem carbon exchange of a dry temperate eucalypt forest. **Biogeosciences**, v. 14, p. 3781-3800, 2017. DOI: https://doi.org/10.5194/bg-14-3781-2017.

HOTT, M. C.; CARVALHO, L. M. T.; ANTUNES, M. A. H.; RESENDE, J. C.; ROCHA, W. S. D. Analysis of grassland degradation in Zona da Mata, MG, Brazil, based on NDVI time series data with the integration of phenological metrics. **Remote Sensing**, v. 11, n. 24, 2019. DOI: https://doi.org/10.3390/rs11242956.

HOWE, J. P. This is nature; this is un-nature: reading the keeling curve. **Environmental History**, v. 20, p. 286-293, 2015. DOI: https://doi.org/10.1093/envhis/emv005.

HUETE, A.; DIDAN, K.; MIURA, T.; RODRIGUEZ, E. P.; GAO, X.; FERREIRA, L. G. Overview of the radiometric and biophysical performance of the MODIS vegetation indices. **Remote Sensing of Environment**, v. 83, p. 195-213, 2002. DOI: https://doi.org/10.1016/S0034-4257(02)00096-2.

HUFFMAN, G. J.; ADLER, R. F.; BOLVIN, D. T.; GU, G.; NELKIN, E. J.; BOWMAN, K. P.; HONG, Y.; STOCKER, E. F.; WOLFF, D. B. The TRMM Multisatellite Precipitation Analysis (TMPA): quasi-global, multiyear, combined-sensor precipitation estimates at fine scales. **Journal of Hydrometeorology**, v. 8, p. 38-55, 2007. DOI: https://doi.org/10.1175/JHM560.1.

HUMBORG, C.; GEIBEL, M. C.; SUN, X.; MCCRACKIN, M.; MÖRTH, C. M.; STRANNE, C.; JAKOBSSON, M.; GUSTAFSSON, B.; SOKOLOV, A.; NORKKO, A.; NORKKO, J. High emissions of carbon dioxide and methane from the coastal Baltic Sea at the end of a summer heat wave. **Frontiers in Marine Science**, v. 6, 2019. DOI: https://doi.org/10.3389/fmars.2019.00493.

HUMPHREY, M. D.; ISTOK, J. D.; LEE, J. Y.; HEVESI, J. A.; FLINT, A. L. A new method for automated dynamic calibration of tipping-bucket rain gauges. **Journal of Atmospheric and Oceanic Technology**, v. 13, p. 364-374, 1996.

IBEBUCHI, C. C.; ABU, I. O. Characterization of temperature regimes in Western Europe, as regards the summer 2022 Western European heat wave. **Climate Dynamics**, v. 61, p. 3707-3720, 2023. DOI: https://doi.org/10.1007/s00382-023-06760-4.

IBGE. Conheça cidades e estados do Brasil. [S. l.]: IBGE, 2020. Disponível em: https://www.ibge.gov.br. Acesso em: 8 jan. 2022.

INTERGOVERNMENTAL PANEL ON CLIMATE CHANGE – IPCC. IPCC – Intergovernmental Panel on Climate Change. Disponível em: https://www.ipcc.ch/. Acesso em: 8 jan. 2022.

INTERGOVERNMENTAL PANEL ON CLIMATE CHANGE – IPCC. Global warming of 1.5°C. Cambridge: Cambridge University Press, 2022. DOI: https://doi.org/10.1017/9781009157940.

INTERGOVERNMENTAL PANEL ON CLIMATE CHANGE – IPCC. Global warming of 1.5°C. Cambridge: Cambridge University Press, 2022. DOI: https://doi.org/10.1017/9781009157940.

INTERGOVERNMENTAL PANEL ON CLIMATE CHANGE – IPCC. Climate change 2021: the physical science basis. Contribution of Working Group I to the Sixth Assessment Report of the IPCC. Cambridge: Cambridge University Press, 2021.

INTERGOVERNMENTAL PANEL ON CLIMATE CHANGE – IPCC. Climate change and land ice: IPCC special report on climate change, desertification, land degradation, sustainable land management, food security, and greenhouse gas fluxes in terrestrial ecosystems: summary for policymakers. Geneva: IPCC, 2017.

KEELING, C. D.; BACASTOW, R. B.; BAINBRIDGE, A. E. Atmospheric carbon dioxide variations at Mauna Loa Observatory, Hawaii. **Tellus**, v. 28, p. 538-551, 1976. DOI: https://doi.org/10.3402/tellusa.v28i6.11322.

KERR, D. D.; OCHSNER, T. E. Soil organic carbon more strongly related to soil moisture than soil temperature in temperate grasslands. **Soil Science Society of America Journal**, v. 84, p. 587-596, 2020. DOI: https://doi.org/10.1002/saj2.20018.

KONINGS, A. G.; BLOOM, A. A.; LIU, J.; PARAZOO, N. C.; SCHIMEL, D. S.; BOWMAN, K. W. Global satellite-driven estimates of heterotrophic respiration. **Biogeosciences**, v. 16, p. 2269-2284, 2019. DOI: https://doi.org/10.5194/bg-16-2269-2019.

KRASNOVA, A.; MANDER, Ü.; NOE, S. M.; URI, V.; KRASNOV, D.; SOOSAAR, K. Hemiboreal forests' CO_2 fluxes response to the European 2018 heatwave. **Agricultural and Forest Meteorology**, v. 323, 2022. DOI: https://doi.org/10.1016/j.agrformet.2022.109042.

KUZYAKOV, Y. V.; LARIONOVA, A. A. Contribution of rhizomicrobial and root respiration to the CO_2 emission from soil: a review. **Eurasian Soil Science**, v. 39, p. 753-764, 2006. DOI: https://doi.org/10.1134/S106422930607009X.

TUNNICLIFFE, R. L.; GANESAN, A. L.; PARKER, R. J.; BOESCH, H.; GEDNEY, N.; POULTER, B.; ZHANG, Z.; WALTER, D.; RIGBY, M.; HENNE, S.; YOUNG, D.; O'DOHERTY, S. Quantifying sources of Brazil's CH_4 emissions between 2010 and 2018 from satellite data. **Atmospheric Chemistry and Physics**, v. 20, p. 13041-13067, 2020. DOI: https://doi.org/10.5194/acp-20-13041-2020.

LHOTKA, O.; KYSELÝ, J. The 2021 European heat wave in the context of past major heat waves. **Earth and Space Science**, v. 9, 2022. DOI: https://doi.org/10.1029/2022EA002567.

LIAN, Y.; LI, H.; RENYANG, Q.; LIU, L.; DONG, J.; LIU, X.; QU, Z.; LEE, L. C.; CHEN, L.; WANG, D.; ZHANG, H. Mapping the net ecosystem exchange of CO_2 of global terrestrial systems. **International Journal of Applied Earth Observation and Geoinformation**, v. 115, 2023. DOI: https://doi.org/10.1016/j.jag.2022.103176.

LOPES, F.; MERTEN, G. H.; MIELNICZUK, J.; TORNQUIST, C. G.; OLIVEIRA, E. S. Simulação da dinâmica do carbono do solo numa microbacia rural pelo modelo Century. **Pesquisa Agropecuária Brasileira**, v. 43, p. 1121-1130, 2008.

CARVALHO, J. L. N.; AVANZI, J. C.; SILVA, M. L. N.; MELLO, C. R.; CERRI, C. E. P. Potencial de sequestro de carbono em diferentes biomas do Brasil. **Revista Brasileira de Ciência do Solo**, v. 34, p. 277-289, 2010.

LUYSSAERT, S.; INGLIMA, I.; JUNG, M.; RICHARDSON, A. D.; REICHSTEIN, M.; PAPALE, D.; PIAO, S. L.; SCHULZE, E. D.; WINGATE, L.; MATTEUCCI, G.; ARAGAO, L.; AUBINET, M.; BEER, C.; BERNHOFER, C.; BLACK, K. G.; BONAL, D.; BONNEFOND, J. M.; CHAMBERS, J.; CIAIS, P.; COOK, B.; DAVIS, K. J.; DOLMAN, A. J.; GIELEN, B.; GOULDEN, M.; GRACE, J.; GRANIER, A.; GRELLE, A.; GRIFFIS, T.; GRÜNWALD, T.; GUIDOLOTTI, G.; HANSON, P. J.; HARDING, R.; HOLLINGER, D. Y.; HUTYRA, L. R.; KOLARI, P.; KRUIJT, B.; KUTSCH, W.; LAGERGREN, F.; LAURILA, T.; LAW, B. E.; LE MAIRE, G.; LINDROTH, A.; LOUSTAU, D.; MALHI, Y.; MATEUS, J.;

MIGLIAVACCA, M.; MISSON, L.; MONTAGNANI, L.; MONCRIEFF, J.; MOORS, E.; MUNGER, J. W.; NIKINMAA, E.; OLLINGER, S. V.; PITA, G.; REBMANN, C.; ROUPSARD, O.; SAIGUSA, N.; SANZ, M. J.; SEUFERT, G.; SIERRA, C.; SMITH, M. L.; TANG, J.; VALENTINI, R.; VESALA, T.; JANSSENS, I. A. CO_2 balance of boreal, temperate, and tropical forests derived from a global database. **Global Change Biology**, v. 13, p. 2509-2537, 2007. DOI: https://doi.org/10.1111/j.1365-2486.2007.01439.x.

MAČEK, I.; PFANZ, H.; FRANCETIČ, V.; BATIČ, F.; VODNIK, D. Root respiration response to high CO_2 concentrations in plants from natural CO_2 springs. **Environmental and Experimental Botany**, v. 54, p. 90-99, 2005. DOI: https://doi.org/10.1016/j.envexpbot.2004.06.003.

MACENA, F.; ASSAD, E.; TORRES STEINKE, E.; MÜLLER, A. Clima do bioma Cerrado. **Embrapa Cerrados Documentos**, n. 174, p. 1-28, 2008.

MAJASALMI, T.; RAUTIAINEN, M.; STENBERG, P.; MANNINEN, T. Validation of MODIS and GEOV1 fPAR products in a boreal forest site in Finland. **Remote Sensing**, v. 7, p. 1359-1379, 2015. DOI: https://doi.org/10.3390/rs70201359.

MALONE, B. P.; MCBRATNEY, A. B.; MINASNY, B.; LASLETT, G. M. Mapping continuous depth functions of soil carbon storage and available water capacity. **Geoderma**, v. 154, p. 138-152, 2009. DOI: https://doi.org/10.1016/j.geoderma.2009.10.007.

MARGHANY, M.; HASHIM, M. Robust of Doppler centroid for mapping sea surface current by using radar satellite data. **American Journal of Engineering and Applied Sciences**, v. 2, p. 781-788, 2009. DOI: https://doi.org/10.3844/ajeassp.2009.781.788.

MARIA, L. DE S.; ROSSI, F. S.; COSTA, L. M. DA; CAMPOS, M. O.; BLAS, J. C. G.; PANOSSO, A. R.; DELLA SILVA, J. L.; SILVA JUNIOR, C. A. DA; LA SCALA, N. Spatiotemporal analysis of atmospheric XCH_4 as related to fires in the Amazon biome during 2015–2020. **Remote Sensing Applications: Society and Environment**, v. 30, 100967, 2023. DOI: https://doi.org/10.1016/j.rsase.2023.100967.

MELO, T. M. DE; LOUZADA, J. A. S.; PEDROLLO, O. C. Trends in extreme indices and seasonal analysis of precipitation and temperature in the northwest region of Rio Grande do Sul, Brazil. **American Journal of Climate Change**, v. 4, p. 187-202, 2015. DOI: https://doi.org/10.4236/ajcc.2015.43015.

MENDONÇA, A. K. DE S.; DA SILVA, S. A.; PEREIRA, L. Z.; BORNIA, A. C.; DE ANDRADE, D. F. An overview of environmental policies for mitigation and adaptation to climate change and application of multilevel regression analysis to investigate the CO_2 emissions over the years of 1970 to 2018 in all Brazilian states. **Sustainability**, v. 12, p. 1-18, 2020. DOI: https://doi.org/10.3390/su12219175.

METCALF, C. J. E.; GRAHAM, A. L.; HUIJBEN, S.; BARCLAY, V. C.; LONG, G. H.; GRENFELL, B. T.; READ, A. F.; BJØRNSTAD, O. N. Partitioning regulatory mechanisms of within-host malaria dynamics using the effective propagation number. **Science**, v. 333, p. 984-988, 2011. DOI: https://doi.org/10.1126/science.1204588.

MINASNY, B.; MCBRATNEY, A. B. Limited effect of organic matter on soil available water capacity. **European Journal of Soil Science**, v. 69, p. 39–47, 2018. DOI: https://doi.org/10.1111/ejss.12475.

MOITINHO, M. R.; PADOVAN, M. P.; PANOSSO, A. R.; TEIXEIRA, D. D. B.; FERRAUDO, A. S.; LA SCALA, N. On the spatial and temporal dependence of CO_2 emission on soil properties in sugarcane (Saccharum spp.) production. **Soil & Tillage Research**, v. 148, p. 127–132, 2015. DOI: https://doi.org/10.1016/j.still.2014.12.012.

MORAIS FILHO, L. F. F.; MENESES, K. C. DE; SANTOS, G. A. DE A.; BICALHO, E. DA S.; ROLIM, G. DE S.; LA SCALA, N. xCO_2 temporal variability above Brazilian agroecosystems: A remote sensing approach. **Journal of Environmental Management**, v. 288, 2021. DOI: https://doi.org/10.1016/j.jenvman.2021.112433.

MORARU, P. I.; TEODOR, R. Soil tillage conservation and its effect on soil organic matter, water management and carbon sequestration. **Drylands Facing Change: Interdisciplinary Research on Climate Change, Food Insecurity, Political Instability-COST Action CA16233**.

MORELLATO, L. P. C.; HADDAD, C. F. B. Introduction: The Brazilian Atlantic Forest. **Biotropica**, v. 32, p. 786–792, 2000. DOI: https://doi.org/10.1111/j.1744-7429.2000.tb00618.x.

MOUSAVI, S. M.; FALAHATKAR, S. Spatiotemporal distribution patterns of atmospheric methane using GOSAT data in Iran. **Environment, Development and Sustainability**, v. 22, p. 4191–4207, 2020. DOI: https://doi.org/10.1007/s10668-019-00378-5.

MOUSAVI, S. M.; FALAHATKAR, S.; FARAJZADEH, M. Assessment of seasonal variations of carbon dioxide concentration in Iran using GOSAT data. **Natural Resources Forum**, v. 41, p. 83–91, 2017. DOI: https://doi.org/10.1111/1477-8947.12121.

MURADYAN, V.; TEPANOSYAN, G.; ASMARYAN, S.; SAGHATELYAN, A.; DELL'ACQUA, F. Relationships between NDVI and climatic factors in mountain ecosystems: A case study of Armenia. **Remote Sensing Applications: Society and Environment**, v. 14, p. 158–169, 2019. DOI: https://doi.org/10.1016/j.rsase.2019.03.004.

MUTIIBWA, D.; STRACHAN, S.; ALBRIGHT, T. Land surface temperature and surface air temperature in complex terrain. **IEEE Journal of Selected Topics in Applied Earth Observations and Remote Sensing**, v. 8, p. 4762–4774, 2015. DOI: https://doi.org/10.1109/JSTARS.2015.2468594.

MYNENI, R. B.; HALL, F. G.; SELLERS, P. J.; MARSHAK, A. L. The interpretation of spectral vegetation indexes. **IEEE Transactions on Geoscience and Remote Sensing**, v. 33, p. 481–486, 1995. DOI: https://doi.org/10.1109/TGRS.1995.8746029.

MYNENI, R. B.; HOFFMAN, S.; KNYAZIKHIN, Y.; PRIVETTE, J. L.; GLASSY, J.; TIAN, Y.; WANG, Y.; SONG, X.; ZHANG, Y.; SMITH, G. R.; LOTSCH, A.; FRIEDL, M.; MORISETTE, J. T.; VOTAVA, P.; NEMANI, R. R.; RUNNING, S. W. Global products of vegetation leaf area and fraction absorbed PAR from year one of MODIS data. **Remote Sensing of Environment**, v. 83, p. 195–213, 2002.

NAGLER, P. L.; GLENN, E. P.; KIM, H.; EMMERICH, W.; SCOTT, R. L.; HUXMAN, T. E.; HUETE, A. R. Relationship between evapotranspiration and precipitation pulses in a semiarid rangeland estimated by moisture flux towers and MODIS vegetation indices. **Journal of Arid Environments**, v. 70, p. 443–462, 2007. DOI: https://doi.org/10.1016/j.jaridenv.2006.12.026.

NASA POWER. Prediction Of Worldwide Energy Resources. [S.I.]: NASA, 2023. Disponível em: https://power.larc.nasa.gov/. Acesso em: 30 abr. 2023.

NASCIMENTO, D. T. F.; MARTINS, A. P.; LUIZ, G. C.; LOPES, R. M. Climatologia do Cerrado: Variabilidades, suscetibilidades e mudanças climáticas no contexto do Cerrado brasileiro. **CandA Alfa Comunicação**, 2021.

NEVE, S. DE; PANNIER, J.; HOFMAN, G. Temperature effects on C-and N-mineralization from vegetable crop residues. **Plant and Soil**, v. 181, p. 25–30, 1996.

O'DELL, C. W.; CONNOR, B.; BÖSCH, H.; O'BRIEN, D.; FRANKENBERG, C.; CASTANO, R.; CHRISTI, M.; ELDERING, D.; FISHER, B.; GUNSON, M.; MCDUFFIE, J.; MILLER, C. E.; NATRAJ, V.; OYAFUSO, F.; POLONSKY, I.; SMYTH, M.; TAYLOR, T.; TOON, G. C.; WENNBERG, P. O.; WUNCH, D. The ACOS CO_2 retrieval algorithm – Part 1: Description and validation against synthetic observations. **Atmospheric Measurement Techniques**, v. 5, p. 99–121, 2012. DOI: https://doi.org/10.5194/amt-5-99-2012.

OLIVEIRA SILVA, R.; BARIONI, L. G.; HALL, J. A. J.; MORETTI, A. C.; FONSECA VELOSO, R.; ALEXANDER, P.; CRESPOLINI, M.; MORAN, D. Sustainable intensification of Brazilian livestock production through optimized pasture restoration. **Agricultural Systems**, v. 153, p. 201–211, 2017. DOI: https://doi.org/10.1016/j.agsy.2017.02.001.

PACHECO, A.; DE QUEIROZ CHAVES, R.; MAIA, C.; NICOLI, L. Integration of crops, livestock, and forestry: A system of production for the Brazilian Cerrados. **Eco-efficiency: from vision to reality**, p. 51–60, 2012.

PATERNIANI, E. Agricultura sustentável nos trópicos. **Estudos Avançados**, v. 35, p. 105–120, 2021.

POGGIO, L.; DE SOUSA, L. M.; BATJES, N. H.; HEUVELINK, G. B. M.; KEMPEN, B.; RIBEIRO, E.; ROSSITER, D. SoilGrids 2.0: Producing soil information for the globe with quantified spatial uncertainty. **Soil**, v. 7, p. 217–240, 2021. DOI: https://doi.org/10.5194/soil-7-217-2021.

REEVES, G. D.; MCADAMS, K. L.; FRIEDEL, R. H. W.; O'BRIEN, T. P. Acceleration and loss of relativistic electrons during geomagnetic storms. **Geophysical Research Letters**, v. 30, 2003. DOI: https://doi.org/10.1029/2002gl016513.

REICHSTEIN, M.; BAHN, M.; CIAIS, P.; FRANK, D.; MAHECHA, M. D.; SENEVIRATNE, S. I.; ZSCHEISCHLER, J.; BEER, C.; BUCHMANN, N.; FRANK, D. C.; PAPALE, D.; RAMMIG, A.; SMITH, P.; THONICKE, K.; VAN DER VELDE, M.; VICCA, S.; WALZ, A.; WATTENBACH, M. Climate extremes and the carbon cycle. **Nature**, v. 500, p. 287–295, 2013. DOI: https://doi.org/10.1038/nature12350.

REICHSTEIN, M.; FALGE, E.; BALDOCCHI, D.; PAPALE, D.; AUBINET, M.; BERBIGIER, P.; BERNHOFER, C.; BUCHMANN, N.; GILMANOV, T.; GRANIER, A.; GRÜNWALD, T.; HAVRÁNKOVÁ, K.; ILVESNIEMI, H.; JANOUS, D.; KNOHL, A.; LAURILA, T.; LOHILA, A.; LOUSTAU, D.; MATTEUCCI, G.; MEYERS, T.; MIGLIETTA, F.; OURCIVAL, J. M.; PUMPANEN, J.; RAMBAL, S.; ROTENBERG, E.; SANZ, M.; TENHUNEN, J.; SEUFERT, G.; VACCARI, F.; VESALA, T.; YAKIR, D.; VALENTINI, R. On the separation of net ecosystem exchange into assimilation and ecosystem respiration: Review and improved algorithm. **Global Change Biology**, v. 11, p. 1424–1439, 2005. DOI: https://doi.org/10.1111/j.1365-2486.2005.001002.x.

RUANE, A. C.; ANTLE, J.; ELLIOTT, J.; FOLBERTH, C.; HOOGENBOOM, G.; MASON-D'CROZ, D.; MÜLLER, C.; PORTER, C.; PHILLIPS, M. M.; RAYMUNDO, R. M.; SANDS, R.; VALDIVIA, R. O.; WHITE, J. W.; WIEBE, K.; ROSENZWEIG, C. Biophysical and economic implications for agriculture of +1.5° and +2.0°C global warming using AgMIP Coordinated Global and Regional Assessments. **Climatic Research**, v. 76, p. 17–39, 2018. DOI: https://doi.org/10.3354/cr01520.

RUSSO, S.; SILLMANN, J.; FISCHER, E. M. Top ten European heatwaves since 1950 and their occurrence in the coming decades. **Environmental Research Letters**, v. 10, 2015. DOI: https://doi.org/10.1088/1748-9326/10/12/124003.

SAUNOIS, M.; BOUSQUET, P.; POULTER, B.; PEREGON, A.; CIAIS, P.; CANADELL, J. G.; DLUGOKENCKY, E. J.; ETIOPE, G.; BASTVIKEN, D.; HOUWELING, S.; JANSSENS-MAENHOUT, G.; TUBIELLO, F. N.; CASTALDI, S.; JACKSON, R. B.; ALEXE, M.; ARORA, V. K.; BEERLING, D. J.; BERGAMASCHI, P.; BLAKE, D. R.; BRAILSFORD, G.; BROVKIN, V.; BRUHWILER, L.; CREVOISIER, C.; CRILL, P.; COVEY, K.; CURRY, C.; FRANKENBERG, C.; GEDNEY, N.; HÖGLUND-ISAKSSON, L.; ISHIZAWA, M.; ITO, A.; JOOS, F.; KIM, H.-S.; KLEINEN, T.; KRUMMEL, P.; LAMARQUE, J.-F.; LANGENFELDS, R.; LOCATELLI, R.; MACHIDA, T.; MAKSYUTOV, S.; MCDONALD, K. C.; MARSHALL, J.; MELTON, J. R.; MORINO, I.; NAIK, V.; O'DOHERTY, S.; PARMENTIER, F.-J. W.; PATRA, P. K.; PENG, C.; PENG, S.; PETERS, G. P.; PISON, I.; PRIGENT, C.; PRINN, R.; RAMONET, M.; RILEY, W. J.; SAITO, M.; SANTINI, M.; SCHROEDER, R.; SIMPSON, I. J.; SPAHNI, R.; STEELE, P.; TAKIZAWA, A.; THORNTON, B. F.; TIAN, H.; TOHJIMA, Y.; VIOVY, N.; VOULGARAKIS, A.; VAN WEELE, M.; VAN DER WERF, G. R.; WEISS, R.; WIEDINMYER, C.; WILTON, D. J.; WILTSHIRE, A.; WORTHY, D.; WUNCH, D.; XU, X.; YOSHIDA, Y.; ZHANG, B.; ZHANG, Z.; ZHU, Q. The global methane budget 2000–2012. **Earth System Science Data**, v. 8, p. 697–751, 2016. DOI: https://doi.org/10.5194/essd-8-697-2016.

SELLERS, P. J.; DICKINSON, R. E.; RANDALL, D. A.; BETTS, A. K.; HALL, F. G.; BERRY, J. A.; COLLATZ, G. J.; DENNING, A. S.; MOONEY, H. A.; NOBRE, C. A.; SATO, N.; FIELD, C. B.; HENDERSON-SELLERS, A. Modeling the Exchanges of Energy, Water, and Carbon Between Continents and the Atmosphere. **Science**, v. 275, p. 502–509, 1997. DOI: https://doi.org/10.1126/science.275.5299.502.

SENAPATI, M. R.; MISHRA, S. R.; RANJAN SENAPATI, M.; BEHERA, B. Impact of climate change on Indian agriculture and its mitigating priorities. **American Journal of Environmental Protection**, v. 1, n. 4, p. 109–111, 2013. DOI: https://doi.org/10.12691/env-1-4-6.

SESSO, P. P.; MENDES, F. H.; FILHO, U. A. S.; ZAPPAROLI, I. D. Agribusiness from selected countries: sustainability analysis between GDP and CO_2 emissions. **Revista de Economia e Sociologia Rural**, v. 61, 2023. DOI: https://doi.org/10.1590/1806-9479.2022.258543.

SHEKHAR, A.; CHEN, J.; PAETZOLD, J. C.; DIETRICH, F.; ZHAO, X.; BHATTACHARJEE, S.; RUISINGER, V.; WOFSY, S. C. Anthropogenic CO_2 emissions assessment of Nile Delta using XCO_2 and SIF data from OCO-2 satellite. **Environmental Research Letters**, v. 15, 2020. DOI: https://doi.org/10.1088/1748-9326/ab9cfe.

SIABI, Z.; FALAHATKAR, S.; ALAVI, S. J. Spatial distribution of XCO_2 using OCO-2 data in growing seasons. **Journal of Environmental Management**, v. 244, p. 110–118, 2019. DOI: https://doi.org/10.1016/j.jenvman.2019.05.049.

SIERRA, J. Nitrogen mineralization and nitrification in a tropical soil: effects of fluctuating temperature conditions. **Soil Biology and Biochemistry**, v. 33, p. 2123–2131, 2001.

SILVA, A. R.; SALES, A.; ALBERTO, C.; VELOSO, C. Atributos físicos e disponibilidade de carbono do solo em sistemas de integração Lavoura-Pecuária-Floresta (iLPF), Homogêneo e Santa Fé, no estado do Pará, Brasil. **Agropecuária Técnica**, v. 37, n. 1, p. 1–8, 2016.

SILVEIRA, M. C. T. DA; PEREZ, N. B. Informações sobre Plantas Forrageiras C4 para Cultivo em Condições de Deficiência de Drenagem e Tolerância a Frio. **Bagé (RS)**, Embrapa Pecuária Sul, 2014.

SMITH, P.; ADAMS, J.; BEERLING, D. J.; BERINGER, T.; CALVIN, K. V.; FUSS, S.; GRISCOM, B.; HAGEMANN, N.; KAMMANN, C.; KRAXNER, F.; MINX, J. C.; POPP, A.; RENFORTH, P.; VICENTE, J. L. Land-Management Options for Greenhouse Gas Removal and Their Impacts on Ecosystem Services and the Sustainable Development Goals. **Annual Review of Environment and Resources**, v. 44, p. 255–286, 2019. DOI: https://doi.org/10.1146/annurev-environ-101718-033129.

SOANE, B. D. The role of organic matter in soil compactibility: A review of some practical aspects. **Soil & Tillage Research**, v. 16, p. 179–201, 1990.

SOARES SEVERINO, L.; XAVIER COSTA, F.; ESBERARD DE MACÊDO BELTRÃO, N.; AMADOR DE LUCENA, M. Mineralização da torta de mamona, esterco bovino e bagaço de cana estimada pela respiração microbiana. **Revista de Biologia e Ciências da Terra**, v. 7, p. 69–77, 2007.

SOILGRIDS250M2.0. SoilGrids250m 2.0. Disponível em: https://soilgrids.org/. Acesso em: 4 ago. 2022.

SOMKUTI, P.; O'DELL, C. W.; CROWELL, S.; KÖHLER, P.; MCGARRAGH, G. R.; CRONK, H. Q.; BURGH, E. B. Solar-induced chlorophyll fluorescence from the Geostationary Carbon Cycle Observatory (GeoCarb): An extensive simulation study. **Remote Sensing of Environment**, v. 263, 2021. DOI: https://doi.org/10.1016/j.rse.2021.112565.

SOUZA OLIVEIRA, E.; REATTO, A.; LLACER ROIG, H. Estoques de carbono do solo segundo os componentes da paisagem. **Revista Brasileira de Ciência do Solo**, v. 39, n. 2, p. 435–443, 2015. DOI: https://doi.org/10.1590/01000683rbcs20140333.

TANG, X.; PEI, X.; LEI, N.; LUO, X.; LIU, L.; SHI, L.; CHEN, G.; LIANG, J. Global patterns of soil autotrophic respiration and its relation to climate, soil and vegetation characteristics. **Geoderma**, v. 369, 2020. DOI: https://doi.org/10.1016/j.geoderma.2020.114339.

TODD, M. C.; KIDD, C.; KNIVETON, D.; BELLERBY, T. J. A combined satellite infrared and passive microwave technique for estimation of small-scale rainfall. **Journal of Atmospheric and Oceanic Technology**, v. 18, p. 742–751, 2001.

TOMASELLA, J.; SILVA PINTO VIEIRA, R. M.; BARBOSA, A. A.; RODRIGUEZ, D. A.; DE OLIVEIRA SANTANA, M.; SESTINI, M. F. Desertification trends in the Northeast of Brazil over the period 2000–2016. **International Journal of Applied Earth Observation and Geoinformation**, v. 73, p. 197–206, 2018. DOI: https://doi.org/10.1016/j.jag.2018.06.012.

VASCONCELOS, A. L. S.; CHERUBIN, M. R.; FEIGL, B. J.; CERRI, C. E. P.; GMACH, M. R.; SIQUEIRA-NETO, M. Greenhouse gas emission responses to sugarcane straw removal. **Biomass and Bioenergy**, v. 113, p. 15–21, 2018. DOI: https://doi.org/10.1016/j.biombioe.2018.03.002.

VÉLEZ-MARTIN, E. Bioma Pampa: oportunidades e desafios de pesquisa para o desenvolvimento sustentável. **Pesquisa Agropecuária Gaúcha**, v. 26, n. 1, p. 7–15, 2020.

VICENTINI, M. E.; PINOTTI, C. R.; HIRAI, W. Y.; DE MORAES, M. L. T.; MONTANARI, R.; FILHO, M. C. M. T.; MILORI, D. M. B. P.; JÚNIOR, N. L. S.; PANOSSO, A. R. CO_2 emission and its relation to soil temperature, moisture, and O_2 absorption in the reforested areas of Cerrado biome, Central Brazil. **Plant and Soil**, v. 444, p. 193–211, 2019. DOI: https://doi.org/10.1007/s11104-019-04262-z.

VIEIRA, R. M. D. S. P.; TOMASELLA, J.; BARBOSA, A. A.; MARTINS, M. A.; RODRIGUEZ, D. A.; REZENDE, F. S. D.; CARRIELLO, F.; SANTANA, M. D. O. Desertification risk assessment in Northeast Brazil: Current trends and future scenarios. **Land Degradation & Development**, v. 32, p. 224–240, 2021. DOI: https://doi.org/10.1002/ldr.3681.

VINHOLIS, M. DE M. B.; MACCHIONE SAES, M. S.; CARRER, M. J.; MEIRELLES DE SOUZA FILHO, H. The effect of meso-institutions on adoption of sustainable agricultural technology: A case study of the Brazilian Low Carbon Agriculture Plan. **Journal of Cleaner Production**, v. 280, 2021. DOI: https://doi.org/10.1016/j.jclepro.2020.124334.

WAN, Z.; HOOK, S.; HULLEY, G. MOD11A2 MODIS/Terra Land Surface Temperature/Emissivity 8-Day L3 Global 1km SIN Grid V006. 2015, distributed by NASA EOSDIS Land Processes DAAC. **NASA LP DAAC**, 2015.

WANG, Y.; GAO, S.; LI, C.; ZHANG, J.; WANG, L. Effects of temperature on soil organic carbon fractions contents, aggregate stability and structural characteristics of humic substances in a Mollisol. **Journal of Soils and Sediments**, v. 16, p. 1849–1857, 2016. DOI: https://doi.org/10.1007/s11368-016-1379-4.

WEBB, A. J.; BÖSCH, H.; PARKER, R. J.; GATTI, L. V.; GLOOR, E.; PALMER, P. I.; BASSO, L. S.; CHIPPERFIELD, M. P.; CORREIA, C. S. C.; DOMINGUES, L. G.; FENG, L.; GONZI, S.; MILLER, J. B.; WARNEKE, T.; WILSON, C. CH_4 concentrations over the Amazon from GOSAT consistent with in situ vertical profile data. **Journal of Geophysical Research: Atmospheres**, v. 121, p. 11006–11020, 2016. DOI: https://doi.org/10.1002/2016JD025263.

WOODALL, C. W.; DOMKE, G. M.; MACFARLANE, D. W.; OSWALT, C. M. Forests and climate change: forcings, feedbacks, and the climate benefits of forests. **Forestry: An International Journal of Forest Research**, v. 85, p. 1444–1449, 2012. DOI: https://doi.org/10.1139/X09-086.

YAN, Y.; WANG, J.; TIAN, D.; ZHANG, R.; SONG, L.; LI, Z.; NIU, S. Heterotrophic respiration and its proportion to total soil respiration decrease with warming but increase with clipping. **Catena**, v. 215, 2022. DOI: https://doi.org/10.1016/j.catena.2022.106321.

YANG, D.; LIU, Y.; FENG, L.; WANG, J.; YAO, L.; CAI, Z.; ZHU, S.; LU, N.; LYU, D. The first global carbon dioxide flux map derived from TanSat measurements. **Advances in Atmospheric Sciences**, v. 38, p. 1433–1443, 2021. DOI: https://doi.org/10.1007/s00376-021-1179-7.

YANG, W.; TAN, B.; HUANG, D.; RAUTIAINEN, M.; SHABANOV, N. V.; WANG, Y.; PRIVETTE, J. L.; HUEMMRICH, K. F.; FENSHOLT, R.; SANDHOLT, I.; WEISS, M.; AHL, D. E.; GOWER, S. T.; NEMANI, R. R.; KNYAZIKHIN, Y.; MYNENI, R. B. MODIS leaf area index products: From validation to algorithm improvement. **IEEE Transactions on Geoscience and Remote Sensing**, v. 44, p. 1885–1896, 2006. DOI: https://doi.org/10.1109/TGRS.2006.871215.

YOUNESZADEH, S.; AMIRI, N.; PILESJO, P. The effect of land use change on land surface temperature in the Netherlands. **ISPRS Archives**, v. 40, p. 745–748, 2015. DOI: https://doi.org/10.5194/isprsarchives-XL-1-W5-745-2015.

YU, L.; WEN, J.; CHANG, C. Y.; FRANKENBERG, C.; SUN, Y. High-resolution global contiguous SIF of OCO-2. **Geophysical Research Letters**, v. 46, p. 1449–1458, 2019. DOI: https://doi.org/10.1029/2018GL081109.

ZEMP, D. C.; SCHLEUSSNER, C. F.; BARBOSA, H. M. J.; HIROTA, M.; MONTADE, V.; SAMPAIO, G.; STAAL, A.; WANG-ERLANDSSON, L.; RAMMIG, A. Self-amplified Amazon forest loss due to vegetation-atmosphere feedbacks. **Nature Communications**, v. 8, 2017. DOI: https://doi.org/10.1038/ncomms14681.

ZHANG, P.; BOUNOUA, L.; IMHOFF, M. L.; WOLFE, R. E.; THOME, K. Comparison of MODIS land surface temperature and air temperature over the continental USA meteorological stations. **Canadian Journal of Remote Sensing**, v. 40, p. 110–122, 2014. DOI: https://doi.org/10.1080/07038992.2014.935934.

ZHANG, Q.; SHIA, R. L.; SANDER, S. P.; YUNG, Y. L. XCO_2 retrieval error over deserts near critical surface albedo. **Earth and Space Science**, v. 3, p. 36–45, 2016. DOI: https://doi.org/10.1002/2015EA000143.

ZHANG, W.; LUO, G.; YUAN, X.; LI, C.; XIE, M.; WANG, Y.; MA, XIAOFEI.; SHI, H.; HAMDI, R.; HELLWICH, O.; MA, XIUMEI.; TERMONIA, P.; DE MAEYER, P. New data-driven method for estimation of net ecosystem carbon exchange at meteorological stations effectively increases the global carbon flux data. **Methods in Ecology and Evolution**, v. 14, p. 2449–2463, 2023. DOI: https://doi.org/10.1111/2041-210X.14188.

ZHU, D.; CIAIS, P.; KRINNER, G.; MAIGNAN, F.; JORNET PUIG, A.; HUGELIUS, G. Controls of soil organic matter on soil thermal dynamics in the northern high latitudes. **Nature Communications**, v. 10, p. 1–9, 2019. DOI: https://doi.org/10.1038/s41467-019-11103-1.

ZHU, X.; CHEN, J.; GAO, F.; CHEN, X.; MASEK, J. G. An enhanced spatial and temporal adaptive reflectance fusion model for complex heterogeneous regions. **Remote Sensing of Environment**, v. 114, p. 2610–2623, 2010. DOI: https://doi.org/10.1016/J.RSE.2010.05.032.

CHAPTER 5 - FINAL CONSIDERATIONS

1. Future perspectives: Heatwaves

To address the positive feedback effect between heatwaves and CO_2 emissions from thermally stressed ecosystems, it is crucial to implement effective control mechanisms. First, it is essential to expand monitoring and research on the relationship between heatwaves and CO_2 emissions in order to anticipate and mitigate future impacts resulting from this feedback loop.

The protection of ecosystems such as forests and agriculture ecosystem are fundamental to enhancing the resilience of these systems and their capacity to sequester and store carbon. Furthermore, public policies must be established to reduce greenhouse gas emissions by promoting sustainable forest management practices.

2. Future perspectives: xCO_2, SOC and Priority Zones

As society faces the consequences of climate change, the development and implementation of public policies focused on this issue become crucial, not only to mitigate the impacts, but also to promote resilience to the approaching extreme climate events. Brazil, with its vast natural resources and diverse biomes, plays an important role in atmospheric CO_2 removals on the global stage.

In Brazil, a country with immense natural wealth across different biomes, nature-based solutions (NBS) offer significant potential to promote sustainability and climate resilience. In this context, such solutions serve as mechanisms capable of optimizing ecosystem processes and services to address regional social, economic, and environmental challenges.

3. Maintenance of Soil Carbon Stocks

Soil plays a central role in this context. Its capacity to store carbon cannot be overlooked, making it a key attribute in the fight against climate change. Policies that promote sustainable agricultural practices, such as conservation and regenerative agriculture, supported by crop rotation and integrated management of soil physical, chemical, and biological properties, can help maintain or increase existing carbon stocks. Furthermore, reforestation with native species and the restoration of degraded areas, especially pastures under the current Brazilian context, are essential strategies that should be expanded.